UNIVERSIDAD DE SALAMANCA

DEPARTAMENTO DE INGENIERÍA CARTOGRÁFICA Y DEL TERRENO

TESIS DOCTORAL

Automatización en la extracción del trazado y el inventario geométrico de carreteras mediante sistemas de cartografiado móvil

Alberto Holgado Barco

2016

Departamento de Ingeniería Cartográfica y del Terreno

Escuela Politécnica Superior de Ávila

Universidad de Salamanca

AUTOR:

Alberto Holgado Barco

DIRECTORES:

Dr. D. Diego González Aguilera

Dr. D. Pedro Arias Sánchez

2016

AUTOMATIZACIÓN EN LA EXTRACCIÓN DEL TRAZADO Y EL INVENTARIO GEOMÉTRICO DE CARRETERAS MEDIANTE SISTEMAS DE CARTOGRAFIADO MÓVIL

Tesis Doctoral presentada por Alberto Holgado Barco

INFORME DE LOS DIRECTORES DE TESIS

La Tesis Doctoral "*Automatización en la extracción del trazado y el inventario geométrico de carreteras mediante sistemas de cartografiado móvil*", presentada por Alberto Holgado Barco, se inserta en la línea de investigación de los sistemas autónomos de cartografiado móvil aplicados al mantenimiento e inventariado de carreteras. Mediante esta Tesis Doctoral se han desarrollado metodologías y algoritmos destinados a la automatización de la extracción de información semántica de interés como son la plataforma de la carretera o las marcas viales, a partir de las cuales obtener la delineación de la carretera y su inventario geométrico (nº carriles, ancho plataforma, ancho arcenes, ancho carriles), así como el trazado geométrico tanto horizontal (p. ej.: rectas, curvas circulares, clotoides) como vertical (p. ej.: rasantes, acuerdos verticales, peraltes).

Los resultados obtenidos con todas y cada una de las metodologías presentadas dieron lugar a la publicación de diferentes artículos científicos, todos ellos actualmente publicados en revistas de reconocido prestigio en el ámbito de la geomática y la ingeniería civil, sometidos a la revisión anónima por pares e indexada en las bases de datos del Journal Citation Report (JCR), encontrándose no sólo en el primer cuartil (Q1) de sus categorías sino también en el **primer decil**.

Dadas las condiciones presentadas, se considera que la presente Tesis Doctoral se ajusta, de modo óptimo, a las condiciones requeridas para la presentación de la misma por la modalidad de "compendio de publicaciones", conforme los requisitos expuestos en el Reglamento de Doctorado de la Universidad de Salamanca.

La calidad de las metodologías propuestas, así como los algoritmos desarrollados, queda irrefutablemente reconocida después de su publicación en revistas de reconocido prestigio y alto factor de impacto en el ámbito de la geomática e ingeniería civil.

Y para los efectos oportunos, los directores informan favorablemente la citada Tesis Doctoral para su presentación y defensa pública.

En Ávila, a 20 de abril de 2016

Dr. Diego González Aguilera

NOMBRE ARIAS SANCHEZ PEDRO - NIF 32773491D

Firmado digitalmente por NOMBRE ARIAS SANCHEZ PEDRO - NIF 32773491D
Nombre de reconocimiento (DN): c=ES, o=FNMT, ou=FNMT Clase 2 CA, ou=500052777, cn=NOMBRE ARIAS SANCHEZ PEDRO - NIF 32773491D
Fecha: 2016.04.21 13:45:41 +02'00'

Dr. Pedro Arias Sanchez

Listado de artículos publicados

Esta Tesis Doctoral consiste en un compendio de tres artículos científicos, publicados en revistas internacionales de alto impacto (primer decil). A continuación se enumeran estas publicaciones.

1. **Semiautomatic Extraction of Road Horizontal Alignment from a Mobile LiDAR System**

   Alberto Holgado-Barco[1], Diego González-Aguilera[1], Pedro Arias-Sánchez[2] and Joaquín Martínez-Sánchez[2]

   [1]Department of Cartographic and Land Engineering, University of Salamanca, Higher Polytechnic School of Avila, Hornos Caleros 50, 05003, Avila, Spain

   [2]Department of Natural Resources & Environmental Engineering, University of Vigo, School of Mining Engineering, Maxwell s/n, 36310, Vigo, Spain

   Computer-Aided Civil and Infrastructure Engineering, Septiembre 2014

   DOI: 10.1111/mice.12087

2. **An automated approach to vertical road characterisation using mobile LiDAR systems: Longitudinal profiles and cross-sections**

   Alberto Holgado-Barco[1], Diego González-Aguilera[1], Pedro Arias-Sánchez[2] and Joaquín Martínez-Sánchez[2]

   [1]Department of Cartographic and Land Engineering, University of Salamanca, Higher Polytechnic School of Avila, Hornos Caleros 50, 05003, Avila, Spain

[2]Department of Natural Resources & Environmental Engineering, University of Vigo, School of Mining Engineering, Maxwell s/n, 36310, Vigo, Spain

ISPRS Journal of Photogrammetry and Remote Sensing, Julio 2014

DOI: 10.1016/j.isprsjprs.2014.06.017

3. Automatic inventory of road cross sections from Mobile Laser Scanning system

Alberto Holgado-Barco[1], Belén Riveiro[2], Diego González-Aguilera[1] and Pedro Arias-Sánchez[3]

[1]Department of Cartographic and Land Engineering, University of Salamanca, Higher Polytechnic School of Avila, Hornos Caleros 50, 05003, Avila, Spain

[2]Department of Materials Engineering, Applied Mechanics and Construction, School of Industrial Engineering, University of Vigo, 36208 Vigo, Spain

[2]Department of Natural Resources & Environmental Engineering, University of Vigo, School of Mining Engineering, Maxwell s/n, 36310, Vigo, Spain

Computer-Aided Civil and Infrastructure Engineering

DOI: 10.1111/mice.12213

“Un camino de mil millas
comienza con un paso”

Benjamin Franklin

Agradecimientos

Por fin se cumplió el objetivo de finalizar la Tesis Doctoral. Un objetivo que hace cuatro años y medio veía como muy lejano y que por fin gracias al esfuerzo y trabajo diario se ha hecho realidad. Ha sido una etapa larga en el tiempo que parecía que nunca finalizaría. Pero aquí está, objetivo conseguido, lo que me provoca una gran satisfacción tanto personal como profesional.

A lo largo de esta etapa han sido muchas personas las que me han acompañado y apoyado para recorrer este camino, a todos ellos quiero expresarles mi más sincero agradecimiento.

En primer lugar quiero agradecer a Diego González Aguilera y Pedro Arias Sánchez, directores de Tesis por su ayuda, colaboración y conocimientos en esta etapa tan dura y compleja que ha sido realizar esta Tesis Doctoral. De forma individual, gracias Diego por haberme dado la oportunidad de pertenecer al equipo de investigación TIDOP y haberme permitido realizar otro tipo de investigaciones que no estaban relacionadas con la Tesis Doctoral, ya que de ellas también he aprendido mucho. Gracias Pedro por haberme dado la posibilidad de trabajar con un tipo de tecnología puntera en el ámbito de las geotecnologías. También agradecerte el haberme permitido realizar dos pequeñas estancias en tu grupo de investigación Geotecnologías Aplicadas.

También dar las gracias, como no, a mis compañeros de trabajo y amigos del grupo TIDOP, con los que he pasado muchas horas y buenos momentos dentro de la locura de cada uno con su Tesis Doctoral o proyectos de investigación entre manos.

Dar las gracias a Belén y Joaquín, los cuales me habéis ayudado mucho para conseguir publicar estos artículos en revistas punteras.

Y finalmente como no a mi familia, la cual me ha ayudado mucho a desconectar de la locura que suponía estar continuamente pegado al ordenador. A mis padres por haberme permitido realizar una formación

universitaria completa. A ti, Cris gracias por el apoyo incondicional, ya que has tenido que aguantar todo tipo de situaciones, desde no entender algunas de las cosas que te decía; en las que aguantabas el chaparrón; hasta el que yo estuviera con el ordenador trabajando cuando estábamos de vacaciones.

Gracias a todos.

Resumen

En esta Tesis Doctoral se plantea el uso de los sistemas de cartografiado móvil (MMS-Mapping Mobile System) tanto para la obtención de inventarios geométricos de carreteras como para la automatización del trazado asociado a las mismas. Una de las mayores dificultades que tienen estos sistemas es la falta de software que permita automatizar la extracción de información semántica de interés, como son las marcas viales o la plataforma de la carretera. Y a partir de esta información poder obtener la delineación de la vía, su inventario geométrico (p. ej.: nº carriles, ancho plataforma, ancho arcenes, ancho carriles), así como el trazado geométrico tanto horizontal (p. ej.: rectas, curvas circulares, clotoides) como vertical (p. ej.: rasantes, acuerdos verticales, peraltes). Con este tipo de desarrollos será posible realizar un control exhaustivo y rápido de las carreteras por parte de las administraciones gestoras, debido a que en la información derivada puedan identificarse problemas relacionados con el estado de las infraestructuras viarias, su inventariado geométrico e incluso la mejora de la seguridad vial. No obstante, uno de los mayores problemas a los que se hace frente en esta Tesis Doctoral es el tratamiento de toda la información capturada; más concretamente a los procesos de segmentación y modelización de objetos o entidades, debido al carácter desorganizado y sin semántica de las nubes de puntos.

Por ello planteamos una metodología automática a partir de la cual obtener los diferentes elementos de la carretera mediante el uso de sistemas LiDAR móvil (MLS), en el que un sistema láser activo de medida permite la documentación de las vías mediante nubes de puntos tridimensionales. La primera fase que se llevará a cabo es obtener de manera automática tanto la plataforma de la carretera como las marcas viales. Debido a la gran cantidad de datos capturados por el MLS se ha desarrollado una metodología basada en procesos de segmentación y clasificación a través de la cual detectar tanto la plataforma del vial como reconocer semánticamente la marcas viales (p. ej.: marca vial izquierda/derecha y diferentes marcas centrales), para así poder llevar a

cabo la delineación de la infraestructura viaria en formato CAD. Realizado el proceso de segmentación y clasificación estamos ya en disposición de obtener los diferentes elementos geométricos contenidos en la vía. En primer lugar comenzaremos estimando las características geométricas del trazado horizontal, que cumplen con los requisitos de la instrucción de carreteras (Norma 3.1- IC. Trazado). Dicho proceso se realizará mediante técnicas de parametrización y filtrado de la marca principal de la vía, ya que esta actuará de eje de la carretera y con ella podremos estimar los elementos geométricos que componen su trazado horizontal (p. ej.: líneas rectas, curvas circulares y clotoides). En segundo lugar estimaremos las características geométricas del trazado vertical. Este proceso se llevará a cabo mediante técnicas de regresión ortogonal, a través del análisis de componentes principales (PCA), así como una parametrización y filtrado de la calzada con la que determinar los elementos geométricos que mejor definen su trazado en alzado (p. ej.: rasantes y acuerdos verticales), así como en su sección transversal (p. ej.: peraltes). La última fase de la metodología será obtener los perfiles transversales de la carretera, a partir de la segmentación de la vía como de la clasificación de las marcas viales, con las que poder obtener el inventario geométrico de la sección transversal (p. ej.: nº carriles, ancho plataforma, ancho arcenes, ancho carriles).

Esta Tesis Doctoral es el resultado de un compendio de tres artículos científicos publicados en revistas internacionales de alto impacto (ver Apéndice A).

Abstract

This Doctoral Thesis proposes the Mobile Mapping System (MMS) technology to inventory roads and obtain their geometric sections automatically. One of the greater difficulties that this technique involves is the extraction of semantic information from raw data due to the lack of software capable to extract it automatically. This semantic information includes, for example, the platform dimensions, road markings, signalling, number of lanes, wide of the hard shoulders, horizontal and vertical delineation (straight lines, circular curves, clothoids, road slope, camber, etc.) among others. After the development of this thesis, administrations will carry out quick and comprehensive controls of roads deriving valuable information in order to detect problems related to roads conditions, their geometric sections and even improving roads safety. However, one of the greater challenges is the data processing since an important segmentation and object modeling processes are necessary to extract semantic information from the point cloud.

For that reason, this thesis aims to achieve an automatic methodology from which different elements of the highway will be obtained by using the mobile LiDAR system (MLS), an active laser system that allows the documentation of the roads by three-dimensional point clouds. The first stage will consist on the automatic extraction of the platform as well as the road markings. Due to the great amount of data captured by the MLS, a new methodology based on segmentation and classification processes has been developed to obtain the road platform as well as to recognize the road markings (i.e., left, right and different central marks) to be able to obtain the road section in CAD format. Once this process finishes, it is possible to extract the rest of the elements of the road. First of all, the geometric characteristics of the road in relation with the horizontal delineation will be obtained by full filing the requirements of the Spanish official specifications for road alignments (Norma 3.1 – I.C.: Trazado). This process will be made through different parameterization and filtering techniques applied to the main central mark of the road (the road axis) from which the geometric

elements that compose its horizontal alignment (straight lines, circular curves and clothoids) will be obtained. Secondly, the vertical characteristics of the road will be extracted. In this case, several techniques like orthogonal regressions, principal component analysis (PCA), parameterization and filtration of the road pavement to determine the geometric elements that best define its vertical delineation as well as the cross-sections. Finally, the cross-sections profiles and the classification of the road markings will be obtained from a segmentation process with which the geometric inventory of the road (number of lanes, and width of the road, shoulders and lanes) will be extracted.

This Doctoral Thesis is the result of a compendium of three scientific papers published in high impact international journals (see Appendix A).

Índice

CAPÍTULO 1

INTRODUCCIÓN

INTRODUCCIÓN

El desarrollo de los sistemas de cartografiado móvil (Mobile Mapping Systems - MMS) se inició a finales de 1980 y principios de 1990, cuando el Centro de Cartografía de la Ohio State University desarrollo el primer MMS utilizable en tierra. Su sistema, llamado GPSVan TM, integraba un sistema de navegación por satélite de código (Global Navigation Satellite System - GNSS), dos cámaras digitales CCD (Charge Coupled Device), dos cámaras de vídeo de color y varios sensores inerciales, todos los cuales eran montados sobre una camioneta (Goad, 1991; Novak, 1991). Se trataba del primer sistema MMS que integraba principalmente tres componentes: sensores de cartografiado (activos y pasivos), sensores de posicionamiento y navegación para la referencia espacial y seguimiento de la trayectoria, y una unidad de control que opera e integra todos estos componentes, sincroniza la adquisición de la medición y registra los datos recogidos.

Los sistemas móviles que utilizan el LiDAR como unidad principal de cartografiado (Mobile LiDAR Systems - MLS) constituyen el sistema más desarrollado en la actualidad. La tecnología LiDAR (Light Detection and Ranging), se basa una tecnología activa que permite determinar la distancia desde un emisor láser a un objeto o superficie utilizando un haz láser pulsado. El sistema LiDAR móvil es utilizado con escáneres láser que se implementan en cualquier plataforma móvil, tales como camionetas, lanchas (Alho et al., 2009), motos de nieve (Kaasalainen et al., 2011), o incluso vehículos todo terreno (El-Halawany y Lichti, 2011). Los escáneres láser móviles comparten muchas características con los escáneres láser en el aire (Airborne Laser Scanners - ALS), especialmente aquellas características como los fundamentos de la medición láser, cálculo y ajuste de la trayectoria y el análisis de los datos. Por otra parte, los flujos de trabajo de procesamiento de datos son muy similares en ambos casos (El-Sheimy, 2005).

Debido a la creciente necesidad de información geográfica en 3D y el actual interés en el campo de la cartografía móvil, los parámetros de los escáneres láser y de navegación varían rápidamente como consecuencia del desarrollo tecnológico. Se trata de un mercado global en el que la principal barrera de entrada es el elevado coste de las unidades móviles que son necesarias para llevar a cabo estas tareas, siendo de hecho la razón que explica la reducida cuota de mercado que han alcanzado los MMS montados en vehículos industriales durante los últimos años. Esto también significa que los beneficios del cartografiado urbano — en particular el incremento de la eficiencia en la recogida de datos — no están siendo explotados por una comunidad amplia de usuarios.

1.1. Principios de funcionamiento y flujo de trabajo

Cualquier sistema LiDAR móvil integra varios subsistemas: las cámaras digitales, uno o varios láseres escáner, una unidad de medición inercial (Inertial Measurement Unit - IMU) en combinación con un sistema de navegación global por satélite (GNSS), y una unidad de control que opera todos estos componentes, sincroniza la adquisición de la medición y registra los datos recogidos. La descripción de la tecnología se organizará en dos partes: la primera describe la geo-referenciación de posicionamiento y navegación (espacial y angular) deparada por los sistemas móviles LiDAR, ineludible dado el propio principio de medición de estos sistemas. La segunda referente a la telemetría láser y los dispositivos complementarios de exploración (p. ej.: cámaras fotográficas, video, etc.).

1.1.1. Componentes de posicionamiento y navegación

La geo-referenciación es la determinación variable en el tiempo de los parámetros de posición y orientación para un sistema LiDAR móvil. Estos llevan montado tres tipos de tecnologías para determinar la posición de un vehículo móvil: sistema global de navegación por satélite (GNSS), sistemas de navegación inercial con una unidad de medición inercial (IMU) y los indicadores de medición de distancia (Distance

Measurement Indicators - DMI). Estos sensores nos permiten orientar y posicionar un sistema móvil respecto a un sistema global de coordenadas.

Hay un gran número de receptores GNSS disponibles en el mercado que pueden proporcionar gran calidad en los datos de posición. Estos operan principalmente en tres modos diferentes de obtener datos en función de la calidad de los resultados que necesitemos: el modo diferencial (Differential Global Positioning System - DGPS), cinemático de tiempo real (Real Time Kinematics - RTK) y el post-procesado cinemático (Post Processed Kinematics - PPK) (El-Rabbany, 2002; Huerta et al., 2005). El GNSS es el componente básico de un sistema de posicionamiento de tierra y estos pueden proporcionar una precisión centimétrica, sin embargo, es prácticamente imposible mantener la señal a lo largo de una toma de datos con un sistema móvil debido a los efectos de trayectoria múltiple y los períodos de interrupción del GNSS (p. ej., a cambios de trayectoria, perdidas de ciclo, túneles, edificios altos, las pendientes de la carretera y las copas de los árboles). Esta limitación a menudo conduce a la combinación de GNSS con las unidades de medición inercial (IMU) (Tin Leung et al., 2011; Titterton y Weston, 2004). La navegación a estima (Dead Reckoning - DR) deparada por la medición inercial, es un proceso en el que las nuevas posiciones se calculan exclusivamente en base a las anteriores, no pudiéndose utilizar durante largos períodos de tiempo debido a que la navegación inercial presenta una deriva con el tiempo. Estos errores surgen de los ruidos y los sesgos presentes en las mediciones inerciales. Por este motivo, los sistemas actuales empleados en los sistemas móviles LiDAR emplean una IMU que se basa en sistemas GNSS para recibir correcciones periódicas. Una unidad de medición inercial proporciona información autónoma sobre la posición instantánea, la velocidad y la orientación de un vehículo. Hay tres tipos de dispositivos IMU que son los más utilizados en los sistemas LiDAR móviles (Petrie, 2010; Kavanagh, 2007): micro electro-mecánicos (Micro Electro-Mechanical Systems - MEMS), giróscopos de fibra óptica (Fiber Optic Gyros - FOG) y giróscopos de anillo láser (Ring Laser Gyros - RLG). Los giróscopos MEMS se construyen con silicio micro-mecanizado, y son relativamente baratos de fabricar. La principal desventaja de los MEMS es que son mucho menos precisos que los dispositivos ópticos, que incluyen fibra

óptica y anillo láser. Ambos giróscopos se basan en el efecto Sagnac[1], y requieren de alta precisión de fabricación y técnicas complejas de montaje, debido a ello siguen siendo costosos.

La mayoría de los GNSS y sistemas IMU utilizados en los sistemas LiDAR móviles son compatibles con los instrumentos de medida de distancia (DMI). Estos son dispositivos rentables y fiables para la recogida y transmisión de datos de rotación, que normalmente se transforman en velocidad, distancia y posición. Los codificadores pueden ser mecánicos u ópticos. Estos últimos se utilizan en altas velocidades cuando se requiere un mayor grado de precisión. La DMI se monta en una rueda del vehículo con un cable de transmisión de datos y el cable de alimentación.

En la mayoría de los casos, el filtro de Kalman (Zarchan y Musoff, 2009) se utiliza para la combinación óptima de los datos GNSS, IMU y DMI respecto a una posición y sistema de orientación (Position and Orientation System - POS). El POS lleva a cabo esta tarea mediante la adopción de la ubicación temporal del vehículo combinando la información de los satélites GNSS, la información acerca de la orientación del vehículo con la IMU y la medición de la distancia de la DMI. El procedimiento para el cálculo de la mejor estimación de la trayectoria (Smooth Best Estimate Trajectory - SBET) del vehículo requiere de cinco minutos de registro de datos GNSS estáticos al principio y al final de una toma de datos, con el fin de obtener datos precisos del GNSS. La trayectoria se utiliza para crear una nube de puntos geo-referenciada utilizando los datos del escaneo láser.

[1] El efecto Sagnac es un fenómeno que se ha encontrado en interferometría que se produce por la rotación. El efecto Sagnac se manifiesta en una configuración llamada interferometría de anillo. Desde un punto de este anillo se lanzan dos rayos de luz simultáneamente en direcciones opuestas. Cuando los rayos vuelven al punto de partida tienen entre sí una diferencia de camino óptico que se puede detectar mediante un montaje interferométrico.

1.1.2. Componentes de medición por láser

Un escáner láser es un sistema de medidas automatizadas de ángulos y distancias. En los sistemas móviles actuales los escáneres pueden obtener la información mediante dos técnicas: el tiempo de vuelo y la diferencia de fase. Un escáner de tiempo de vuelo (Time of Flight - ToF) determina la distancia cronometrando el tiempo del viaje de ida y vuelta de un pulso de luz. Algunos de los escáner que utilizan esta técnica son los siguientes: Riegl VZ-400i (Riegl, 2016), Optech (Optech, 2016), Leica Scanstation P40 (Leica, 2016), Trimble TX8 (Trimble, 2016) y la Sick LMS511 (Sick, 2016). Por el contrario los que utilizan la diferencia de fase Z+FImager 5010C (Zoller+Fröhlich, 2016); Faro Focus 3D (Faro, 2016) miden la diferencia de fase entre la onda emitida y la recibida, y utilizan dicha medida para estimar la distancia al objeto. El haz láser emitido por este tipo de escáneres es continuo y de potencia modulada. Los escáneres láser de fase tienen un rango de medición más corto. La combinación de la distancia láser, los ángulos de lectura horizontal y vertical, y el conocimiento de la trayectoria nos permiten la integración de la posición del láser mediante GNSS / IMU / DMI, obteniendo como resultado la posición 3D (*X*,*Y*,*Z*) de los puntos escaneados.

Existe un gran número de escáneres láser que se han utilizado en vehículos de cartografiado móvil pero usando el modo de perfil 2D, con un único ángulo de giro del cabezal. La tercera dimensión de los datos capturados del perfil se obtiene como resultado del movimiento de avance de la plataforma del vehículo (Kutterer, 2009). En la actualizad se están empleando múltiples escáneres láser en una misma plataforma móvil. Estos sistemas utilizan un conjunto de láseres ToF para analizar y medir de forma simultánea y en paralelo, para así poder producir una densidad mayor de puntos y dar una cobertura superior, mejorando la calidad de los datos. Múltiples sistemas de escaneo láser se utilizan para capturar entornos de gran tamaño. La tasa de repetición del pulso de láser (Pulse Repetition Rate - PRR), en combinación con el espejo de exploración, determina la velocidad de toma de datos LiDAR. La velocidad de recogida de datos está entre 50 kHz – 2 MHz (50,000 –

2,000,000 puntos/seg), lo que permite al usuario recoger gran cantidad de datos empleando un período de tiempo muy corto.

1.2. Sistemas LiDAR móviles

A continuación se van a mostrar los diferentes sistemas LiDAR móviles que están en el mercado. Existen dos factores importantes que influyen en la calidad de los datos como son el escáner láser y la exactitud de la posición proporcionada por los sistemas de posicionamiento y navegación. Las propiedades importantes de un escáner láser son: el alcance máximo, el campo de visión, la tasa de repetición del pulso, la frecuencia de barrido, la divergencia del haz, la exactitud y precisión en la medición de la distancia y la densidad de puntos, son algunas de las características técnicas más importantes de los escáneres láser. Los MLS que se van a analizar son los siguientes: IP-S3 HD1 (Topcon), MX8 (Trimble), VMX-1HA (Riegl) y Lynx SG Mobile Mapper (Optech).

1.2.1. IP-S3 HD1– TOPCON

Topcon Positioning Systems (Topcon, 2016) introdujo su nuevo sistema de cartografía móvil, el IP-S3, en la primavera de 2015. Incluye una solución de navegación TOPCON la cual combina tres tecnologías diferentes. Un receptor GNSS de doble frecuencia y un sistema inercial. El resultado de la posición GNSS / IMU es complementado por un DMI. Las especificaciones del sistema una vez realizado el post-proceso son las siguientes: precisión en la posición *X Y* de 0.030 m y en *Z* de 0.030 m.

El sistema de imagen que lleva montado el IP-S3 es una unidad multicámara que se compone de seis cámaras de 5 Mpx, cinco situadas en un anillo horizontal y una en la parte superior. Esta cámara realiza imágenes panorámicas de 360 º con velocidades de hasta 10 fps.

La toma de datos láser del sistema IP-S3 HD1 (Topcon, 2016) cuenta con un campo de vista horizontal de 360º (Horizontal Field Of View - HFOV) y un campo de vista vertical de 30º (Vertical Field Of View - VFOV). El sistema está compuesto por 32 rayos láser internos

que cubren la totalidad de los 360º, proporcionando 700,000 puntos por segundo. El LiDAR opera a una longitud 100 m de distancia con un 100% de reflectividad, la distancia típica es de 70 m.

1.2.2. MX8 – TRIMBLE

El Sistema Móvil Trimble MX8 es un sistema avanzado que combina tanto la captura de imágenes como de nubes de puntos a través del sistema láser. Ha estado disponible desde el tercer trimestre de 2010 a través de TRIMBLE.

Los MX8 cuentan con un diseño tipo cápsula que pueden ser instalados en una gran variedad de vehículos. El sistema de captura de datos incluye dos receptores GNSS TRIMBLE (para determinar la posición inicial y la dirección del vehículo) y un sistema inercial APPLANIX POS LV 520, la combinación de manera óptima de los datos inerciales con los observables GNSS brutos procedentes de los satélites con una frecuencia de hasta 200 Hz se lleva a cabo con el software PosPac MMS. El sistema tiene cuatro componentes principales: una unidad de medición inercial (IMU) que es el corazón del sistema POS LV, un sistema informático POS, dos antenas GNSS y una DMI que calcula la información de rotación de la rueda para ayudar en la medida de distancia del vehículo. POS LV puede ser utilizado con DGPS y correcciones RTK, o en post-proceso para mejorar la calidad de los datos obtenidos. Con post-procesamiento, las especificaciones son las siguientes: precisión en la posición *X Y* de 0.020 m, precisión de la posición *Z* de 0.050 m, roll / pitch de 0.005º y el yaw de 0.015 °.

El sistema también tiene dos posibles configuraciones en cuanto a sistemas LiDAR se refiere. La versión más alta integra dos escáneres Riegl VQ-450 y un sistema de imágenes panorámicas compuesto por seis cámaras digitales de 5 Mpx con una tasa de captura 12 fps. Los láser pueden medir distancias de hasta 800 m (con un 80% de reflectividad) a una velocidad de 550,000 puntos por segundo. La unidad de control del MX8 es de gran tamaño y se encuentra en el interior del vehículo. La empresa TRIMBLE también ha integrado una pantalla doble para el seguimiento de la toma de datos en la posición del copiloto (Trimble, 2014).

1.2.3. VMX-1HA – Riegl

El Riegl VMX-1HA es un láser de escaneo móvil muy compacto y fácil de usar. El sistema va montado sobre bastidores en el techo del vehículo o sobre diferentes plataformas (automóviles, vehículos 4x4, trenes o barcos) está compuesto por dos escáneres Riegl VUX-1HA que pueden medir distancias de hasta 420 m (con un 80% de reflectividad) a una velocidad de 500,000 puntos por segundo, un sistema inercial VMX-MH, un odómetro VMX-DMI que se coloca en una de las ruedas del vehículo, un sistema de navegación y varias cámaras digitales o equipos de vídeo. Las especificaciones del sistema una vez realizado el post-proceso son las siguientes: precisión en la posición *X Y* de 0.020 m y en *Z* de 0.050 m (Riegl, 2016). El sistema de exploración se complementa con el sistema de imagen VMX-CS6, que soporta hasta 6 cámaras digitales de color. La orientación y la posición de cada cámara es seleccionable por el usuario, la velocidad de captura es de hasta 9 fps. También puede integrar una unidad multicámara LADYBUG5, que se compone de seis cámaras Sony de 5 Mpx, cinco situadas en un anillo horizontal y una en la parte superior. Esta cámara realiza imágenes panorámicas de 360 º con velocidades de hasta 10 fps. Los datos se visualizan en una pantalla colocada en el interior, la cual está conectada a la unidad de control VMX-CU.

1.2.4. Lynx SG Mobile Mapper – OPTECH

El Lynx SG Mobile Mapper fue lanzado a finales de 2007 por OPTECH. Es capaz de generar datos LiDAR e imágenes a alta velocidad. El LYNX se basa en una cabeza LiDAR, de Optech con la tecnología iFlex, para capturar datos a una velocidad de 600,000 puntos por segundo con un campo de visión horizontal de 360 º. El sistema de posicionamiento ha sido diseñado por Applanix, POS 520, con 2 antenas GNSS para un mejor cálculo inicial y dirección del vehículo: utiliza receptores GNSS TRIMBLE. OPTECH proporciona hasta cuatro cámaras digitales de 5 Mpx que adquieren imágenes geo-referenciadas. La orientación de las cámaras es seleccionable por el usuario. Estas pueden producir velocidades de hasta 6.5 fps. También puede montar un sistema multicámara LADYBUG. Los sensores del LYNX están

montados en una plataforma rígida que se puede colocar en los bastidores del techo de los vehículos o en instalaciones personalizadas para embarcaciones o trenes. OPTECH no vende sus escáneres por separado como Riegl, sino que los incorporan en exclusiva en su sistema de cartografía móvil LYNX SG1.

Las unidades de escáner láser tienen un alcance máximo de 250 m y proporcionan una cobertura horizontal de 360 º, a una velocidad de 600,000 puntos por segundo. Cada sensor detecta y registra hasta cuatro mediciones de retorno distinto para cada pulso láser (Optech, 2016).

La unidad de control / rack del LYNX (con la solución de navegación integrada) se encuentra dentro del vehículo. La unidad de control controla los datos LiDAR, que se fusionan con los datos GNSS / INS del sistema POS LV520 de Applanix, los datos DMI y las imágenes de las cámaras. Desde un ordenador portátil conectado a la unidad de control un operador puede controlar y supervisar el trabajo, ya que este proporciona los datos en tiempo real, el monitoreo de imágenes y los códigos de color que indican el estado del sistema.

1.3. Aplicaciones de los sistemas LiDAR móviles

Los sistemas Mobile LiDAR System (MLS) se están utilizando en múltiples aplicaciones, como son los inventarios de carreteras o la modelización de entornos urbanos. Las mayores dificultades que tienen estos sistemas es la falta de software capaz de automatizar la extracción de información semántica de interés como son las marcas viales, a partir de las cuales obtener la delineación de la carretera así como su inventario geométrico. Con este tipo de tecnología es posible realizar un control exhaustivo y rápido de las carreteras por parte de las administraciones gestoras, ya que a través de la información derivada podrían identificarse problemas relacionados con el estado de las carreteras, su inventariado geométrico e incluso la mejora de la seguridad vial. No obstante, uno de los mayores problemas a los que se enfrenta esta tecnología es el tratamiento de toda la información capturada y más concretamente la segmentación y modelización de objetos y entidades a partir del carácter desorganizado y sin topología de las nubes de puntos.

La extracción automática de las marcas viales y perfiles transversales nos permite avanzar en el inventario de la carretera a través de la extracción de sus elementos geométricos (p. ej.: nº carriles, ancho plataforma, ancho arcenes, ancho carriles, peralte) al igual que en la delineación automática de la carretera en formato CAD. En este contexto, son diversos los autores que han avanzado soluciones interesantes como son: la obtención de un modelo superficial de la carretera (Gräfe, 2008), el inventario automático de las marcas viales que se centran en dos aspectos principales: la detección y clasificación de las señales de tráfico puntuales (p. ej.: pasos de cebra, ceda el paso, límites de velocidad, etc.) (Guan et al., 2015), así como el inventario de diferentes tipos de marcas viales con diferentes formas y orientaciones (Yu et al., 2015).

Por otro lado, existen diversas investigaciones que se centran en entornos urbanos a través de la extracción de las calles y sus marcas viales utilizando tan solo imágenes capturadas desde sistemas Mapping Mobile System (MMS). Dichas investigaciones se centran en la detección de marcas viales en el contexto de la visión computacional, donde la información 3D se calcula utilizando imágenes estereoscópicas (Soheilian et al., 2010) o mediante imágenes panorámicas (Cheng et al., 2008). A pesar de los intereses reales de dichos métodos, la información 3D extraída de imágenes estereoscópicas sigue siendo incierta, ya que el ángulo de incidencia generado por las imágenes no es el óptimo para reconstruir la misma zona de carretera que con un LiDAR. También, las imágenes sufren las condiciones de luz desfavorable o condiciones climáticas (p. ej.: cielo cubierto, resplandor del sol, sombras, etc.), que en el caso del LiDAR no le influyen pudiendo realizar capturas incluso de forma nocturna.

En el mismo contexto urbano pero utilizando datos LiDAR, son diversos los autores los que han avanzado soluciones interesantes como son la detección de calles (Hervieu y Soheilian, 2013), la diferenciación del tipo de material con el que está construida la calle (asfalto, pavimento de piedra) (Díaz-Vilariño et al., 2016) y la delineación de zonas urbanas (Yang et al., 2013). También existe otro tipo de clasificación de objetos urbanos como son: objetos sobre el suelo (p. ej.: señales, farolas, muros, árboles, etc.), objetos fuera del suelo como es la vegetación baja (p. ej.:

matorrales) y la propia superficie del terreno. Dicha clasificación de elementos se basa en características geométricas y relaciones topológicas (Pu et al., 2011).

Bajo el contexto de la extracción topográfica del trazado de carreteras, cabe reseñar la disponibilidad de crear detallados mapas de carreteras digitales que contienen información precisa sobre parámetros geométricos ampliamente utilizados, tanto horizontales (líneas rectas, curvas circulares y clotoides) así como verticales (rasantes, curvas verticales y peraltes). Un gran número de autores han empleado recientemente el uso de sistemas de mapeo móvil (MMS) para obtener información precisa sobre la geometría del trazado horizontal (Di Mascio et al., 2012), vertical (Lakakis et al., 2013) y el peralte (Tsai et al., 2013) de la carretera mediante los sistemas globales de navegación por satélite (GNSS). En estos acercamientos realizan la captura de los datos de la carretera mediante los registros de ida y vuelta de la misma, a partir del cuales estimar el eje para posteriormente reconocer los elementos horizontales, verticales de la carretera u obtener los peraltes de la carretera. Las limitaciones más importantes que presentan estos acercamientos radica en el uso exclusivo del GNSS, ya que la obtención de la geometría de la trayectoria seguida por el vehículo no es la geometría real de la carretera, sin embargo con los acercamientos que proponemos evitamos esa dependencia debido a que hacemos uso de la información aportada por los sensores LiDAR y por tanto el vehículo podría circular con total libertad por cualquier tipo de carreteras.

CAPÍTULO 2

HIPÓTESIS DE TRABAJO Y OBJETIVOS

HIPÓTESIS DE TRABAJO Y OBJETIVOS

En el apartado anterior se ha mostrado una visión general de las diversas técnicas geomáticas aplicadas al reconocimiento e inventario de carreteras. El contexto de aplicación de la metodología y herramientas desarrolladas es el del Inventario Geométrico de Carreteras, particularmente las autovías. No obstante, el rango de aplicación de los métodos propuestos no está restringido exclusivamente a autovías, pudiendo extrapolarse a carreteras e incluso ferrocarriles.

2.1. Hipótesis de trabajo

La base de esta investigación es el desarrollo de diferentes herramientas que nos permitan automatizar la extracción de información de las carreteras, especialmente el trazado y su inventariado geométrico. Para dar respuestas a esta investigación, se plantean las siguientes hipótesis:

- Los sistemas LiDAR móvil son herramientas potentes que permiten el modelado de las infraestructuras lineales de una forma rápida y eficaz, a partir de la información tridimensional que generan.

- Es posible la segmentación automática de nubes de puntos procedentes de MLS con el objetivo de obtener la digitalización de las marcas viales.

- Es posible automatizar la extracción y cálculo de los elementos geométricos característicos del trazado, tanto horizontales (p. ej.: rectas, curvas circulares, clotoides) como verticales (p. ej.: rasantes, acuerdos verticales, peraltes)

- Es factible la creación de una herramienta informática para la extracción y gestión en base de datos de los atributos del

inventario vial (p. ej.: nº carriles, ancho plataforma, ancho arcenes, ancho carriles)

2.2. Objetivos

Con relación a los objetivos de la Tesis Doctoral podríamos destacar un objetivo general y varios objetivos específicos.

El **objetivo general** es el desarrollo y puesta en práctica de métodos automáticos y herramientas para extraer el trazado horizontal y vertical de las carreteras así como su inventario geométrico de la sección transversal, a partir de la información capturada por un sistema LiDAR móvil (MLS).

Los **objetivos específicos** de la Tesis Doctoral son:

- Desarrollar un protocolo para la detección de las calzadas a partir de datos LiDAR.
- Establecer una metodología que nos permita detectar las marcas viales longitudinales de la carretera a partir de la calzada detectada anteriormente.
- Clasificar semánticamente las marcas detectadas anteriormente en función de la posición espacial de la nube de puntos e incluso la clasificación de las distintas marcas discontinuas.
- Convertir las marcas clasificadas a formas geométricas del tipo splines, para su posterior exportación a un fichero CAD.
- Desarrollar una estrategia que nos permita obtener el trazado geométrico horizontal (rectas, curvas circulares y clotoides) en función de la marca que consideremos que actúa de eje en cada tipo de carretera.
- Generar una metodología mediante la cual obtener el trazado vertical tanto en la dirección longitudinal (rasantes y acuerdos

verticales) como transversal (peraltes), a partir de la calzada detectada.

- Crear una estrategia que nos permita obtener los perfiles transversales de la carretera a partir de la detección de la calzada, así como de la clasificación de las marcas viales con las cuales poder obtener el inventario geométrico de la sección transversal de la carretera (nº carriles, ancho plataforma, ancho arcenes, ancho carriles).

CAPÍTULO 3

ARTÍCULOS CIENTÍFICOS

ARTÍCULOS CIENTÍFICOS

3.1. Semi-Automatic extraction of road horizontal alignment from a mobile LiDAR system

Resumen: El objetivo principal del artículo es desarrollar un método que nos permita obtener las características geométricas del trazado horizontal a partir de los datos capturados con un sistema LiDAR móvil. En particular, el enfoque desarrollado tiene dos componentes: (1) la extracción de los datos LiDAR para modelar el eje de la carretera y (2) la estimación de las características geométricas del trazado horizontal que cumplen con los requisitos de la instrucción de carreteras (Norma 3.1- IC. Trazado). Dado el carácter masivo y complejo de los datos capturados por el sistema, se ha implementado una estrategia jerárquica basada en procesos de segmentación, parametrización y filtrado que determine la línea central de la carretera junto con los elementos geométricos que componen su trazado horizontal: líneas rectas, arcos circulares y clotoides. El proceso desarrollado ha sido validado con datos simulados y reales. Los resultados experimentales obtenidos en ambos casos garantizan precisiones relativas del 2%, siendo un método útil para automatizar de forma precisa las características geométricas asociadas al trazado horizontal de la carretera.

Palabras clave: sistema de cartografía móvil; sistema LiDAR móvil; información geo-espacial; escaneado láser; mantenimiento de carreteras; inventarios de carretera; trazado horizontal; segmentación; filtrado; parametrización; extracción de características.

COMPUTER-AIDED CIVIL AND INFRASTRUCTURE ENGINEERING

Computer-Aided Civil and Infrastructure Engineering **30** (2015) 217–228

Semiautomatic Extraction of Road Horizontal Alignment from a Mobile LiDAR System

Alberto Holgado-Barco & Diego González-Aguilera*

Department of Cartographic and Land Engineering, University of Salamanca, Higher Polytechnic School of Avila, Hornos Caleros 50, 05003, Avila, Spain

Pedro Arias-Sanchez & Joaquin Martinez-Sanchez

Department of Natural Resources & Environmental Engineering, University of Vigo, School of Mining Engineering, Maxwell s/n, 36310, Vigo, Spain

Abstract: *This article proposes a method to semiautomatically extract the road axis through a mobile LiDAR system, a recent popular technology for transportation-related applications, road estimation and even to enhance driver safety. In particular, the approach developed has two components: (1) the feature extraction from LiDAR data to model the road axis, and (2) the estimation of the horizontal alignment that meets the requirements and practice for a transportation authority. Given the massive and complex character of the data captured by the system, a hierarchical (coarse-to-fine) and robust strategy based on segmentation, parameterization and filtering, which determine the road centerline together with the geometric elements that compose its horizontal alignment, such as straight lines, circular arcs, and clothoids, has been developed and implemented. Test results using a simulated and a real data are discussed and validated. The experimental results obtained with real cases guarantying relative accuracies under 2%, being a useful approach to produce accurate estimations of the horizontal geometric features of the road alignment.*

1 INTRODUCTION

Usefulness of road digital maps goes beyond topographic applications as they are already a real demand in the development of advanced driving assistance systems, vehicle-based safety improvement, and traffic accident reduction (GIM, 2013). Simple navigation maps, placed nowadays in most of the car models, can easily become safety maps by using additional digital information. This may help the driver in a number of ways, such as adapting the speed to the road condition, interpreting signals, and even avoiding collisions.

Within this context, the automatic extraction of road axis is the first step for the generation of detailed digital road maps. Such maps should contain accurate and reliable information about the vertical (slopes and cambers) and horizontal (straight lines, circular arcs, and clothoids) road features.

The application of Mobile Mapping Systems (MMS) to road characterization is straightforward. MMS began to be used in the late 1980s and early 1990s and were composed of a navigation system and a set of digital cameras (photogrammetric systems). Currently, the navigation system of a MMS is typically integrated by three sensors: Global Navigation Satellite System (GNSS), Inertial Measurement Unit (IMU), and Distance Measuring Indicator (DMI). In addition, an important evolution of MMS has occurred in the last decades, incorporating and integrating LiDAR (Light Detection and Ranging) sensors. A decreasing cost of acquisition and some improvements in accuracy and point cloud density have made LiDAR a widely preferred technology for surveying. Moreover, LiDAR has been successfully used in a wide variety of civil engineering applications. Park et al. (2007) have used Terrestrial Laser Scanning (TLS) for health monitoring of structures. In this work, TLS-based displacement measurements were tested against three different techniques: (1) linear variable displacement transducers, (2) electric strain gages, and (3) long gage fiber optic sensors. Truong-Hong

*To whom correspondence should be addressed. E-mail: *daguilera@usal.es*.

DOI: 10.1111/mice.12087

et al. (2013) presented a technique for transforming point clouds into solid models based on the combination of an angle criterion and voxelization. Complete building models are generated using this technique. Aerial laser scanning (ALS) was used by Deshpande (2013) for floodplain delineation. A time-efficient delineation method that divides the LiDAR data into regular tiles was presented in this work. LiDAR data was saved at pyramid levels and preprocessed to obtain elevation information. This information was used to filter and process only those tiles that contribute to the floodplain, resulting in a time-saving methodology.

Accordingly, LiDAR point clouds and RGB images are directly georeferenced under a mapping system (in our case, ETRS89-European Terrestrial Reference System 1989, UTM-Universal Transverse Mercator-30N).

Besides that, mobile LiDAR system (MLS) synchronization capabilities allow integration of additional data acquired from auxiliary sensors, such as thermal information provided by thermographic cameras, subsoil data coming from a ground penetrating radar (GPR), and even information about the pavement international roughness index (IRI) using profilometers. Saarenketo and Scullion (2000) provide a status report of the principles of operation of GPR systems for road evaluation. GPR techniques have been used to nondestructively identify soil type, to estimate the thickness of overburden and to evaluate the compressibility and frost susceptibility of subgrade soil. Lorenzo et al. (2011) present a special trailer designed to adapt a multipurpose GPR system to road evaluation using two bowtie-antennas. As a result, both commercial (Puente et al., 2013) or custom developed (Tao, 2000; Moreno et al., 2013) MLSs constitute an ideal system to capture massive and detailed data for accurate and reliable road geometric characterization and centerline generation.

MLS is an accurate and time-saving technology that increases productivity in capturing road networks. On the other hand, we must keep in mind that, for instance, the Optech system used in this work can provide up to a million points per second. This pulse repetition rate (PRR) would result, depending on the scanned geometry, in approximately 500 million points for a road section of 10 km, at an average speed of 60 km/h.

This article presents a methodology for the automated extraction of the topographical parameters of road axes (i.e., straight lines, circular arcs, and clothoids) using a dataset obtained by an MLS. One of the main advantages of this approach is that both point cloud segmentation and road axis extraction can be solved with a one-way travel.

The article is structured as follows: after this introduction; Section 2 describes the related work regarding road geometric characterization; Section 3 explains the materials used and the developed method, with special emphasis on algorithms for segmentation, parameterization, and filtering; Section 4 shows the experimental results obtained considering simulated and real data; the last section describes the most relevant conclusions along with possible future work directions.

2 RELATED WORK

There are several examples in the literature regarding road geometric characterization based on imaging technologies and MMS. Toth and Grejner-Brzezinska (2004) present a custom-designed van-based mapping system that delivers road centerline positions obtained from a GNSS/IMU navigation system and an imaging subsystem, which supports mono and stereo processing. Based on stereovision, Nedevschi et al. (2004) propose a 3D lane detection system. The lane is modeled as a 3D surface defined by the vertical and horizontal clothoid curves, the lane width and the roll angle. These values are detected by the system and detection results are used to update the lane through Kalman filtering. A single camera and 3D road model are used by Ishikawa et al. (2007) for precise road line localization. In this work, a MMS provides a highway alignment database and measures road center and side lines positions based on camera and laser scanners. In Cheng et al. (2008), a robust automatic road geometry characterization is presented. Based on panoramic imagery, the extracted information includes 3D lane lines, road edges, and lane lines attributes. Soheilian et al. (2010) deal with the problem of road marking reconstruction using stereo pairs gathered by a MMS in a dense urban area. Zebra crossings and dashed lines are detected by using geometric specifications of road markings. Tsai et al. (2013) propose the use of vision technology for horizontal roadway curvature computation. The proposed algorithm consists of four steps: (1) curve edges image processing, (2) mapping edges from image space to real-world space, (3) camera parameters calibration, and (4) curve center and radius calculation. Foucher et al. (2011) focus on the detection of urban road markings such as zebras, arrows, and crosswalks and propose an algorithm for the detection and recognition of repetitive markings as well as single patterns.

The road geometric characteristics are extracted in other studies from the data provided by dynamic mapping systems. Cremean and Murray (2006) presented a methodology to extract a clothoid road model based on features extracted from single-axis LiDAR and extended Kalman filter techniques. A methodology for the extraction of road horizontal alignment based on GNSS/IMU is presented in Choi and Sung (2007), where an algorithm was proposed according to the statistical inference. This algorithm is subdivided by

three steps: (1) data grouping by tangent/curve/clothoid sections, (2) tangent/curve/clothoid analysis, and (3) tangent/curve/clothoid position estimation. Jiménez et al. (2009) presented a fast and accurate on-board inertial system together with an algorithm for segmenting straight alignments, circular curves, and transition curves. Segmented sections are afterwards fitted to geometric curves following highway standards. Stratakos et al. (2009) proposed a strategy of multiscale correlation and a method of curve matching that identify the traditional geometric elements that define the centerline. Karamanou et al. (2010) proposed the use of a survey based on the geodetic positioning of a suitably equipped vehicle, moving along the road in a two-way journey. The acquired data were used to extract the road centerline. The parameters of horizontal and vertical features of the road are afterwards estimated based on a least squares adjustment of the characteristic curves. Di Mascio et al. (2012) presented a procedure to determine the geometry of road alignment using GNSS dynamic measurements. For single carriageway, two datasets are logged, one for each traffic way. The centerline is estimated as the middle point between both trajectories. Another algorithm is applied afterwards to recognize horizontal and vertical road elements by least squares optimization. The main drawback of the previous approaches based on dynamic mapping systems is that the geometry of the road axis is computed after two surveys in both traffic ways. Moreover, geometric design elements obtained in these studies rely heavily on the trajectories described by the MMS.

As mentioned in the introduction, MLS are a state-of-the-art technology for road inspection and characterization. Due to the huge datasets acquired, there is a need for automatic road data processing. Yang et al. (2013) presented a semiautomated approach for road extraction and delineation in urban scenes. Taking into account that MLS point clouds are a set of consecutive scan lines, road curb points are obtained based on a moving window operator that filters point cloud data line by line. Guan et al. (2014) presented a stepwise procedure for road marking recognition based on MLS point clouds. The raw dataset is partitioned, according to the vehicle trajectory, into a set of profiles that are inspected afterwards for road surface segmentation. These road surfaces are interpolated into a georeferenced image, which is used for road marking recognition.

3 MATERIALS AND METHODS

This section is divided in five subsections. The first one deals with the Optech Lynx MLS used in the work and presents its properties and characteristics. The second one includes a comprehensive analysis of the errors and their propagation. After a brief overview of the methods developed in Section 3.3, a detailed description of the main processing steps is provided. In particular, the point cloud segmentation and centerline extraction is described in Section 3.4, whereas the procedure for road horizontal alignment and its mathematical modeling is detailed in Section 3.5.

Table 1
Technical specifications regarding the accuracy thresholds of the Optech Lynx mobile LiDAR system

Technical features	*Lynx Mobile Mapper*
X, *Y* position	0.020 m
Z position	0.050 m
Roll and pitch	0.005°
True heading	0.015°
Measuring principle	Time of flight (ToF)
Maximum range	200 m
Precision range	8 mm, 1σ
Ranging accuracy	±10 mm, (1σ)
Laser measurement rate	75–500 kHz
Measurement per laser pulse	Up to 4 simultaneous
Scan frequency	80–200 Hz
Laser wavelength	1,550 nm (near infrared)
Angular resolution	0.001°

3.1 The acquisition system: Optech Lynx

The acquisition system used in this work is the Lynx Mobile Mapper by Optech. This MLS can acquire a LiDAR point cloud together with RGB imagery of the scanned scene. The capture system itself integrates a navigation system, two LiDAR sensors, and four RGB cameras (Puente et al., 2012).

The navigation system of the vehicle is the Applanix POS LV 520 that consists of a GNSS system, an IMU, and a DMI. The IMU is the center of the vehicle coordinate system, and, accordingly, the other sensors must be aligned with it. The positioning GNSS system is used for mapping vehicle local coordinates to absolute coordinates with a planimetric precision of about 0.02 m. It should be noted that precision properties are highly dependent on GNSS availability, which can be considered good for open-space road scanning. The MLS used is manufactured by Optech, Inc. and its technical specifications are described in Table 1.

3.2 Mobile LiDAR system: budget error

The error budget of a MLS is developed based on a direct sensor orientation process that integrates GNSS, IMU, and LiDAR observations. There are several

random and systematic error sources that contribute to the final positional (X, Y, Z) accuracy of the processed MLS point cloud. Apart from the calibration parameters (e.g., boresight, offset, time, etc.) the main factors to a MLS error budget are: (i) the GNSS precision to provide position information, (ii) the IMU precision to provide attitude determination, and (iii) the LiDAR unit to obtain distances. The measured distances are coupled with the position and attitude information from the GNSS/IMU integration process, as well as the calibration parameters relating the coordinate system components. As a result, the derivation of the final accuracy of the point cloud is not clear and transparent to the final user.

To this end, a budget error of MLS based on the variance–covariance propagation law is proposed (Mikhail and Ackermann, 1976). The evaluation of the results considers the estimated residuals $\boldsymbol{v}$ and their covariance matrix $\mathbf{C_{vv}}$:

$$C_{vv} = C_{ll} - AC_{xx}A^T \quad (1)$$

where $\mathbf{C_{ll}}$ is the covariance matrix of observations, $\mathbf{A}$ is the Jacobian design matrix, and $\mathbf{C_{xx}}$ is the covariance matrix of the estimated parameters.

It should be remarked that the magnitude of the random errors depends on the accuracy of the system's measurements, which include position and orientation measurements from the GNSS/IMU unit and scanning angles and distances from the LiDAR system. Systematic errors, on the other hand, are mainly due to biases in the boresight-offset parameters relating the coordinate system components as well as biases in the LiDAR system measurements (e.g., scaling factor and zero-offset).

The equation that relates random and systematic errors for computing the final position of the ground point, i, in the mapping system could be expressed as follows:

$$r_i^m = r^m{}_{\text{imu/gnss}(t)} + R_b^m(t)\left[R_l^b r_i^l(t) + a^b\right] \quad (2)$$

where r_i^m is the final position of the point i in the mapping reference system (ETRS89,UTM-30N); $r^m{}_{\text{imu/gnss}}$ is the IMU positioning under the mapping reference system and based on the GNSS system; $\mathbf{R}_b{}^m$ is the rotation matrix coming from the IMU that encloses the attitude under the mapping reference system; $\mathbf{R}_l{}^b$ contains the boresight misalignment between the LiDAR and the IMU computed in a calibration process; r_i^l is the vector that includes the distances measured from the LiDAR system; a^b is the spatial offset between the IMU and the LiDAR system, also determined in the calibration process.

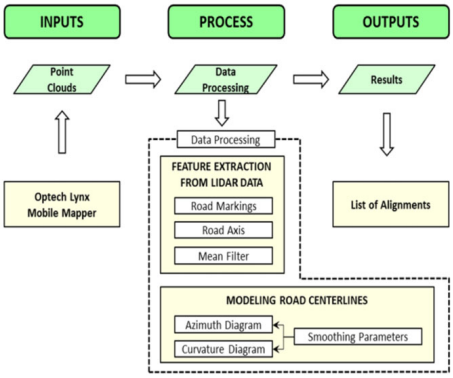

Fig. 1. Workflow for the semiautomatic extraction of the geometric parameters of the road using a MLS-acquired point cloud.

3.3 Methods overview

The methodology proposed in this article is divided into three steps: (1) segmentation, (2) filtering, and (3) parameterization of the collected point cloud (Figure 1). More specifically, the amount of points in the input point cloud is reduced by the segmentation procedure (1). As a result of this procedure, a road axis or centerline is obtained. Due to the presence of random errors, this centerline is filtered (2) using a robust approach to improve the latter parameterization process. In the parameterization step (3), the geometric design elements of the road are computed based on the azimuth and curvature diagrams. The entire process has been developed in Matlab as a prelude to its final implementation in the open source library, PCL (Point Cloud Library).

3.4 Segmentation of the point cloud and extraction of the road axis

It should be noted that Spanish official specifications for road alignments (Norm 3.1) were considered in this study to be practical, although the resulting methodology would be application dependent.

The point cloud collected by the MLS is segmented semiautomatically using intensity and scan-angle thresholds. Pavement marking lines of the road are segmented using the intensity values captured by the LiDAR and taking into account their higher reflectivity. All points with an intensity value higher than 180 are classified and labeled as road-marking points. This threshold was determined adaptively using the

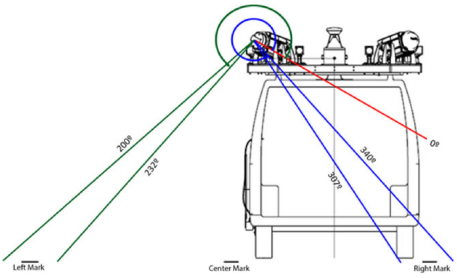

Fig. 2. Determination of the scan angle thresholds for the segmentation of the road platform together with its pavement marking lines.

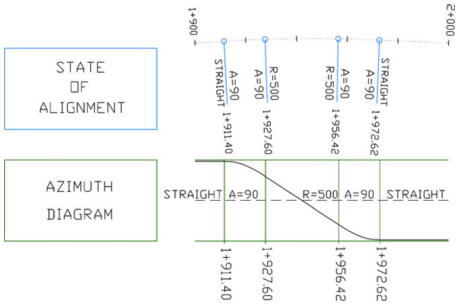

Fig. 3. Example of the parameterization of the road according to the azimuth diagram, being A the clothoid parameter and R the radius of the circular curve.

histogram of the point intensity values. In the second step of the segmentation, the points that belong to the left and right pavement marking lines are segmented. This segmentation is achieved by establishing a scan-angle threshold between 200° and 232° for the left marking line and between 307° and 340° for the right marking line. Figure 2 outlines the implemented segmentation process.

To reduce the number of points to be processed in subsequent steps, points segmented as marking-lines are clustered every 0.5 m by using point time stamps and scan-angles. Segmented points are put in order depending on their time stamp and scan-angle to obtain the different scan-lines of the MLS. These scan-lines are clustered based on the distance between lines. Finally, the centroid of each cluster (Equation 3) is saved as a centerline point:

$$\bar{x} = \frac{\sum_{i=1}^{n} x_i}{N} \quad \bar{y} = \frac{\sum_{i=1}^{n} y_i}{N} \tag{3}$$

where $\bar{x}$, $\bar{y}$ are the centroid coordinates, x_i, y_i, and N are, respectively, the coordinates of the points and the number of points in the cluster.

3.5 Calculation of the geometric design of the horizontal alignments

The elements of the horizontal alignment (i.e., straight lines, circular arcs, and clothoids) can be determined using the centerline extracted in the previous section. The geometric parameters of the horizontal road alignment have been obtained based on azimuth and curvature information.

The azimuth of the centerline is determined as follows:

$$a = \operatorname{arctg}\left(\frac{\Delta x_i^{i-1}}{\Delta y_i^{i-1}}\right)\frac{180}{\pi} \tag{4}$$

where Δx, Δy are the X and Y planimetric coordinate difference between consecutive points (i, $I-1$) along the road axis.

The segmentation of the road according to its different elements is possible based on graphical analyses of the azimuth, where straight lines correspond to horizontal lines, circular arcs correspond to straight lines, and clothoids correspond to second degree curves or parabolas (Figure 3). The curvature of a circular arc can be derived from the slope of its corresponding line. In Figure 3, the azimuth diagram of a road is shown. This diagram consists of two straight segments (horizontal lines) and a circular arc (straight line). The clothoids are the elements between a straight line and a circular arc.

A second parameter, the curvature, can be calculated using the first derivative of the azimuth according to Equation (5).

$$a' = \frac{a_{i+1} - a_i}{s_{i+1} - s_i} \tag{5}$$

where a_i is the azimuth value in position i and the difference $(s_{i+1} - s_i)$ is the length between points. Through this parameterization, straight lines correspond to zero-curvature values, circular arcs correspond to constant-curvature values and clothoids correspond to variable curvature values (straight line with a slope depending on the clothoid parameter) (Figure 4).

Due to measurement errors and their propagation through the previous steps in the methodology, an antialiasing filter is applied before the parameterization

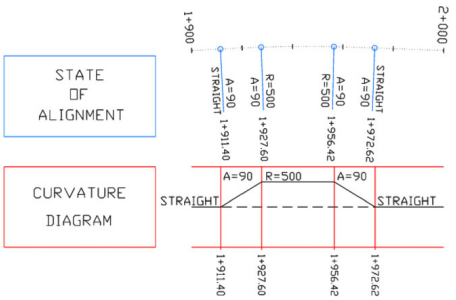

Fig. 4. Example of the parameterization of the road according to the curvature diagram, being A the clothoid parameter and R the radius of the circular curve

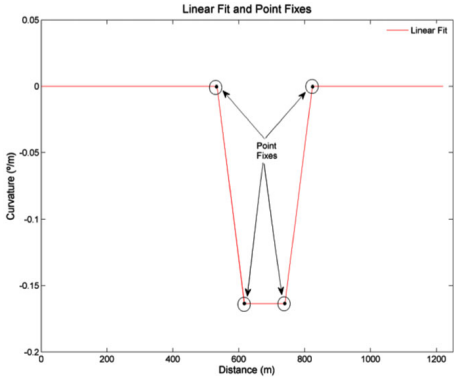

Fig. 5. Example of road segmentation based on curvature values: linear fit of the curvature (red line) and point fixes obtained from clothoid parameterization (see color figure in online version).

steps. The antialiasing filtering used is a locally weighted regression curve (Cleveland and Devlin, 1988) where the fitting function is applied locally and moved along the centerline to smooth the data.

The filtered curvature diagram can be used for segmentation. A threshold value of ±0.005°/m was set, because this value corresponds to curvature radius not considered in the road technical specifications. Segments with a curvature parameter lower than this threshold are classified as straight lines. The other segments in the road axis should be detected and labeled either as circular arcs or as clothoids.

The histogram of curvature values can be used for circular arc detection, because the curvature value of a circular arc corresponds with the maximum value of such a histogram. The radius of the circular arc is obtained by using Equation (6).

$$R = \frac{180}{\pi \cdot a'} \tag{6}$$

where a' corresponds to the curvature associated with the circular arc and R is the radius of the circular curve.

At this point, straight lines and circular arcs in the road axis were detected and classified. Unclassified points are grouped and labeled as clothoid points. To group the clothoid points, we take into account the distance between successive points and the curvature value increments: curvature increases (decreases) for clothoids preceding (succeeding) a circular arc. Every detected clothoid is modeled with a parameter A that is obtained by applying Equation (7).

$$A^2 = R \cdot L \tag{7}$$

where A is the clothoid parameter, R is the radius of the adjacent circle arc computed in the previous step, and L is the transition length. This transition length is derived in three steps: (1) a linear model is fitted to curvature values through least squares adjustment, (2) this line is intersected with the adjacent horizontal lines (view Figure 5) to find the fixed transition points, and (3) transition length is the distance between fixed points.

The different geometric elements forming the horizontal alignment are classified and filtered according to the Spanish official specifications for road alignments (Norm 3.1), and the horizontal design elements are calculated using least-squares adjustment. In the case of the straight lines: the initial point, the length and the slope are calculated. In the case of the circular arcs: the radius, the center of the circle and the length of the arc are calculated. In the case of the clothoids: apart from the A parameter, the point fixes coordinates, the clothoid length, the radius of the adjacent circle arc and the value of the tangent at the origin are calculated. All this information is stored in a text file that contains the list of the horizontal alignment of the road.

4 EXPERIMENTAL RESULTS

The proposed methodology has been implemented in a software package developed in Matlab. Both simulated and real data were used to test this methodology.

4.1 Simulated study case

For a better validation of the developed methodology, a simulated experimental case was established. In this

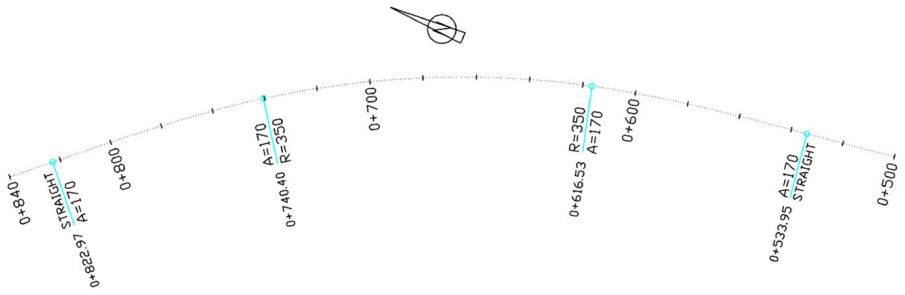

Fig. 6. Simulated study case: road axis that contains two straight lines, a circular curve ($R = 350$), and two clothoids ($A = 170$).

study case, a road axis was generated using topographical commercial software and used as an input for the algorithms to obtain the geometric design of the alignments. The dataset consists of a road section of 1,220 m that contains two straight lines, a circular arc, and two clothoids (Figure 6). This road axis was sampled with a spacing of 0.5 m, obtaining a centerline with 2,440 points. Random Gaussian noise was added to the planimetric coordinates (X, Y) with a standard deviation of 0.02 m.

According to Section 3.5, the first step of the simulation is to obtain the azimuth diagram. The azimuth diagram before and after antialiasing filtering is shown in Figure 7a. To improve readability, a close-up of the diagram is detailed in Figure 7b. Both Figures 7a and b show the smoothing of the Azimuth diagram after noise filtering.

Following, the curvature diagram is derived by using the filtered azimuth diagram and shown in Figure 7c. The geometric information of the road is obtained using this diagram in a more intuitive fashion, because the geometric elements are transformed into straight lines.

As mentioned in the methodology, the road axis is segmented and classified into the different road elements based on the curvature diagram of Figure 7c. Searching for the maximum value of the curvature histogram, a circular arc is matched with a curvature value of –0.1636°/m, and a circular radius of 350.26 m. These values are shown in Table 2 along with the rest of the road design elements' information.

Figure 8a shows the linear adjustment of the curvature values, used to classify the different geometric elements and to derive the fixed points of the clothoids. Although from Figure 8a at first sight it could seem that the linear adjustment fits very well along its curvature, several discrepancies remain between the linear adjustment and the curvature (Figure 8b). It is important to note that major discrepancies are coincident with

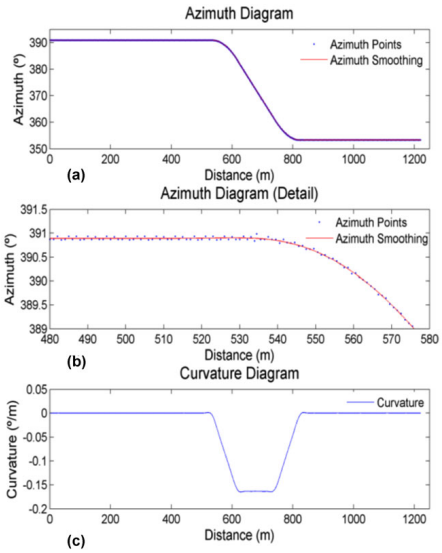

Fig. 7. (a) Azimuth diagram of the simulated road. (b) Details of the azimuth diagram and antialiasing filtering. (c) Curvature diagram of the simulated road.

the point fixes, due to the curvature associated to these areas.

Finally, the result of the different geometric design elements is shown in Table 2, which establishes an accuracy assessment based on a comparison with the ground truth provided by the simulated road axis. In particular, the lengths of the different geometric design elements (straight lines, circular arcs, and clothoids)

Table 2
Results of the geometric design elements of the simulated road (estimated) and its accuracy assessment (ground truth) in absolute (discrepancy) and relative (ε) terms

Geometric design parameters													
		Ground truth (m)			*Estimated (m)*			*Discrepancy (m)*			*ε (%)*		
ID	*Parameter*	*L*	*R*	*A*	*L*	*R*	*A*	*dL*	*dR*	*dA*	ε_L	ε_R	ε_A
1	Line	533.95	–	–	533.57	–	–	0.4, 1σ	–	–	0.1, 1σ	–	–
2	Clothoid (first)	82.57	–	170.00	83.35	–	170.87	–0.8, 1σ	–	–0.9, 1σ	–1.0, 1σ	–	–0.5, 1σ
3	Curve	123.88	350.00	–	123.05	350.26	–	0.8, 1σ	–0.3, 1σ	–	0.7, 1σ	–0.1, 1σ	–
4	Clothoid (last)	82.57	–	170.00	83.48	–	171.00	–0.9, 1σ	–	–1.0, 1σ	–1.1, 1σ	–	–0.6, 1σ
5	Line	397.03	–	–	396.54	–	–	0.5, 1σ	–	–	0.1, 1σ	–	–

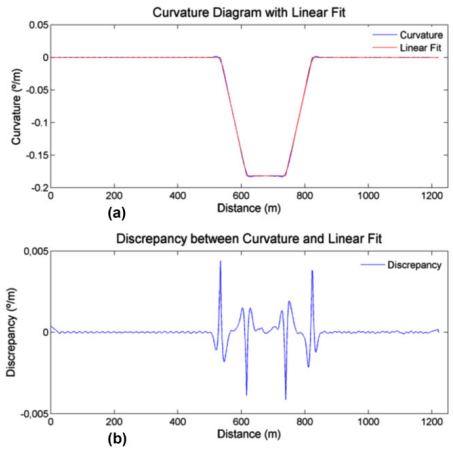

Fig. 8. (a) Curvature diagram obtained after the classification and linear adjustment of the different geometric elements along with the point fixes. (b) Discrepancy between curvature and linear fit.

together with the radius for circular curves, R, and the clothoid parameter, A, have been taken as the accuracy parameters. For a better assessment of the accuracy, the different geometric design elements are analyzed in relative terms through the relative error (ε).

According to the results outlined in Table 2, it can be stated that the algorithm identifies successfully the horizontal geometric elements. In particular, geometric design elements (straight lines, circular arcs, and clothoids) present a maximum variation in length of −0.9 m (–1.1%) corresponding to a clothoid, whereas the mean variation in length for the geometric design elements is of –0.2%. In the case of circular arcs radius, a maximum discrepancy of –0.3 m (–0.1%) is obtained. Similar values are obtained from the clothoids parameters with a maximum discrepancy of –1.0 (–0.6%).

4.2 Real study case: A-52 highway

A study case with real-world data was carried out in a road section belonging to the A-52 highway. The length of this road section is 3,210 m and it is located in the NW of Spain. The acquired point cloud contains 97.2 million points. Because of the massive nature of the initial data, a segmentation process is carried out using the scan-angle and intensity thresholds described in the workflow. The first segmentation consists of applying a threshold of 180 to the 12 bit-encoded intensity value.

As a result, the pavement markings of the road are represented by a total of 1 million points.

Finally, the second segmentation is performed to extract the road axis or centerline and is supported by scan angle thresholds between 307° and 340° because the study case is a dual carriageway and the road axis is located in the left pavement marking of the road. This segmentation is applied over the clustered left pavement marking of the road based on the angular threshold established, obtaining a point cloud of the road axis that is composed of only 361,809 points (Figure 9a). However, the result of these sequential segmentations provide the whole left pavement marking footprint with a resolution of 5 cm between profiles, containing 25 points per profile. Therefore, to work with the most probable value that defines the road axis, a mean filter is applied along the centerline (i.e., left pavement marking) (Figure 9b), obtaining a point cloud with a total of 10,252 points. This centerline is ready for computing the azimuth and curvature diagrams.

After the segmentation process, a total of 10,252 points are obtained for the extraction of the road axis.

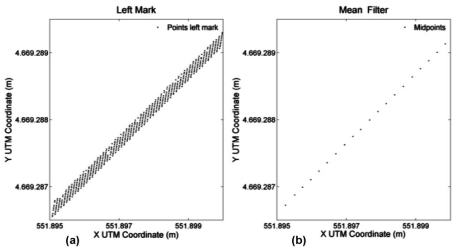

Fig. 9. (a) Road axis segmentation by the scan angle threshold. (b) Simplification of the road axis with the mean filter.

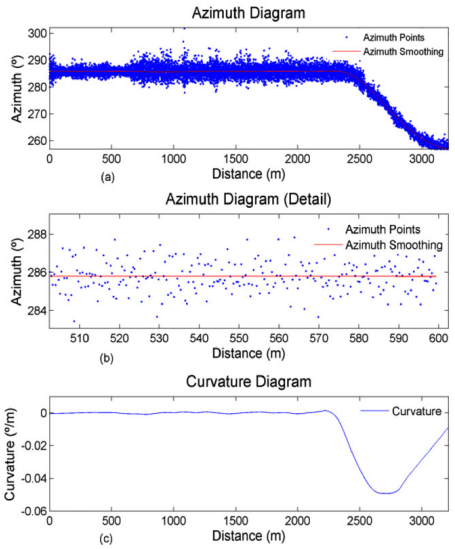

Fig. 10. (a) Azimuth diagram of the real data, A-52 highway. (b) Details of the azimuth diagram and antialiasing filtering. (c) Curvature diagram of the real data, A-52 highway.

Once the road axis or centerline points are segmented, the next step is to calculate the geometric design elements as explained in Section 3.5. First, the azimuth diagram is derived to have a first estimation of the design elements that define the road axis (Figure 10a). Figure 10b shows a close-up view of the antialiasing filtering. Taking into account Figures 10a and b, it should be noted that small variations in the alignment of

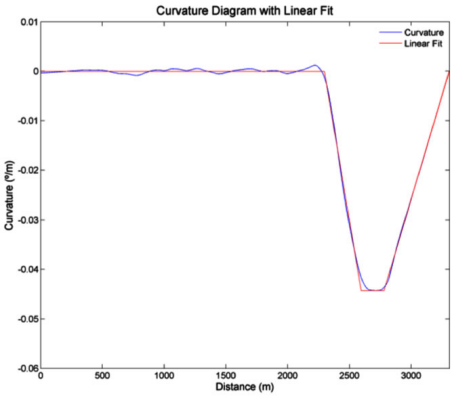

Fig. 11. Curvature diagram obtained after the classification and linear adjustment of the different geometric elements along with the singular points.

planimetric points, produce big differences in azimuth values due to azimuth computation. As a consequence, antialiasing filtering is mandatory.

After that, and based on the previous results, the second parameterization based on the curvature diagram is carried out. From this second parameterization, all the information of the road axis geometric design elements can be obtained (Figure 10c).

In particular, the curvature of the circular arc is obtained, –0.0443°/m, using the curvature histogram, in which the maximum value corresponds to the circular radius, 1,294 m. The rest of the curvature values based on the different geometric elements, such as the straight lines, circular arcs, and clothoids together with their points fixes, are determined (Figure 11). From Figure 11 it is showed that the linear adjustment does not fit well, because smaller variations in planimetric coordinates generate bigger variations in azimuth and curvature, especially in the point fixes areas.

Finally, the results of the geometric design elements are compared against a ground truth reference provided by an experienced topographer by road alignment software. Error values and comparison are outlined in Table 3.

According to the results showed in Table 3, it can be confirmed that the algorithm identifies successfully the horizontal alignment. In particular, geometric design elements (straight lines, circular arcs, and clothoids) present a maximum variation in length of 3.8 m (2.0%) corresponding to circular arcs, whereas the mean variation in length for geometric design elements is of

Table 3
Results of the geometric design elements of the A-52 highway (estimated) and its accuracy assessment (ground truth) in absolute (discrepancy) and relative (ε) terms

A-52 Highway: geometric design parameters													
		Ground truth (m)			*Estimated (m)*			*Discrepancy (m)*			*ε (%)*		
ID	*Parameter*	*L*	*R*	*A*	*L*	*R*	*A*	*dL*	*dR*	*dA*	ε_L	ε_R	ε_A
1	Line	2,300.00	–	–	2,296.86	–	–	3.1, 1σ	–	–	0.1, 1σ	–	–
2	Clothoid (first)	300.00	–	624.50	297.99	–	621.07	2.0, 1σ	–	3.4, 1σ	0.7, 1σ	–	0.6, 1σ
3	Curve	190.00	1,300.00	–	186.20	1,294.44	–	3.8, 1σ	5.6, 1σ	–	2.0, 1σ	0.4, 1σ	–
4	Clothoid (last)	525.00	–	826.14	526.82	–	825.79	–1.8, 1σ	–	0.4, 1σ	–0.4, 1σ	–	0.0, 1σ

1.8 m (0.6%). In the case of circular radius, a maximum discrepancy of 5.6 m (0.4%) is obtained. Similar values are obtained from the clothoids parameters with a maximum discrepancy of 3.4 (0.6%), whereas the mean discrepancy for clothoids parameters is of 1.9 (0.3%).

The final results were satisfactory for both study cases analyzed. In the real study case, larger errors are reached because the highway construction plans could not be located. Therefore, an experienced topographer had to adjust the geometric elements to the point cloud. These results are quite similar to the results obtained through the developed methodology. The simulated study case confirms that good results are achieved with the methodology developed in this article.

5 CONCLUSIONS

Efficient methods for extracting road axes and their topographical design elements from dense and huge point clouds acquired by MLS systems are crucial for transportation-related applications, road "as-built" plans, and even to provide road accident maps. In this article, a novel method for the semiautomatic extraction of the road axis together with the estimation of its horizontal alignment according to the Spanish official specifications has been developed. The proposed method utilizes the point clouds acquired by the MLS to successfully segment, filter, and parameterize the road axis in three types of geometric design elements: straight lines, circular arcs, and clothoids. In particular, the road axis is extracted and parameterized supported by a twofold approach:

1. First, the road centerline is extracted and modeled based on scan angle and intensity segmentations applied to the right and left pavement marking lines together with a filtering of the profiles acquired by the MLS based on the mean filter. This step requires extracting road lane markings for the estimation of road axis because several regional roads do not have a centerline. In addition, the user should manually adapt the scan angle threshold according with the type of road.
2. Second, the horizontal alignment of the road axis is parameterized based on azimuth and curvature parameters. Other approaches based on the least squares adjustment of circular arcs were unsuccessfully tested for the parameterization.

Based on the methodology and the experimental results it could be stated that an optimal method has been developed and validated for the extraction of the road horizontal alignment, guarantying good precision and without requiring a high computational cost. However, two main limitations, both related with the establishment of thresholds, arise from the road axis extraction: the first based on the angular threshold required for scanning angles; the second based on the intensity threshold needed for the detection of pavement marking lines. As a consequence, it should be remarked that the proposed approach is a first approximation tested only over simple and regional roads. It is not the scope of this article to provide a universal or commercial solution for any type of road.

Regarding future perspectives, the extraction of marking lines should be performed more robustly, that is, using adaptive thresholds and without a fixed range of incidence angles that depends on the trajectory followed by the vehicle. On the other hand, the georeferenced information captured by the MLS system could be integrated with other sensors such as a thermal camera, ground penetrating radar, and a profiler. In addition, additional information (signals, slopes, structures, tunnels, etc.) can be linked to the different design elements that define the road axis, offering a complete tool for road maintenance and quality control.

ACKNOWLEDGMENTS

The authors want to give thanks to Ministerio Ciencia e Innovación (Grant No. IPT-2012–1092–120000; INNPACTO program) for the financial support given. Furthermore, part of the human resources of this work has been supported by the European Regional Development Fund (FEDER) and the Spanish Centre for Technological and Industrial Development (Grant No. IDI-20101770; Human Resources programs BES-2010–034106 and IPP055 – EXP44).

REFERENCES

Cheng, W., Hassan, T., El-Sheimy, N. & Lavigne, M. (2008), Automatic road vector extraction for mobile mapping systems, *The International Archives of the Photogrammetry, Remote Sensing and Spatial Information Sciences*, **37**(Part B3b), 515–21.

Choi, S. & Sung, J. (2007), Data generalization algorithm for the extraction of road horizontal alignment design elements using the GPS/INS data. *Advances in Hybrid Information Technology*, Vol. 4413, Springer-Verlag, Berlin Heidelberg, 51–62.

Cleveland, W. S. & Devlin, S. J. (1988), Locally weighted regression: an approach to regression analysis by local fitting, *Journal of the American Statistical Association*, **83**(403), 596–610.

Cremean, L. B. & Murray, R. M. (2006), Model-based estimation of off-highway road geometry using single-axis ladar and inertial sensing, in *Proceedings of the IEEE International Conference on Robotics and Automation*, 2006, 1661–666.

Deshpande, S. S. (2013), Improved floodplain delineation method using high-density LiDAR data, *Computer-Aided Civil and Infrastructure Engineering*, **28**(1), 68–79.

Di Mascio, P., Di Vito, M., Loprencipe, G. & Ragnoli, A. (2012), Procedure to determine the geometry of road alignment using GPS data, *Procedia-Social and Behavioral Sciences*, **53**, 1203–16.

Foucher, P., Sebsadji, Y., Tarel, J. P., Charbonnier, P. & Nicolle, P. (2011), Detection and recognition of urban road markings using images, *Proceedings of the 14th International IEEE Conference on Intelligent Transportation Systems*, 1747–52.

Frank, D. (1996), Road markings recognition, in *Proceedings of the International Conference on Image Processing*, 1996, 1669–672.

Gikas, V. & Stratakos, J. (2012), A novel geodetic engineering method for accurate and automated road/railway centerline geometry extraction based on the bearing diagram and fractal behavior, *IEEE Transactions on Intelligent Transportation Systems*, **13**(1), 115–26.

GIM International (2013), Mobile mapping to create road map of Brazil. Available at: http://www.gim-internationalcom/news/id7510-Mobile_Mapping_to_Create_Road_Map_of_Brazil.html, accessed July 26, 2013.

Guan, H., Li, J., Yu, Y., Wang, Ch., Chapman, M. & Yang, B. (2014), Using mobile laser scanning data for automated extraction of road markings, *ISPRS Journal of Photogrammetry and Remote Sensing*, **87**(1), 93–107.

Ishikawa, K., Amano, Y., Hashizume, T., Takiguchi, J. & Kajiwara, N. (2007), A mobile mapping system for precise road line localization using a single camera and 3D road model, *Journal of Robotics and Mechatronics*, **19**(2), 174–80.

Jiménez, F., Aparicio, F. & Estrada, G. (2009), Measurement uncertainty determination and curve-fitting algorithms for development of accurate digital maps for advanced driver assistance systems, *Transportation Research Part C: Emerging Technologies*, **17**(3), 225–39.

Karamanou, A., Papazissi, K., Paradissis, D. & Psarianos, B. (2010), Precise estimation of road horizontal and vertical geometric features using mobile mapping techniques, *Boletim De Ciências Geodésicas*, **15**(5), 762–75.

Lakakis, K., Savvaidis, P. & Wunderlich, T. (2013), Evaluation of a low-cost mobile mapping and inspection system for road safety classification, *American Journal of Geographic Information System*, **2**(1), 6–14.

Lorenzo, H., Rial, F. I., Pereira, M. & Solla, M. (2011), A full non-metallic trailer for GPR road surveys, *Journal of Applied Geophysics*, **75** (2011), 490–97.

Mikhail, E. M. & Ackermann, F. E. (1976), Observations and Least Squares, IEP-Dun-Donnelley, Harper and Row, New York, p. 497.

Ministerio de Fomento (2000), Instrucción de carreteras. norma 3.1 – I.C.: Trazado. Boletín Oficial Del Estado, Número 28, De 2 De Febrero De 2000, Madrid.

Moreno, F. A., Gonzalez-Jimenez, J., Blanco, J. L. & Esteban, A. (2013), An instrumented vehicle for efficient and accurate 3D mapping of roads, *Computer-Aided Civil and Infrastructure Engineering*, **28**(6), 403–19.

Nedevschi, S., Schmidt, R., Graf, T., Danescu, R., Frentiu, D., Marita, T., Oniga, F. & Pocol, C. (2004), 3D lane detection system based on stereovision, in *Proceedings of the 7th International IEEE Conference on Intelligent Transportation Systems*, 161–66.

Park, H. S., Lee, H. M., Adeli, H. & Lee, I. (2007), A new approach for health monitoring of structures: terrestrial laser scanning, *Computer-Aided Civil and Infrastructure Engineering*, **22**(1), 19–30.

Puente, I., González-Jorge, H., Martínez-Sánchez, J. & Arias, P. (2013), Review of mobile mapping and surveying technologies, *Measurement*, **46**(7), 2127–45.

Puente, I., González-Jorge, H., Riveiro, B. & Arias, P. (2012), Accuracy verification of the Lynx mobile mapper system, *Optics & Laser Technology*, **45**, 578–86.

Saarenketo, T. & Scullion, T. (2000), Road evaluation with ground penetrating radar, *Journal of Applied Geophysics*, **43**, 119–138.

Soheilian, B., Paparoditis, N. & Boldo, D. (2010), 3D road marking reconstruction from street-level calibrated stereo pairs, *ISPRS Journal of Photogrammetry and Remote Sensing*, **65**(4), 347–59.

Stratakos, J., Gikas, V. & Fragos, K. (2009), A multi-scale curve matching technique for the assessment of road alignments using GPS/INS data, *6th International Symposium on Mobile Mapping Technology*, Sao Paolo, Brazil, July 21–24.

Tao, C. V. (2000), Mobile mapping technology for road network data acquisition, *Journal of Geospatial Engineering*, **2**(2), 1–14.

Toth, C. & Grejner-Brzezinska, D. (2004), Redefining the paradigm of modern mobile mapping: an automated

high-precision road centerline mapping system, *Photogrammetric Engineering and Remote Sensing*, **70**(6), 685–94.

Truong-Hong, L., Laefer, D. F., Hinks, T. & Carr, H. (2013), Combining an angle criterion with voxelization and the flying voxel method in reconstructing building models from LiDAR data, *Computer-Aided Civil and Infrastructure Engineering*, **28**(2), 112–29.

Tsai, Y. and Wu, J. (2010), Horizontal roadway curvature computation algorithm using vision technology, *Computer-Aided Civil and Infrastructure Engineering*, **25**(2), 78–88.

Tsai, Y. J., Ai, C., Wang, Z. & Pitts, E. (2013), A mobile cross slope measurement method using LiDAR technology 2, *Technology*, **2**(3), 53–59.

Yang, B., Fang, L. & Li, J. (2013), Semi-automated extraction and delineation of 3D roads of street scene from mobile laser scanning point clouds, *ISPRS Journal of Photogrammetry and Remote Sensing*, **79**, 80–93.

3.2. An automated approach to vertical road characterisation using mobile LiDAR systems: Longitudinal profiles and cross-sections

Resumen: Las características de los perfiles longitudinales y transversales de las carreteras son importantes para verificar si hay errores en la construcción de las mismas e incluso en la prevención de accidentes de tráfico. El objetivo de este trabajo es la automatización en la extracción del trazado vertical asociado a las carreteras mediante el procesamiento automático de nubes de puntos capturadas por un sistema LiDAR móvil (MLS). Dado el carácter masivo y complejo de los propios datos capturados por el sistema, se ha implementado una estrategia jerárquica sustentada en procesos de segmentación, regresión ortogonal a través del análisis de componentes principales (PCA), parametrización y filtrado que nos permite determinar los elementos geométricos que mejor definen su trazado vertical tanto en la dirección longitudinal (rasantes y acuerdos verticales), como transversal (peraltes). El proceso desarrollado ha sido validado con datos reales arrojando unas precisiones relativas del 3.5% en el escenario analizado, siendo un método útil para automatizar de forma precisa las características geométricas asociadas al trazado vertical de la carretera.

Palabras clave: sistema de cartografía móvil; sistema LiDAR móvil; información geo-espacial; escaneado láser; mantenimiento de carreteras; inventarios de carretera; trazado vertical; segmentación; filtrado; parametrización; extracción de características.

ISPRS Journal of Photogrammetry and Remote Sensing 96 (2014) 28–37

Contents lists available at ScienceDirect

ISPRS Journal of Photogrammetry and Remote Sensing

journal homepage: www.elsevier.com/locate/isprsjprs

An automated approach to vertical road characterisation using mobile LiDAR systems: Longitudinal profiles and cross-sections

Alberto Holgado-Barco [a], Diego Gonzalez-Aguilera [a,*], Pedro Arias-Sanchez [b], Joaquín Martinez-Sanchez [b]

[a] Department of Cartographic and Land Engineering, University of Salamanca, Higher Polytechnic School of Avila, Hornos Caleros 50, 05003 Avila, Spain
[b] Department of Natural Resources & Environmental Engineering, University of Vigo, School of Mining Engineering, Maxwell s/n, 36310 Vigo, Spain

ARTICLE INFO

Article history:
Received 9 February 2014
Received in revised form 28 June 2014
Accepted 30 June 2014
Available online 24 July 2014

Keywords:
Mobile mapping system
Mobile LiDAR system
Geospatial information
Laser surveying
Road maintenance
Road inventories
Vertical alignment
Segmentation
Filtering
Parameterisation
Feature extraction

ABSTRACT

The characterisation the vertical profiles and cross-sections of roads is important for the verification of proper construction and road safety assessment. The goal of this paper is the extraction of geometric parameters through the automatic processing of mobile LiDAR system (MLS) point clouds. Massive and complex datasets provided by the MLS are processed using a hierarchical strategy that includes segmentation, principal component analysis (PCA)-based orthogonal regression, filtering and parameter extraction procedures. Best-fit geometric parameters act as a vertical road model for both linear parameters (slope and vertical curves) and cross-sections (superelevations). The proposed automatic processing approach gives satisfactory results for the analysed scenario.

1. Introduction

The availability of a detailed digital cartography for road geometry is of great importance when working with topographic applications centred on road characterisation for engineering purposes such as route modifications (i.e., lane additions). In the same way, the analysis of digital road maps can enhance road-safety verification, the identification of potentially dangerous points or black-spot localisation and the influence of road conditions on accident forensics (Gomes, 2013).

The literature contains numerous examples of the use of road planning for road-safety-based modification. Sentouh et al. (2006) conducted a road speed analysis for accident prevention. In this work, the vehicle, driver and infrastructure were modelled to obtain the maximal speed in curve, and the infrastructure characteristics included both the horizontal and vertical geometric information. Taylor et al. (2007) proposed a speed model based on artificial neural networks for road-safety analysis. The inputs to the model included horizontal and vertical road alignment. The European project SAFESTAR-Safety Standards for Road Design and Redesign (Institute for Road Safety Research, 2002) attached great importance to the knowledge of road layouts, assessing the safety of road infrastructure during road planning and design.

Applying mobile LiDAR systems (MLS) to road surveying is straightforward and allows for a wide range of possible applications. Gräfe (2008) presented a capture system that allows a surface model to be obtained for the planning and design of roads. Ai and Tsai (2012) presented and assessed an automated method for traffic sign detection using LiDAR point clouds. El-Halawany and Lichti (2011) proposed a pipeline for road pole detection through MLS processing. This method is based on the eigenvalue analysis of the covariance matrix in a local neighbourhood. Yang et al. (2012) presented an approach to automated road-marking extraction based on a hierarchical segmentation methodology using point-intensity and point-height thresholds, followed by a knowledge-based extraction. Wang et al. (2013) focused on obtaining data of interest on excavation volume extraction for road construction through MLS data processing.

The automatic extraction of road layouts from MLS makes possible the availability of detailed digital road maps that contain precise information on widely used geometric parameters, both

* Corresponding author.
E-mail address: daguilera@usal.es (D. Gonzalez-Aguilera).

http://dx.doi.org/10.1016/j.isprsjprs.2014.06.017
0924-2716/

horizontal (straight lines, circular curves and clothoids) and vertical (slope, vertical curves and superelevations). A number of authors recently employed mobile mapping systems (MMS) to derive precise information on horizontal and vertical road parameters. Karamanou et al. (2010) proposed the use of a survey based on the geodetic positioning of a suitably equipped vehicle moving along the road in a two-way journey. The acquired data were used to extract the road's centreline. The parameters of the road's horizontal and vertical features were then estimated based on a least squares adjustment of the characteristic curves. Di Mascio et al. (2012) presented a procedure to determine the geometry of horizontal and vertical road alignment using a global navigation satellite system's (GNSS) dynamic measurements. Two datasets were logged for a single carriageway, one for each traffic direction, and the centreline was estimated as the middle point between both trajectories. Another algorithm was then applied to recognise the horizontal and vertical road elements through least squares optimisation. Gikas and Stratakos (2012) proposed a method, based on the trajectory captured by a GNSS, for deriving curvature diagrams and analysing the horizontal geometric elements of a road/railway. Lakakis et al. (2013) developed a low-cost system supported only by two GNSS sensors that could obtain the vertical alignment of a road. Again, a two-way journey was required to survey the road. Tsai et al. (2013) presented a method based on MLS acquisition, but focused only on the computation of superelevations. More recently, (Holgado-Barco et al., 2014) proposed a method for the extraction of horizontal geometric road alignments based on MLS processing. This method was followed by an assessment of the obtained road alignment using official ground-truth data.

One of the main disadvantages of these studies is that results analysis and comparison are usually non-quantitative due to the lack of a comparative ground-truth. Among the studies that provide a vertical road analysis, their analysis is usually limited to the vehicle lane, extracting cross-section slopes with no linear slope extraction. In addition, those approaches based only on GNSS measurements require a two-way journey, whereas the studies performed with a MLS do not provide a complete vertical alignment analysis. Within this context, this paper presents a workflow for the automatic extraction of geometric vertical road parameters through MLS data processing, distinguishing linear (i.e., slopes and vertical curves) and cross-sectional (i.e., superelevations) parameters. Finally, the parameters are created according to Spanish road regulations and their absolute and relative errors are estimated to evaluate the method's accuracy.

In Section 2, the materials and methods used in the study are explained, emphasising segmentation, principal component analysis (PCA)-based orthogonal regression, setup and filtering. Section 3 provides the experimental results obtained using a dataset, while the last section describes the conclusions drawn from this work and future research suggestions.

2. Materials and methods

2.1. Capture system: Optech LYNX MMS

The capture system used in this work is a LYNX Mobile Mapper manufactured by Optech (Optech, 2013) (see Fig. 1). This system is composed of two LiDAR sensors, four RGB cameras, and an Applanix POS LV 520 IMU. The system is configured to take 500,000 points per second with a scan frequency of 200 Hz. The maximum range of the sensors is 200 m, with a precision of 8 mm (one sigma) and permission to obtain up to 4 echoes of the signal and the intensity reflected by the objects at a 1550 nm wavelength (Puente et al., 2012). These and other characteristics are listed in Table 1.

Fig. 1. The Optech LYNX Mobile Mapper.

Table 1
Technical characteristics of Optech LYNX Mobile Mapper.

Technical features	LYNX Mobile Mapper
X, *Y* position	0.020 m
Z position	0.050 m
Roll and pitch	0.005°
True heading	0.015°
Measuring principle	Time of flight (TOF)
Maximum range	200 m
Range precision	8 mm, 1σ
Range accuracy	±10 mm, (1σ)
Laser measurement rate	75–500 kHz
Measurement per laser pulse	Up to 4 simultaneous
Scan frequency	80–200 Hz
Laser wavelength	1550 nm (near infrared)
Scanner field of view	360°
Operating temperature	10°–40 °C
Angular resolution	0.001°

2.2. Methodology overview

The proposed methodology is carried out in four steps (see Fig. 2). The first step is data capture through MLS, and the following processing steps are focused on segmentation, plane adjustment and point cloud parameter extraction. Specifically, the goal of the segmentation is to simplify the point cloud to extract a road platform and provide cross-sections along with the trajectory. Next, a process for creating a best-fit plane is performed using PCA. This plane adjustment of the road allows the geometric parameters of the vertical and cross-sections to be extracted, accounting for slope and superelevation diagrams. More precisely, these geometric parameters are obtained from the eigenvalues and eigenvectors computed with the PCA. Due to the presence of gross and accidental errors in the input data and the parameter extraction, data filtering and processing are needed. A prototype of the process is fully developed in MatLab, due mainly to its ease of use in testing algorithms and obtaining research results, the goal being to extrapolate the developed approach to a powerful point cloud library (PCL) and an open source C++ library. The main advantage of using PCL is that many of its functions are parallelised and thus improve the software's performance.

2.3. Point cloud segmentation

The input point cloud provided by the MLS is segmented in a two-step approach. The first segmentation phase is achieved by setting angular thresholds in a road function with user interaction

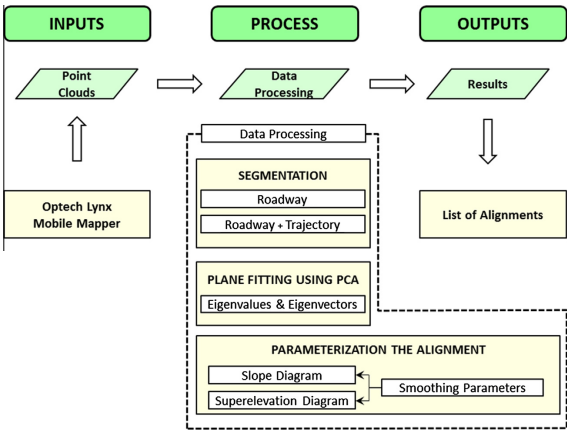

Fig. 2. Workflow of the developed processing.

and the second phase based on the generation of the road's cross-sections.

The goal of the first segmentation phase is to set the angular thresholds and produce a rough calculation of the road platform. Noting that the laser heads consist of a laser distance meter that is deflected by a mirror to create 2D sections, we can define a polar local coordinate system centred in each laser (see Fig. 3). During the first segmentation phase, this local coordinate system is used to set the minimum and maximum values for the angular coordinate. In our case, for highways that obey the Spanish Road Rules, minimum and maximum values of 196° and 336° are derived when the MLS is travelling in the right lane. These values should be refined for different road types or rules.

Once the platform segmentation is completed, the next step consists of generating 1 m long cross-sections, with respect to the MLS travelling route, that contain approximately 8800 points. The cross-sections are obtained using the trajectory of the MLS as a reference based on the *XY* coordinates and the azimuth of 1 m spaced points. Two anchor points are computed from these reference points on the trajectory using Eq. (1):

$$\begin{aligned} x &= x_0 + r \cdot \cos\theta \\ y &= y_0 + r \cdot \sin\theta \end{aligned} \tag{1}$$

where x and y are the coordinates of the anchor points, x_0 and y_0 are the coordinates of the reference point on the trajectory, r is the distance between the trajectory and the road platform's extreme points and θ is the direction orthogonal to the trajectory. These auxiliary anchor points are used for segmentation (see Fig. 4).

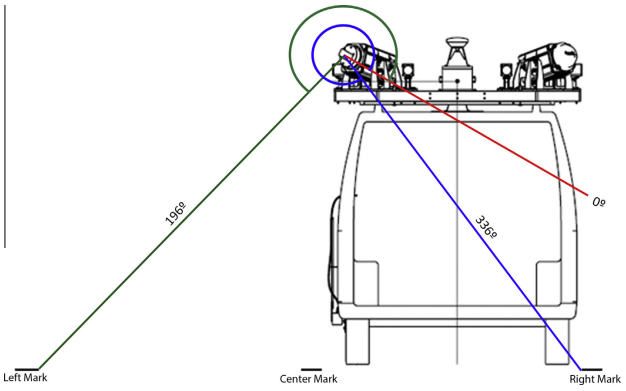

Fig. 3. Angular segmentation angles for road platform determination.

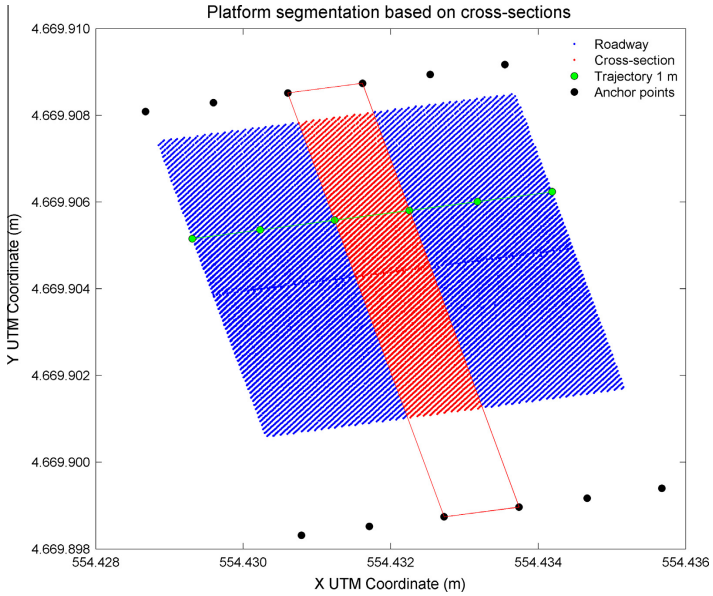

Fig. 4. Platform segmentation based on 1 m-long sections. Selected points are highlighted in red. The width of the cross-sections equals the width of the road platform, which is 7 m in our case. (For interpretation of the references to colour in this figure legend, the reader is referred to the web version of this article.)

2.4. Slope and superelevation computation using PCA

After the angular and cross-section segmentation is applied, selected points belonging to rectangular regions between the anchor points are processed for plane adjustment using PCA. The plane adjustment, based on a covariance matrix, allows for computation of the slope and superelevation (Belton and Lichti, 2006; Pauly et al., 2002) using the eigenvalues and eigenvectors corresponding to each cross-section.

By using PCA, a linear transformation to a new coordinate system is achieved to reduce the dimensionality of the original dataset (Jolliffe, 2002). The basis vectors of this new coordinate system are given by the principal components in the data. The first step in the PCA is to obtain the covariance matrix, which is described by Eq. (2):

$$\Sigma = COV(X) = \begin{bmatrix} \sigma_x^2 & \sigma_{xy} & \sigma_{xz} \\ \sigma_{xy} & \sigma_y^2 & \sigma_{yz} \\ \sigma_{xz} & \sigma_{yz} & \sigma_z^2 \end{bmatrix} \quad (2)$$

where σ_x^2 and σ_{xy} represent the variance and covariance, respectively:

$$\sigma_x^2 = \mathrm{var}(x) = E(x^2) - E(x)^2 = \frac{1}{k}\sum_{i=1}^{k}(x_i - \bar{x})^2 \quad (3)$$

$$\sigma_{xy} = \mathrm{cov}(x,y) = E(xy) - E(x)E(y) = \frac{1}{k}\sum_{i=1}^{k}(x_i - \bar{x})(y_i - \bar{y}) \quad (4)$$

x_i, y_i and z_i are the coordinates of the segmented points, k is the number of points in the original dataset and $\bar{x}, \bar{y}$ are the data centroid coordinates.

The next step involves the calculation of the eigenvalues and eigenvectors of this matrix. The eigenvalues can be derived from Eq. (5):

$$|\Sigma - \lambda \cdot I| = 0 \quad (5)$$

Given that Σ is a symmetric matrix, its corresponding eigenvectors form a basis of the vector space and obey Eq. (6):

$$\Sigma \cdot v = \lambda \cdot v \quad (6)$$

where Σ is the covariance matrix and v are the eigenvectors ($v_0 v_1 v_2$) associated with the eigenvalues λ ($\lambda_0 \lambda_1 \lambda_2$). The transformation from the original vector basis to this new basis is the linear transformation that reduces the dataset dimensionality.

Three eigenvalues and eigenvectors of the matrix are obtained using PCA. These values contain geometric information that is suitable for geometric characterisation of the road's vertical profile. Specifically, the eigenvector, v_0, corresponding to the smallest eigenvalue, λ_0, contains information about the adjusted normal plane, while the eigenvalues λ_1 and λ_2 and the corresponding eigenvectors v_1 and v_2 contain information about the slope (longitudinal) and superelevation (transversal). Fig. 5 shows the correspondence between the eigenvectors and eigenvalues and the road's geometric parameters. In the end, the percentage slope and superelevation are computed using Eq. (7) as a function of the corresponding eigenvector:

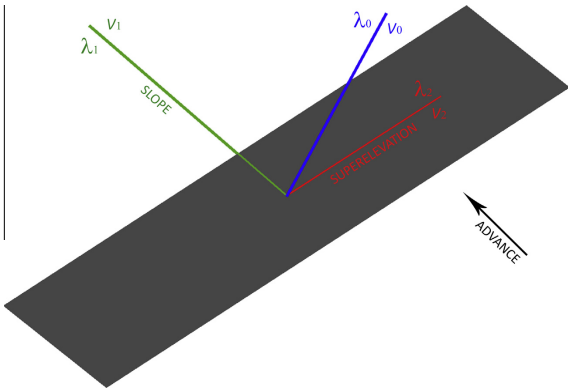

Fig. 5. Drawing showing the correspondence between PCA-based eigenvalues and eigenvectors with vertical geometric parameters of the road.

$$\text{Inclination } (\%) = \frac{v_z}{\sqrt{v_x^2 + v_y^2}} \cdot 100 \quad (7)$$

where v_x, v_y and v_z are the coordinates of each eigenvector.

2.5. Slope and superelevation smoothness filtering and geometric characterisation

Once the slope and superelevation are computed, a graphical parameterisation is implemented to improve the readability of the data. Graphical diagrams are commonly used as an accurate and detailed topographical representation of a road's vertical parameters.

Regarding the slope of the road, these vertical parameters are characterised in two ways, through vertical curves and slopes. In the first case, the slopes are drawn as straight lines that possess the same slope as the road, and the vertical agreement is modelled as a parabola. In the second case, the slope diagram consists of horizontal slope lines with straight vertical agreements. These two approaches are depicted in Fig. 6.

A relationship exists between a road's superelevation and its horizontal profile. Fig. 7 shows a graphical diagram of this relationship. The straight sections in the horizontal alignment correspond to normal crown zones in the superelevation diagram, whereas the circular arcs are related to the full superelevation that counteracts centrifuge. These sections are both depicted as horizontal lines in the superelevation diagram. The superelevation transition sections corresponding to clothoid arc alignments are modelled as lines with the slope in the superelevation diagram, adapting the road's superelevation.

At this point, it should be noted that the results will yield noisy values due primarily to accidental errors by the MLS and the noise added by the parameterisation process itself. A smoothing filter is applied to the diagrams to reduce these errors, and consists of locally weighted scatterplot smoothing (LOWESS). The anti-aliasing filtering used is a locally weighted regression curve (Cleveland, 1979; Cleveland and Devlin, 1988) based on the local adjustment of polynomial models that are joined in a subsequent step. The observations' weights in the adjustment are modified by accounting for their distance from the model (Eq. (8)):

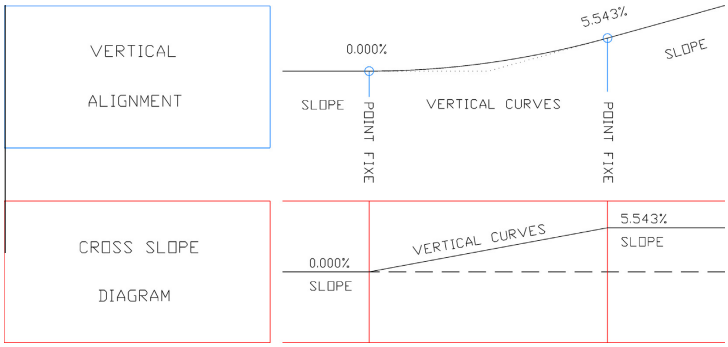

Fig. 6. Road parameterisation example taking into account the slope diagram. Road vertical alignment (top) and slope diagram parameterisation (bottom).

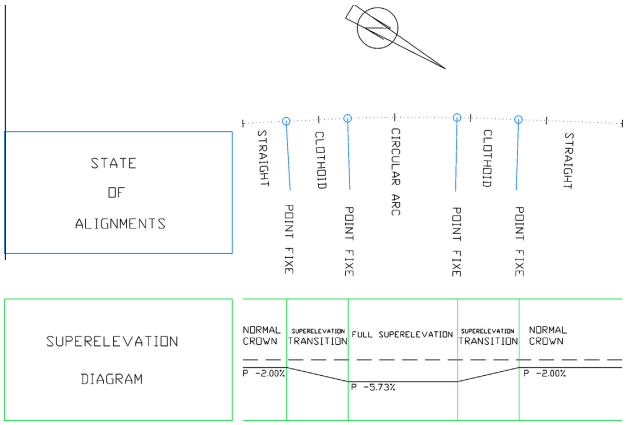

Fig. 7. Parameterisation of a road regarding cross-section slopes. Related floor plan of the road (top) and superelevation diagram (bottom) are shown in the diagram.

$$\omega_i = \left(1 - \left|\frac{x - x_i}{d(x)}\right|^3\right)^3 \tag{8}$$

where x is the predictor value associated with the response value to be smoothed, x_i are the nearest neighbours of x, and $d(x)$ is the distance along the abscissa from x to the most distant predictor value.

After applying the anti-aliasing filter to both the slope and superelevation values, the data are suitable for a classification in terms of the road's vertical geometric parameters.

Given that the road is segmented into equally spaced sections, the classification sections are distinguishable through histogram inspection. In fact, the histogram maxima correspond to a constant slope (slope diagram) as normal crown zones and full superelevation (superelevation diagram). Once the constant sections are classified, the joining sections must be modelled in both the slope and superelevation diagrams. These sections act as a connection of the constant zones in the diagrams and are modelled using least-square linear regression (Toutenburg, 2008) of the variable of interest using Eqs. (9)–(11):

$$y = \beta_1 + \beta_2 \cdot x + \varepsilon \tag{9}$$

$$y = \begin{bmatrix} p_1 \\ p_2 \\ \vdots \\ p_n \end{bmatrix} \quad x = \begin{bmatrix} 1 & s_1 \\ 1 & s_2 \\ \vdots & \vdots \\ 1 & s_n \end{bmatrix} \quad \beta = \begin{bmatrix} \beta_1 \\ \beta_2 \end{bmatrix} \quad \varepsilon = \begin{bmatrix} \varepsilon_1 \\ \varepsilon_2 \\ \vdots \\ \varepsilon_n \end{bmatrix} \tag{10}$$

$$\begin{bmatrix} p_1 \\ p_2 \\ \vdots \\ p_n \end{bmatrix} = \begin{bmatrix} 1 & s_1 \\ 1 & s_2 \\ \vdots & \vdots \\ 1 & s_n \end{bmatrix} \cdot \begin{bmatrix} \beta_1 \\ \beta_2 \end{bmatrix} + \begin{bmatrix} \varepsilon_1 \\ \varepsilon_2 \\ \vdots \\ \varepsilon_n \end{bmatrix} \tag{11}$$

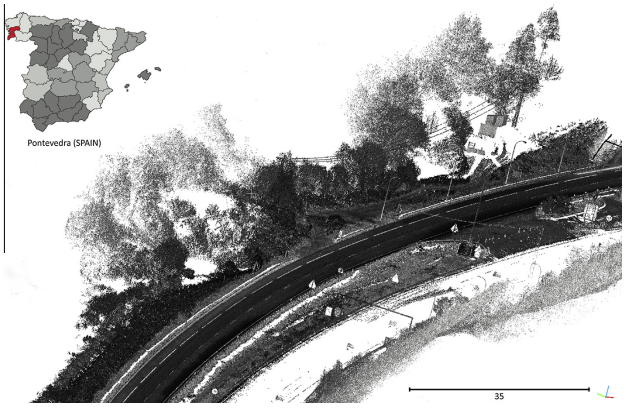

Fig. 8. Raw point cloud captured by LYNX Mobile Mapper on A-52 highway, in NW Spain.

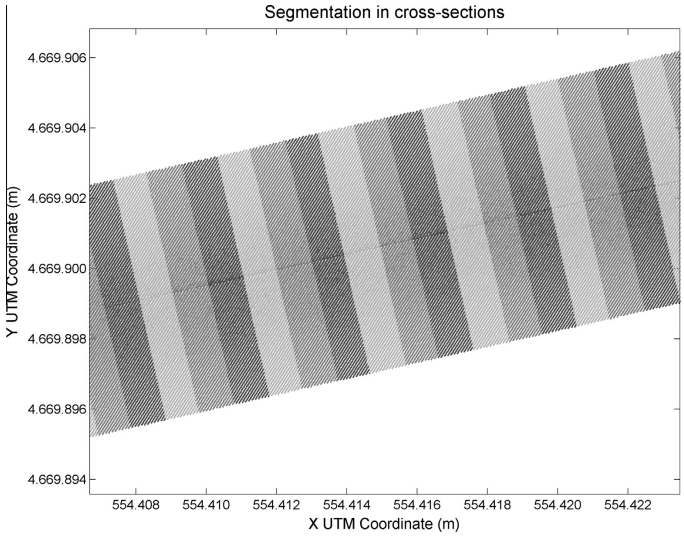

Fig. 9. Segmentation of the platform in cross-sections.

Table 2
Segmentation summary.

Segmentation	Points	Percentage (%)
Raw point cloud	97,214,162	100
Road platform point cloud	33,054,744	34
Cross-section (3747) points	8820	0.009

where p is the variable of interest (slope or superelevation, respectively), s is the distance between points, β_1 and β_2 are the parameters of the line and ε are the errors of the points.

When the diagrams are classified through histogram processing and linear adjustment, point fixes are extracted from the intersection of these lines and the horizontal lines in the diagram. Point fixes are the points where constant horizontal lines and transition straight lines meet (Figs. 6, 7 and 11). Other geometric characteristics of the road, such as section lengths, percentage slope and slope variation, can be calculated using these point fixes.

The sections and parameters obtained from this process are suitable for storage in a database that complies with the Spanish Official Road Rules regarding a road's route and geometric characteristics.

3. Experimental results

To test the developed methodology, a dataset is captured from the Spanish highway A-52 between marker posts 278/500 and 282/250. The point cloud obtained by the system is captured with a scanning frequency of 500,000 points per second and generated 97.2 million data points (Fig. 8).

Given the massive amount of input data, a segmentation is performed using angular thresholds and PCA-based adjustment, as described in the previous section (Fig. 2).

As a result, two angle thresholds between 196° and 336° are set. These values permit the road platform to be segmented, for a total of 33 million points. This segmentation is performed for the entire dataset because the case study consists of a highway where the superelevation is equal in all of the lanes.

Finally, the second segmentation provides 1 m spaced cross-sections along the MLS trajectory. These profiles are obtained based on the trajectory of the vehicle, as detailed in Section 2.3. 3747 Cross-sections are obtained in the case study and are 7 m wide, corresponding to the width of the platform. Each of the resulting rectangular areas comprises approximately 8800 points (Fig. 9).

As a summary of the segmentation process, Table 2 shows the number of points used for calculation and the reduction in the numbers of points needing processing in a row.

After segmentation is finished, a PCA-based adjustment is performed, supported by points belonging to the cross-sections. A sequence of planes along the trajectory is obtained as a result, which are processed to estimate the road slope and superelevation. As explained in Section 2.4, we perform the estimation using the covariance method. By using the covariance matrix's three eigenvalues and their corresponding eigenvectors, a vertical road alignment is computed for each of the 3747 cross-sections, and this is the number of vector sets defining the slope (v1) and the superelevation (v2) (Fig. 5). These vectors are used to compute a percentage parameter value.

Once the calculations of both the slope and superelevation are completed, we differentiate the geometric elements, as explained in Section 2.5. First, we obtain graphical diagrams for both the slope and superelevation (Fig. 10). Further analysis permits the sections in the diagrams to be differentiated and the data smoothing to be performed through LOWESS.

The different geometric elements are classified based on these graphical diagrams. The geometric parameters of interest are constant slopes and vertical curves (slope diagram) and normal crown zones and superelevation transitions and full superelevation

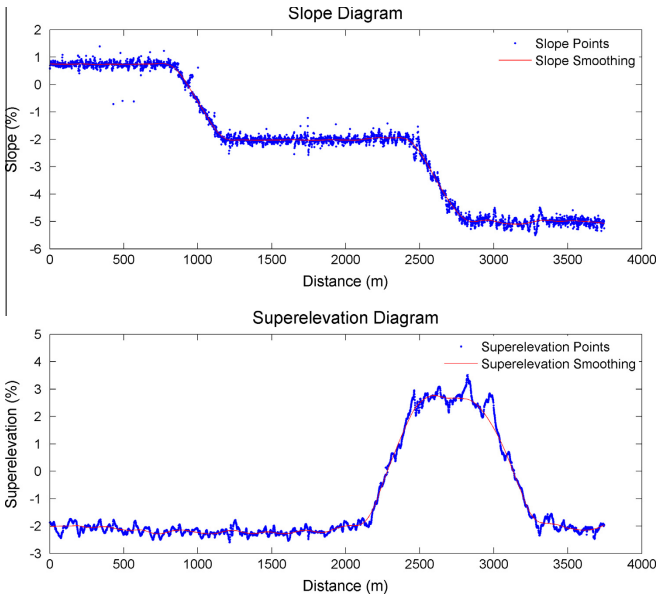

Fig. 10. Slope diagram (top) and superelevation diagram (bottom).

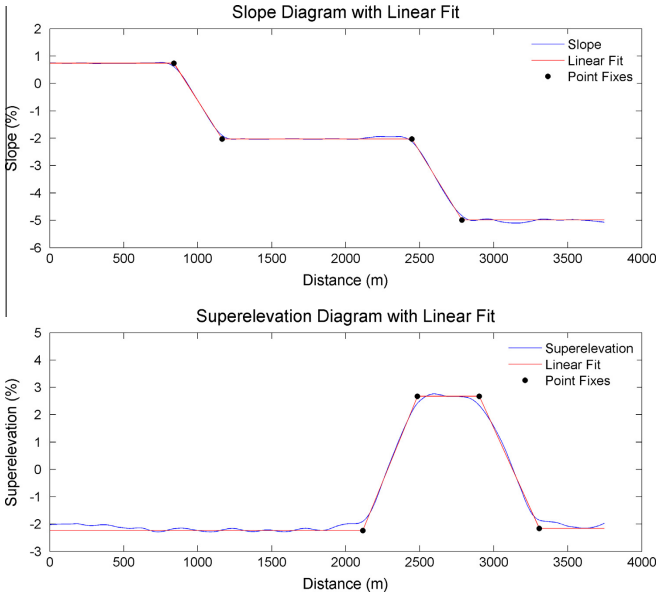

Fig. 11. Graphical diagrams after classification and linear adjustment of geometric elements and fixed points of: slope diagram and (top) superelevation diagram (bottom).

Table 3
Results compared to official data for geometric slope parameters.

Ground truth values		Calculated values (PCA)		Differences			Error (%)		
Length (m)	Slope (%)	Length (m)	Slope (%)	PK's	Slope	Length	PK's	Slope	Length
Slope extraction from A-52 highway									
0.000	0.717	0.000	0.741	0.000	−0.024	4.775	0.000	3.287	−0.566
843.049	0.717	838.274	0.741	4.775	−0.024	−4.396	−0.566	3.287	1.364
1165.458	−2.083	1165.080	−2.029	0.379	−0.054	0.252	−0.032	−2.572	−0.020
2447.267	−2.083	2446.636	−2.029	0.630	−0.054	−3.629	−0.026	−2.572	1.086
2781.375	−5.083	2784.374	−4.989	−2.999	−0.094	2.999	0.108	−1.841	−0.311
3746.028	−5.083	3746.028	−4.989	0.000	−0.094	–	0.000	−1.841	–

Table 4
Results compared to official data for geometric superelevation parameters.

Ground truth values		Calculated values (PCA)		Differences			Error (%)		
Length (m)	Super-elevation (%)	Length (m)	Super-elevation (%)	PK's	Super-elevation	Length	PK's	Super-elevation	Length
Superelevation extraction on A-52 highway									
0.000	−2.292	0.000	−2.238	0.000	−0.054	−1.138	0.000	−2.340	0.054
2113.139	−2.292	2114.277	−2.238	−1.138	−0.054	1.493	0.054	−2.340	−0.403
2483.902	2.768	2483.547	2.672	0.355	0.096	−0.263	−0.014	−3.482	0.063
2901.997	2.768	2901.905	2.672	0.092	0.096	−2.186	−0.003	−3.482	0.543
3304.788	−2.132	3306.881	−2.158	−2.093	0.026	2.093	0.063	1.238	−0.474
3746.028	−2.132	3746.028	−2.158	0.000	0.026	–	0.000	1.238	–

(superelevation diagram). The constant values (slope, normal crown and full superelevation) are obtained from the histogram of alignment, in which the maximum values correspond to these elements. Once the values are classified based on the histograms, we can determine inflection points by the intersection of constant values with linear fit slopes and superelevations belonging to the vertical curves and superelevation transitions, respectively (Fig. 11).

The results of the obtained slope's geometric elements are shown in Table 3, while the geometric elements of the superelevation are shown in Table 4. In both cases, the results are compared to the ground truth values provided by the Spanish Ministry of Development.

Analysing the data in Table 3, we can see the differences in both quantitative value and percentage, resulting in a maximum length difference of 4.775 m for the first slope and a maximum slope difference of −0.094%. The mean difference in the slope results is −0.06%. Regarding the relative errors in percentage, the biggest obtained mistake is 3.3%, while the average percentage relative error was −0.38%. These error values show that the developed methodology offers satisfactory results.

Analysing the data in Table 4, we can see a differences in both quantitative value and percentage. The maximum length difference is −2.186 m for the second superelevation transition, a percentage of 0.096%. The mean difference in the superelevation values is 0.03%. In terms of the relative errors, we obtain a maximum value of 3.482%, while the average percentage relative error for superelevation is −1.53%. In conclusion, the superelevation of the road calculated with the proposed methodology yields satisfactory results.

Overall, in both conducted analyses, the results extracted for slopes and are very similar, where the absolute length differences for linear elements become greater as the sections increase. On the contrary, the differences in superelevation become smaller as the methodology operates in a smaller range. The percentage relative errors are higher for angular measurements than for linear measurements in terms of both slope and superelevation. Noting the absolute differences in slope and superelevation, we can see that the results are below 0.1%, which is the maximum error considered in the inventory of Spanish roads.

4. Concluding remarks

This paper presented a contribution to data processing tasks for MLS. The developed methodology for road characterisation is based on segmentation processes, orthogonal regression through PCA and filtering. These procedures permit the determination of geometric parameters that best define vertical road alignments, such as slope, vertical curves, normal crown, full superelevation and superelevation transitions. The extracted geometric parameters comply with the Spanish normative.

In short, this paper's novel contribution is to propose an alternative for the automated development of "as-built" road plans. Based on the results, users can perform various analyses of interest about road conditions to determine constructive errors and prevent accidents.

The experimental results validate the use of the proposed method, guaranteeing relative accuracies under 3.5%. However, it should be noted that the proposed approach is a first approximation tested only for simple regional roads. It is not within the scope of this paper to provide a universal or commercial solution for any type of road.

Accounting for the results and comparing them with existing research (Lakakis et al., 2013; Tsai et al., 2013), the present study provides comprehensive information on vertical alignments, both longitudinally and transversely and for both lanes of a road. The methodology presented in this article goes a step further in the extraction of information. An input LiDAR point cloud enables for the precise analysis of road conditions and does not rely on the trajectory followed by the driver.

Despite the large volume of information generated by this type of system, the developed methodology obtains detailed information easily and smoothly due to the simple algorithms implemented. The automatic extraction of road elevations and cross-sections in an accurate manner will be important to further studies on road visibility.

In the future, the georeferenced information captured by the MLS, horizontal alignment and vertical alignment could be used for visibility studies and serve as a complete tool for road maintenance and quality control.

Acknowledgements

The authors would like to thank the Ministerio Ciencia e Innovación (Grant No. IPT-2012-1092-120000; INNPACTO program) for the financial support given. Furthermore, a portion of human resources for this work has been supported by the European Regional Development Fund (FEDER), the Spanish Centre for Technological and Industrial Development (Grant No. IDI-20101770) and Xunta de Galicia (Competitive Referenced Research Groups, Grant No. 2012/269) (Human Resources programs BES-2010-034106 and IPP055 – EXP44).

References

Ai, C., Tsai, Y.J., 2012. Critical assessment of automatic traffic sign detection using three-dimensional LiDAR point cloud data. In: Transportation Research Board 91st Annual Meeting, pp. 12–3214.

Belton, D., Lichti, D.D., 2006. Classification and Segmentation of Terrestrial Laser Scanner Point Clouds using Local Variance Information. IAPRS, XXXVI, 5.

Cleveland, W.S., 1979. Robust locally weighted regression and smoothing scatterplots. J. Am. Stat. Assoc. 74 (368), 829–836.

Cleveland, W.S., Devlin, S.J., 1988. Locally weighted regression: an approach to regression analysis by local fitting. J. Am. Stat. Assoc. 83 (403), 596–610.

Di Mascio, P., Di Vito, M., Loprencipe, G., Ragnoli, A., 2012. Procedure to determine the geometry of road alignment using GPS data. Procedia-Soc. Behav. Sci. 53, 1203–1216.

El-Halawany, S.I., Lichti, D.D., 2011. Detection of road poles from mobile terrestrial laser scanner point cloud. In: Multi-Platform/Multi-Sensor Remote Sensing and Mapping (M2RSM), 2011 International Workshop on, pp. 1–6.

Gikas, V., Stratakos, J., 2012. A novel geodetic engineering method for accurate and automated road/railway centreline geometry extraction based on the bearing diagram and fractal behavior. IEEE Trans. Intell. Transp. Syst. 13 (1), 115–126.

Gomes, S.V., 2013. The influence of the infrastructure characteristics in urban road accidents occurrence. Accid. Anal. Prevent 60, 289–297.

Gräfe, G., 2008. Kinematic 3D laser scanning for road or railway construction surveys. In: Proceedings of the International Conference on Machine Control & Guidance, pp. 24–26.

Holgado-Barco, A., González-Aguilera, D., Arias-Sanchez, P., Martinez-Sanchez, J., 2014. Semi-Automatic extraction of road horizontal alignment from a mobile LiDAR system. Comput.-Aided Civil Inf. Eng. http://dx.doi.org/10.1111/mice.12087.

Institute for Road Safety Research, 2002. Safety Standards for Road Design and Redesign SAFESTAR, pp. 1–118.

Jolliffe, I.T., 2002. Principal Component Analysis, second ed. New York, Springer.

Karamanou, A., Papazissi, K., Paradissis, D., Psarianos, B., 2010. Precise Estimation of Road Horizontal and Vertical Geometric Features using Mobile Mapping Techniques. Boletim De Ciências Geodésicas, 15(5).

Lakakis, K., Savvaidis, P., Wunderlich, T., 2013. Evaluation of a low-cost mobile mapping and inspection system for road safety classification. Am. J. Geogr. Inf. Syst. 2 (1), 6–14.

Optech Inc., 2013. Home page of The Company Optech Inc. <http://optech.ca> (3.12.2013).

Pauly, M., Gross, M., Kobbelt, L.P., 2002, October. Efficient simplification of point-sampled surfaces. In: Proceedings of the Conference on Visualization'02, IEEE Computer Society, pp. 163–170.

Puente, I., González-Jorge, H., Riveiro, B., Arias, P., 2012. Accuracy verification of the LYNX mobile mapper system. Opt. Laser Technol.

Sentouh, C., Glaser, S., Mammar, S., 2006. Advanced vehicle–infrastructure–driver speed profile for road departure accident prevention. Vehicle Syst. Dyn. 44 (sup1), 612–623.

Taylor, D.R., Muthiah, S., Kulakowski, B.T., Mahoney, K.M., Porter, R.J., 2007. Artificial neural network speed profile model for construction work zones on high-speed highways. J. Transport. Eng. 133 (3), 198–204.

Toutenburg, H., 2008. Linear Models and Generalizations: Least Squares and Alternatives. Springer.

Tsai, Y.J., Ai, C., Wang, Z., Pitts, E., 2013. A mobile cross slope measurement method using LiDAR technology 2. Technology 2 (3), 4.

Wang, J., González-Jorge, H., Lindenbergh, R., Arias-Sánchez, P., Menenti, M., 2013. Automatic estimation of excavation volume from laser mobile mapping data for mountain road widening. Remote Sens. 5 (9), 4629–4651.

Yang, B., Fang, L., Li, Q., Li, J., 2012. Automated extraction of road markings from mobile LiDAR point clouds. Photogramm. Eng. Remote Sens. 78 (4), 331–338.

3.3. Automation in the geometric inventory of roads from a Mobile LiDAR System

Resumen: El objetivo del presente artículo es obtener de manera automática las marcas viales del pavimento de la carretera junto con el inventario geométrico de la sección transversal de la carretera (nº carriles, ancho plataforma, ancho arcenes, ancho carriles, peralte) mediante la utilización de un Mobile LiDAR System (MLS). Debido a la gran cantidad de datos capturados por el MLS hemos desarrollado una metodología basada en procesos de segmentación, clasificación y extracción de perfiles transversales que nos permite determinar los elementos del inventario de la carretera contenidos en los perfiles transversales al igual que la delineación automática de la misma en formato CAD. El proceso desarrollado ha sido validado con datos reales arrojando resultados satisfactorios en los escenarios analizados, detectando tanto la plataforma de la carretera como las diferentes marcas viales presentes, teniendo en cuenta que las carreteras analizadas tenían múltiples carriles así como variación de los mismos.

Palabras Clave: sistema LiDAR móvil; automatización en la inspección de carreteras; información geo-espacial; mantenimiento de carreteras; inventarios de carretera; segmentación; extracción de características.

COMPUTER-AIDED CIVIL AND INFRASTRUCTURE ENGINEERING

Computer-Aided Civil and Infrastructure Engineering **00** (2016) 1–15

Automatic Inventory of Road Cross Sections from Mobile Laser Scanning System

Alberto Holgado-Barco

Department of Cartographic and Land Engineering, University of Salamanca, Higher Polytechnic School of Avila, Hornos Caleros, Avila, Spain

Belén Riveiro*

Department of Materials Engineering, Applied Mechanics and Construction, School of Industrial Engineering, University of Vigo, Vigo, Spain

Diego González-Aguilera

Department of Cartographic and Land Engineering, University of Salamanca, Higher Polytechnic School of Avila, Hornos Caleros, Avila, Spain

&

Pedro Arias

Department of Natural Resources & Environmental Engineering, University of Vigo, School of Mining Engineering, Vigo, Spain

Abstract: *This article aims to automatically obtain the geometrical inventory of road cross sections (i.e., number of lanes, width of the roadway, width of the shoulders, width of the lanes, superelevation) using a mobile laser scanning (MLS) system. Because of the large amount of data captured by the MLS, we have developed a methodology that is based on a process of segmentation, classification and extraction, which allows us to determine the geometrical cross-section parameters. The process was validated with real data from motorways, and satisfactory results were obtained in the analyzed scenarios.*

1 INTRODUCTION

Mobile laser scanning (MLS) is increasingly expanding toward management applications, principally in applications related to road inventory (Zhou et al., 2013) and urban landscape modeling (Deshpande, 2013), and even structural applications (Park et al., 2007; Truong-Hong et al., 2013; Park et al., 2015). This technology allows quick and exhaustive control of the roads, and Transport Administrations have begun to demand this technology because of its ability to perform accurate geometric inventories (Tsai et al., 2013) and detect damages and pathologies that may reduce road safety. However, the data that are gathered through MLS systems must be accordingly processed, and a currently important bottleneck for the implementation of this technology is related to this issue. Specifically, point cloud segmentation and 3D modeling are not trivial tasks because a point cloud is a collection of unorganized points that lack semantic information (Vosselman and Maas, 2010; Gómez-García-Bermejo et al., 2013). Thus, the geometry is required, and the semantic data are challenging for 3D modeling. Additionally, specialized software for automated processing is demanded in many fields where laser scanning may provide useful information,

*To whom correspondence should be addressed. E-mail: *belenriveiro@uvigo.es*.

DOI: 10.1111/mice.12213

such as road marks that must be detected and properly classified according to their function on the road.

Currently, the digital cartography provided by MLS goes further than inventory purposes. For example, in the case of the driverless-car philosophy, proper maps may assist the automatic driving system (Guo et al., 2014) to improve road safety. Some authors have developed solutions for lane detection and tracking which could be interesting for security purposes. Actually, there are different techniques for lanes detection (Hillel et al., 2014). In particular, Thuy et al. (2010) presented a methodology for the detection and tracking of lanes using LiDAR data. Huang et al. (2009) developed a method for the detection and tracking of lanes in real time using LiDAR and camera sensors, so they can support the automatic driving of vehicles. In this manner, some of these approaches for lane detection and tracking could become in future navigation safety maps uploaded on-board to help the driver.

Recently, an intensity activity related to automatic detection of road features from MLS data has been reported in the literature. In general, the works related to automatic inventory of road markings focus on two main features: detection and classification of punctual road signs (such as zebra crossing, give way, stop, speed limits, etc.) as presented by Guan et al. (2014); or detection and delineation of longitudinal road lines (Yu et al., 2015).

The automatic extraction of road marks and cross sections allows us to advance in inventorying a road by extracting its geometric elements (i.e., the number of lanes, width of the roadway, width of the shoulders, width of the lanes, superelevation; for more information about the road parameters, see Highway Design Manual (2012) and automatically vectorizing the road in the CAD format. In this context, different authors have addressed interesting solutions: Chen et al. (2009) located road-marking candidates using adaptive thresholding, where thresholds were invariant to absolute values of laser beam returns. They also extracted road markings with Hough transform clustering, followed by a refinement step with trajectory constraint and geometry check. Kumar et al. described an algorithm for extracting road edges from mobile LiDAR data that improved the parametric active contour or snake model by introducing navigation information (Kumar, 2012; Kumar et al., 2013). Yang et al. (2013) proposed an approach that allowed the semi-automatic extraction and delineation of roads using evaluation point clouds based on consecutive sets of scanner cross sections, where a moving window operator was used to remove nonground points from each line and curb points were detected based on curb patterns. Kumar et al. presented an automatic algorithm for the extraction of road marks using MLS data (Kumar, 2012; Kumar et al., 2014). The approach presented is supported by the intensity values recorded by the LiDAR sensor and the use of morphological operators, as well as the knowledge of the dimensions of road marks. Yang et al. (2012) presented a methodology to automatically extract the road marks of the point clouds from a MLS. In the first phase, they detected such marks based on the intensity georeferenced image, which included the elevation data. In the second phase, they extracted the boundaries of the marks using semantic knowledge (i.e., shape and size). The methodology presented is suited for the detection and classification of different types of road marks. However, they do not provide any geometric inventory of the road. More recently, Takahashi et al. (2014) developed an efficient method to automatically draw the road lines using LiDAR data. The method is based on the extraction of lines through the Hough transform and uses profile intensity as a parameter. However this approach presents two main limitations: first, they do not perform any detection of road edges and second, they do not provide a geometric inventory of the road using road marks.

Finally, and in the context of topographic mapping of road alignment, Holgado-Barco et al. (2014) proposed a method to extract the horizontal alignment of roads based on the MLS data. However, the approach proposed requires a lot of fixed thresholds which must be defined or tested by the user.

This article presents the development and testing of a methodology to convert an unorganized point cloud from MLS data into standardized geometric inventory of road cross sections which can be applied to roads that do not contain any semantic information. Currently, the Road Administrations use both images and LiDAR data to manage and conduct inventories (Spear et al., 2010). LiDAR data are also used to obtain manual measurements from qualified staff (Catálogo de la RCE, 2010). Comparing this process with the existing approaches, our method performs the semantic recognition of road marks and provides the geometric inventory of cross sections: number of traffic lanes, width of the roadway, width of traffic lanes and shoulders, and superelevation. The article starts with an introduction; then, Section 2 presents the developed methodology, which is composed of three main steps: (1) road segmentation, (2) detection and classification of road marks, and (3) roadway geometric inventory for each cross section. Section 3 presents the materials and case studies. Section 4 outlines the obtained results in the real case studies, which corresponded to three roadways with different geometric characteristics and road marks. Finally, the conclusions and future study are stated in Section 5.

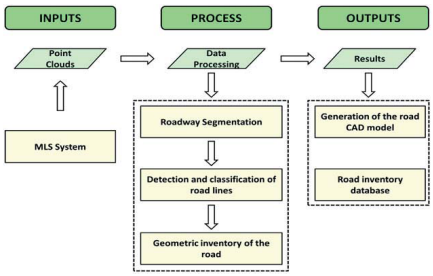

Fig. 1. General workflow of the methodology for the automatic delineation and roadway measurement from MLS data.

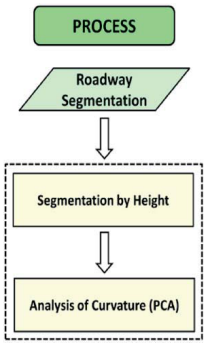

Fig. 2. Workflow for roadway segmentation.

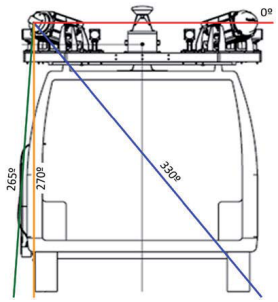

Fig. 3. Reference angles in a sensor head that corresponds to the horizontal projection of the vehicle.

2 METHODS

2.1 Methodology

The methodology presented in this work is composed of four main steps (Figure 1). First, data are acquired using the MLS in the road, and a 3D point cloud is prepared. Then, the data processing is divided into the three remaining steps: (1) roadway segmentation from the global point cloud, (2) detection and classification of the road lines, and finally, (3) roadway geometric inventory based on cross sections of the road. The process was fully developed and tested with a library developed by authors (GeoRoad), using MATLAB language.

2.2 Roadway segmentation

One of the most challenging tasks of the process is the automatic segmentation of the points that correspond with the roadway from the global point cloud. This segmentation was performed in two consecutive steps: the first step was based on an adaptive height threshold, and the second step was based on a curvature analysis using the principal component analysis (PCA) (Ghosh-Dastidar et al., 2008) (Figure 2). These segmentation steps were applied to each laser profile, which was collected using a LiDAR sensor head. Although all points are evaluated in 2D, the segmented points remain in the 3D space.

The first segmentation is performed to remove all points whose height is out of the range of the roadway height (e.g., traffic signs, trees, poles, and traffic lights). The height threshold is automatically computed from the set of points that correspond to the horizontal projection of the vehicle. Thus, for each profile, the height is computed to account for the points whose angle is in the interval of 265–330° (Figure 3).

After the points that are far from the road are removed, a PCA-based curvature analysis is applied to the remaining points to filter the outlier points (i.e., those that do not belong to the roadway) of the laser profile. The principal direction for each profile is estimated using those points whose angle is in the interval of 265–330°. Using the covariance method (Pauly et al., 2002; Belton and Lichti, 2006), the principal directions for each profile (calculating eigenvectors and eigenvalues) are determined; consequently, it is possible to obtain the direction of the straight line that best fits the road points.

With this vector and a point in the set of points below the vehicle, the straight line that best fits the points of the roadway is used as the reference line. Next, the minimum distance between each point in the profile and the reference line is calculated.

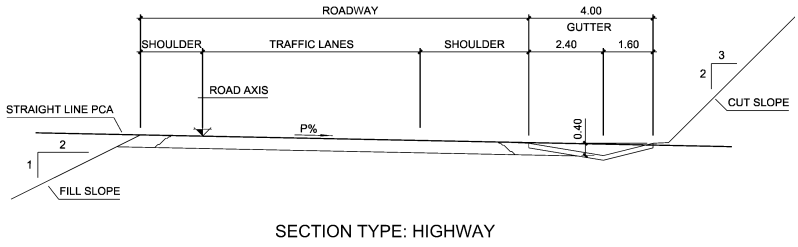

Fig. 4. Cross section of a motorway and straight line obtained using PCA.

All points whose aforementioned distance is greater than 15 cm are removed (Figure 4). This distance was determined based on the depth of gutter and the height of lateral curbs of roads using the official Standard for Roads Design, so only the points that are within this range are initially considered to be the points of the roadway.

The next step in the segmentation consists of establishing both ends of the straight line, so the points that correspond to other elements such as drainages, vegetation, and slopes are removed. Note that to avoid the effects of noisy points or outliers, a filter based on number of neighbor points was applied so isolated points were removed. Hence, the distance between consecutive points is calculated (points are sorted by time stamp), and a large distance denotes the end of the roadway points. This distance threshold is calculated to the geometry of the drainage element according to the standards for road design. The ends of the roadway are marked at the points that first reach the distance threshold in both directions from an angle of 270° (Figure 3). By repeating this operation for all surveyed profiles, a segmented point cloud that corresponds to only the roadway is obtained.

2.3 Detection and classification of the road lines

After the point cloud of the roadway is obtained, the next step involves detecting road lines using the attribute of intensity and subsequent clustering of road lines (Figure 5).

The intensity attribute of LiDAR points is used to distinguish the road marks and pavement because these elements are made of materials that have significantly different reflectivity. Road marks are composed of the points that present a local maximum in the intensity response (analysis performed by LiDAR profile). Because some reflective marks may appear in the road (e.g., reflective material in the road, painting spots), a distance filter is imposed to minimize the number of

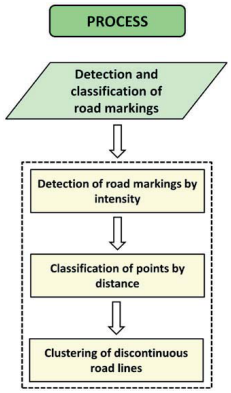

Fig. 5. Workflow of the process of detection, classification and clustering of road lines.

false positives. The filtering is performed to introduce the logical constrains according to the standards for road painting (in the Spanish case, Norma 8.2- IC. Marcas Viales; in the U.K. case, Traffic Signs Manual; in the Brazil case, Manual de Sinalização Rodoviária and in the Portugal case, Norma de Marcas Rodoviárias, 1995), which establishes that the maximum width of the road lines is 30 cm, being also compatible with those road marks with lower widths. Thus, when the distance between consecutive points is higher than this value, these points are discarded.

After the points that belong to the road lines are detected, they must be classified into groups that correspond to different road lines (Figure 6). The points are coded after computing the distance between them and the set of points of the previous LiDAR profiles. In addition, it is verified that the computed distance is shorter than 30 cm (according to the aforementioned

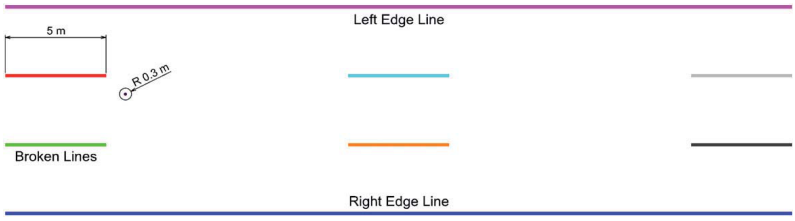

Fig. 6. First automatic coding and dimensional characteristics (meters) of road lines for the motorways in Spain, United Kingdom, Brazil, and Portugal.

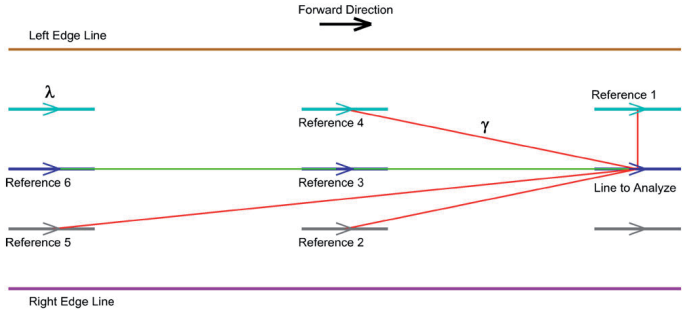

Fig. 7. Clustering of broken lines based on the relationship between the direction vector of the road marks (PCA) and the azimuths to the neighbor broken lines.

standards). The points are consequently grouped into different line groups; each time a point does not have close points in the previous profiles, a new road line group is started (Figure 6). At this stage, the road lines are also semantically classified as left mark, right mark, or central mark. Road markings are classified into left, right, and central according to the acquisition order performed by LiDAR, that is, MLS starts acquiring information from the left edge to the right edge, so the first road mark detected will be the left mark and the last road marking detected will be the right mark. Depending on the number of lanes several central marks (central lines) may be detected in the same road cross-section. When a central line is composed of consecutive broken lines, each segment is classified as an independent mark, as shown in Figure 6.

Consequently, the next step consists of clustering all individual marks into a common broken line. This problem is challenging when there are several broken lines in a roadway and when the number of traffic lanes changes along the road route. A two-stage process was developed to achieve efficient clustering.

First, only the road mark groups with a length of fewer than 6 m are candidates to belong to a broken line. This threshold is established according to the maximum length of a broken line (Figure 6). Although the logical thresholds were established according to the analyzed standards (representative of most European and South American countries), they might be adapted to any other geometric relation according to national standards.

Second, after the broken lines are selected, they are compared according to their principal direction (Figure 7). Thus, from a PCA analysis, the direction vector of each mark is obtained and converted to an azimuth angle (λ_n). In addition, the azimuths (γ_{n-m}) that result from joining the centroid of each mark (n) and the centroids of the previous marks (m) are computed (Figure 7). Finally, the ratio between both angles λ_n/γ_{n-m} is computed to evaluate the parallelism (values close to 1 denote parallelism). In positive case, both marks are clustered into the same broken line.

Based on the previous conditions, different road marks, such as speed reduction, arrows, Give Way, and

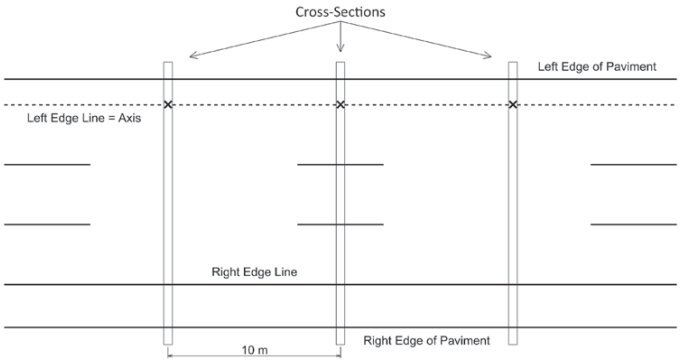

Fig. 8. Plan view of a road and its component elements, where the cross sections are separated by 10 m from one another.

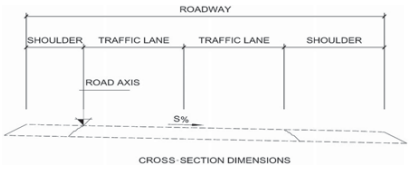

Fig. 9. Geometric information of the cross-sectional profiles, which is automatically collected using the proposed algorithm.

Chevron Markings, that can be contained in the point cloud are discarded from the classified marks, primarily because of the condition of the minimum number of points contained in each individual mark along the forward direction. In addition, for discontinuous road lines, a minimum number of consecutive marks is required to define a longitudinal road line.

After all road lines are detected, classified and clustered, the classes with fewer than 30 points are discarded to avoid including arrows or other road marks that do not belong to the longitudinal road lines. Then, to define an accurate and reliable geometry associated to each road mark, a spline is fitted to each class of road mark. The code for the curve fitting can be found in the work by Lundgren (2011). Thus, the road is automatically drawn from the mobile LiDAR data and delivered to the CAD (exported as a DXF format).

2.4 Geometric inventory of cross sections

This step is the last step where cross-sectional profiles of the roadway are generated to perform its geometric

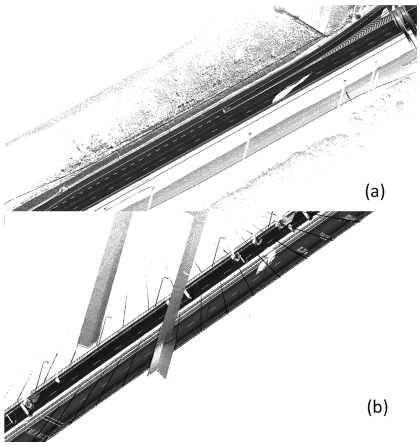

Fig. 10. (a) Point cloud of a motorway with variation in the number of lanes; (b) point cloud of a motorway with different types of road marks.

inventory (i.e., number of lanes, width of the roadway, width of the traffic lane, width of the shoulder, superelevation). At this stage, the user must define the type of road (i.e., motorway, national or local roads) and then the library assists the user in the road axis definition. Note that this information does not depend on the segmentation and classification strategy because even when the inventory is performed manually, this information must be provided by the road owner or manager. Because the point clouds are evaluated in

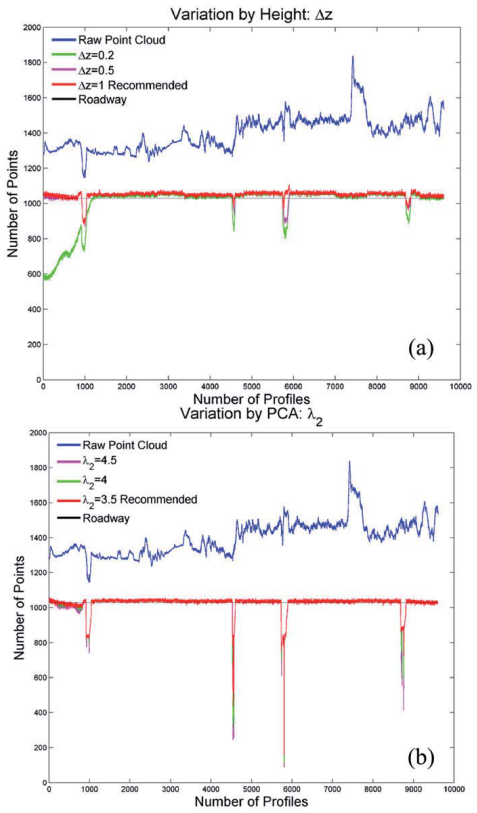

Fig. 11. Sensibility analyses for the parameters defined in the road segmentation: (a), gradient in Z coordinate (Δz); and (b) second eigenvalue (λ_2) of the PCA analysis.

strips, the proposed algorithm maintains the same axis for the entire strip; if the road axis changes, this information must be provided, as would occur in a manual inventory. Using the road axis as the reference, the remaining inventory parameters are automatically made at the cross-sectional profiles, which are separated by 10 m from one another (Figure 8).

Thus, continuous road lines are fitted to a spline, and discontinuous road lines are joined using a common spline, so the inventory can be properly done at each cross section, even when the road mark is not painted at the point of inventory (e.g., the first and third cross sections in Figure 8).

Then, the azimuthal vector at each cross-sectional profile is calculated along the road axis. This vector is used to define the cross-sectional plane in which all points in a neighborhood of 10 cm are projected to perform the inventory measurements. The cross-sectional profile is represented in a vertical plane, which is computed as perpendicular to the plane defined by the direction vector of the road axis every 10 m and in the vertical direction.

As shown in Figure 9, the information collected at every 10 m includes the following: kilometric point of the roadway, number of traffic lanes, superelevation (S%), roadway width, shoulder width, and traffic lane

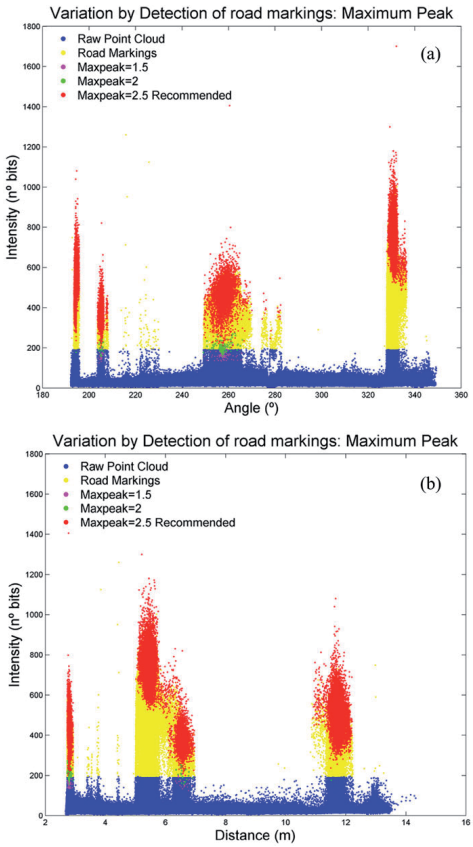

Fig. 12. (a) Sensibility analysis for the threshold for local maximum of the intensity represented by deflection angle; (b) sensibility analysis for the threshold for local maximum of the intensity represented by distance to the scanner axis.

widths. This information is stored in a database as a part of the geometric inventory of the roadway.

3 CASE STUDIES

3.1 The capture system: Optech Lynx MMS

The MLS system selected for the case study was the Lynx Mobile Mapper, which was released the end of 2007 by OPTECH Inc. (Optech, 2012). The Lynx MLS is composed of a LiDAR subsystem and a navigation system. Two LiDAR sensor heads with a nominal accuracy of 8 mm (1σ) are mounted to form an angle of 90° between their respective rotation axes and 45° with respect to the trajectory of the vehicle. These sensors enable survey-grade LiDAR data to be collected at 500,000 measurements per second with a 360° FOV (each scanner). The navigation system incorporates the POS LV 520 produced by Applanix, which integrates an Inertial Measurement Unit (IMU) with a 2-antenna heading measurement system Global Navigation Satellite Systems (GNNS) and provides 0.015° in heading, 0.005° in roll and pitch, 0.02 m in X,Y

Table 1
Summary of the segmentation and detection processes. Point reduction and computation time

Segmentation	*Number of points*	*Reduction of points (%)*	*Computation times*
Raw point cloud	10,021,417	100%	1' 9.38"
Roadway (threshold by heights)	8,357,978	83.4%	11' 27.51"
Roadway (analysis of curvature (PCA))	8,100,991	80.8%	20' 14.82"
Detection of road lines (threshold by intensity)	22,343	0.22%	10.68"

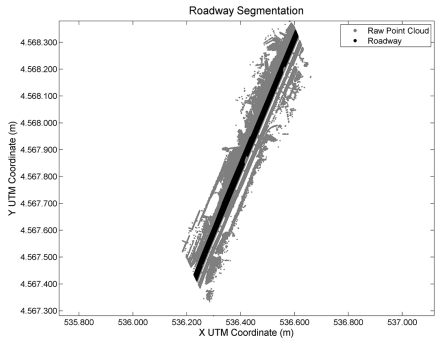

Fig. 13. Raw point cloud (in gray color) and segmentation of the roadway (in black color).

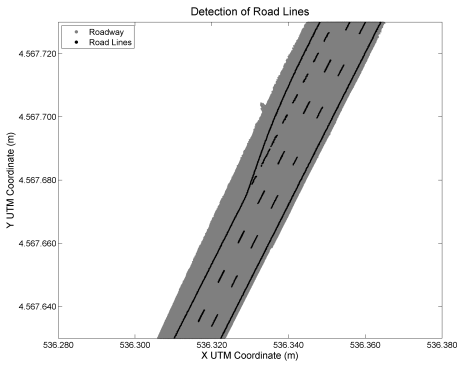

Fig. 14. Detection of the road lines (in black color) based on the intensity values.

position and 0.05 m in the Z position. These values were determined using differential GPS (Global Positioning System) postprocessing after data collection using GPS base station data (Puente et al, 2013). The Optech LiDAR provides up to four echoes per pulse with their respective intensity attribute, whose wavelength is 1550 nm. The Lynx Mobile Mapper also contains four Jai 500GE cameras with a resolution of 5 megapixels. The three sensors of the Lynx Mobile Mapper (navigation system, LiDAR, and cameras) are time-synchronized with the GPS time.

The point clouds to validate the method were acquired at an averaged constant vehicle speed of 80 km/h, which ensures a separation of 11 cm between consecutive laser profiles, being also optimal for higher vehicle speeds (up to 120 km/h). The acquisition rate allows an angular resolution of 0.14° in each laser profile (equivalent to a resolution of 6.1 cm at a range of 25 m). In addition, the survey was performed in normal traffic conditions. Because of the presence of cars in the road that appear in the point cloud because of overtaking, the algorithm presented by Varela-González et al. (2014) was used to preprocess the point cloud and remove noisy points.

3.2 Case study 1: with variation in the number of lanes

The second case study corresponds to at a stretch of motorway, with a length of 1 km, where there is variation in the number of lanes. Again, the point cloud was acquired using the MLS with a 500 MHz scan frequency and provided 10 million points in total (Figure 10a).

3.3 Case study 2: with different types of road marks

The third case study corresponds to a stretch of motorway, with a length of 400 m, where the most difficulty is the presence of different types of road marks (speed reduction, arrows, etc.). Again, the point cloud was acquired using the MLS with a 500 MHz scan frequency and provided 4.7 million points in total (Figure 10b).

4 EXPERIMENTAL RESULTS

During the development of the algorithm several parameter had to be fixed empirically. For that purpose,

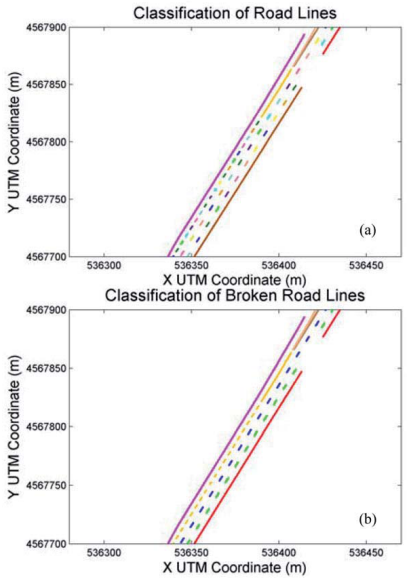

Fig. 15. (a) Classification of the road lines. (b) Clustering of the broken road lines.

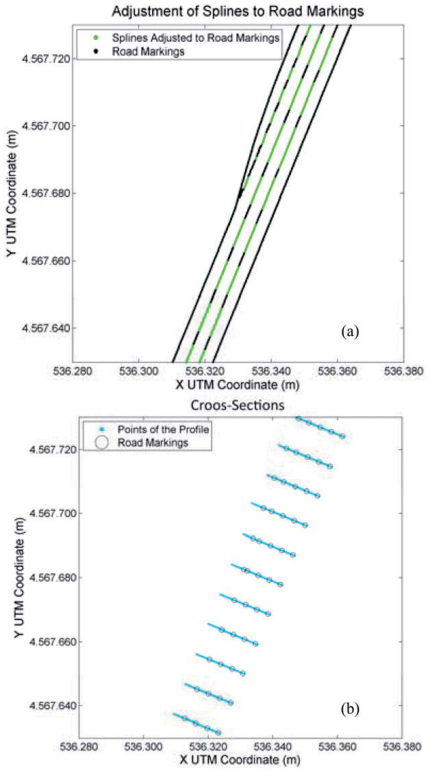

Fig. 16. (a) Splines fitted to different road lines. (b) Generation of cross sections with footprints (circular elements) of the road lines along the cross sections.

sensibility analyses were performed to evaluate the influence of those parameters for the results in terms of segmentation of roadway and extraction of road marks. Later, the methodology described in Section 2 was validated through two different data sets presented in Sections 4.2 and 4.3.

4.1 Sensibility analyses

Sensitivity analyses were performed to evaluate the optimal value of those parameters that cannot be assumed from logical constraints. The following plots show the sensibility analysis for the parameters used for the road segmentation: "Δz" for the segmentation based on point height, and "λ_2" for the segmentation based on PCA.

The results for three different values of those parameters (two unfavorable and the recommended value) are shown, using the number of points of each profile to evaluate the goodness of the parameters (black line).

In Figure 11a we can see that the vehicles or other obstacles affect the number of points in each profile. Also, when the parameter is too restrictive, a significant number of points are missing if the road has a significant camber. However, in Figure 11b we can see that the parameter is less sensitive to the road geometry and is mainly affected by occlusions due to vehicles.

Two parameters were empirically set according to the robustness of the results during the detection of road marks: angle of deflection of points and distance to the scanner axis. The results are evaluated using the intensity value of points, and manual segmentation of roads marks was performed as ground truth (yellow points). Original point cloud is presented in blue color.

In Figures 12a and b we can see that the recommended parameter provides good results in the detection of the road marks. If this parameter is lower,

Table 2
Results of the geometrical inventory of the road and comparison of its different geometric elements

KPs	*Number of lanes*	*Superelevation %*	*Width roadway (m)*	*Right shoulder (m)*	*Left shoulder (m)*	*Width Lane 1 (m)*	*Width Lane 2 (m)*	*Width Lane 3 (m)*	*Width Lane 4 (m)*
50	3	2.49	15.37	3.66	0.44	3.77	3.90	3.60	
100	3	2.38	15.18	3.60	0.29	3.79	3.74	3.76	
150	3	2.35	15.13	3.36	0.51	3.74	3.76	3.76	
200	3	2.43	15.04	3.33	0.43	3.78	3.73	3.76	
250	3	2.41	15.23	3.58	0.37	3.79	3.78	3.72	
300	3	2.33	15.22	3.40	0.54	3.78	3.77	3.73	
350	3	2.37	15.30	3.44	0.57	3.79	3.73	3.78	
400	3	2.35	15.23	3.54	0.41	3.77	3.82	3.69	
450	4	2.38	17.00	2.60	0.33	2.80	3.75	3.84	3.67
500	4	2.29	16.95	1.20	0.51	3.88	3.83	3.75	3.77
550	4	2.53	17.52	2.43	0.37	3.48	3.74	3.76	3.73
600	4	2.57	17.83	2.48	0.60	3.40	3.87	3.73	3.75
650	4	2.57	17.75	2.64	0.46	3.45	3.76	3.74	3.71
700	4	2.18	16.81	4.15	0.53	1.07	3.62	3.76	3.68
750	3	2.30	15.51	3.74	0.54	3.78	3.75	3.69	
800	3	0.98	15.23	3.53	0.46	3.77	3.74	3.73	
850	3	–2.19	15.27	3.63	0.29	3.77	3.78	3.79	
900	3	–3.08	15.30	3.57	0.39	3.80	3.81	3.73	
950	3	–3.90	15.17	3.31	0.49	3.86	3.77	3.74	

Table 3
Summary of the segmentation and detection processes. Point reduction and computation time

Segmentation	*Number of points*	*Reduction of points (%)*	*Computation times*
Raw point cloud	4,765,186	100%	40”
Roadway (threshold by heights)	4,203,805	88.2%	16”
Roadway (analysis of curvature (PCA))	3,533,818	74.2%	1’ 31”
Detection of road lines (threshold by intensity)	9,926	0.21%	27”

then many other nondesired marks appear in the segmentation (as shown by green and magenta points in both plots).

4.2 Results of case study 1

The first step is the roadway segmentation based on the height thresholds, which reduced the point cloud to 8.3 million points. Based on these results, the roadway segmentation was refined using the eigenvalues and eigenvectors associated with each cross section. As a result, the roadway was defined using 8.1 million points (Figure 13), which represents a 19.2% reduction compared with the original “raw” point cloud.

After the roadway was segmented, the road lines were extracted based on the intensity value, which was acquired using LiDAR, to obtain a total of 22,343 points that belonged to road lines (Figure 14).

After the roadway segmentation and road line detection, Table 1 shows the percentage of reduction of points and required computation time. We may observe that the roadway is defined using 8.1 million points, whereas the road lines are defined using 22,343 points.

The next phase is the semantic classification of road lines, which allows us to classify different road lines (Figure 15a).

After the road lines were classified, a clustering of different broken lines of the roadway along their principal direction was performed (Figure 15b).

Supported by the road line classification, the geometric inventory of the road cross sections was obtained (Section 2.4). To successfully determine the cross sections (Figure 16b), the road axis must be defined, and the road lines must be fitted to the splines (Figure 16a).

Finally, with the obtained cross sections, we could provide its geometric inventory (Table 2). This table shows the KP position, number of lanes, superelevation,

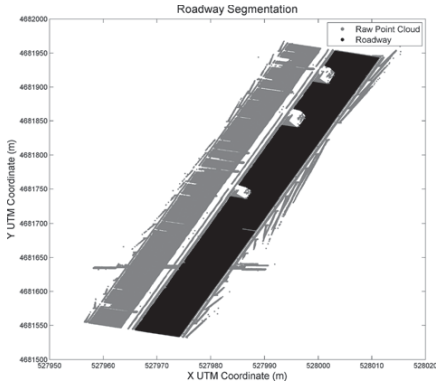

Fig. 17. Raw point cloud (in gray color) and segmentation of the roadway (in black color).

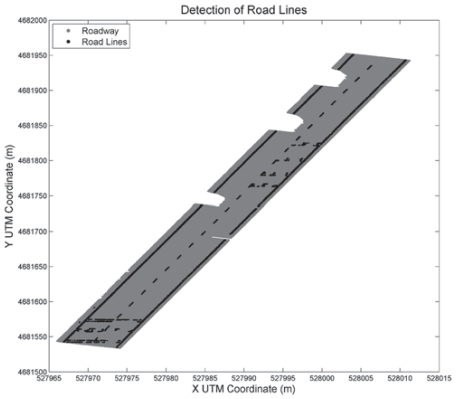

Fig. 18. Detection of the road lines (in black color) based on the intensity values.

width of the roadway, shoulders and lanes. Because of the huge volume of information, Table 2 only shows the results for the cross sections that were generated every 50 m.

The results in Table 2 show the variation in the number of traffic lanes between KP 450 and KP 700 because of an additional lane, which increases the roadway width. In addition, the dimensions of lane 1 decrease because of the presence of this additional lane. Analyzing the remaining data, we may observe that the superelevation remains constant until KP 800 because it

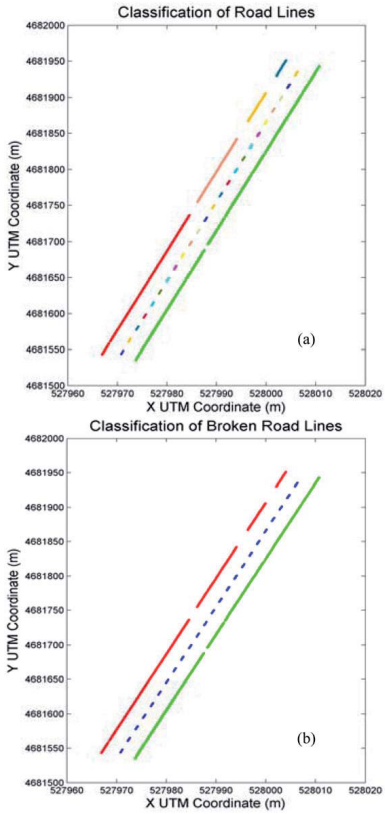

Fig. 19. (a) Classification of the road lines. (b) Clustering of the broken road lines.

corresponds with a straight stretch, which begins to change at the beginning of the curve.

4.3 Results of case study 2

The first step is the road segmentation based on the height threshold, reducing the point cloud to 4.2 million points. Based on these results, the road segmentation was refined using the eigenvalues and eigenvectors associated with each cross section. As a result, the road was defined using 3.5 million points (Figure 17), which represents a 25.8% reduction compared with the original "raw" point cloud.

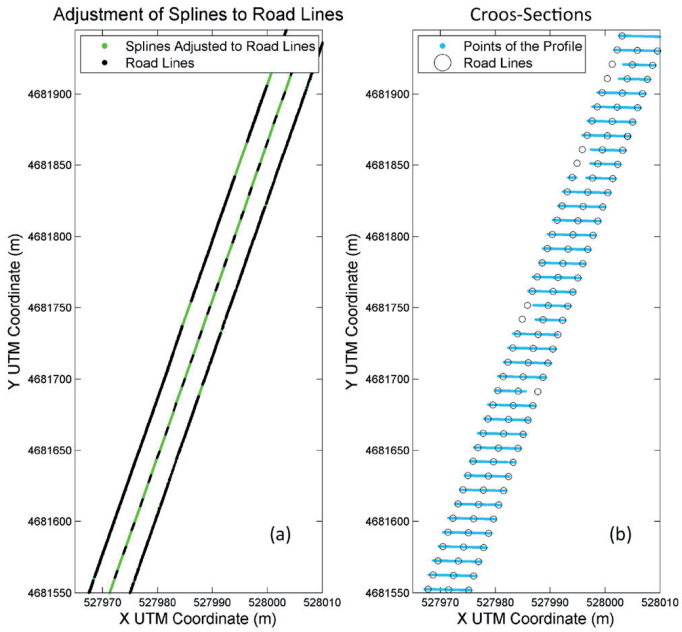

Fig. 20. (a) Splines fitted to different road lines. (b) Generation of cross sections with footprints (circular elements) of the road lines along the cross sections.

After the roadway segmentation, road lines were extracted using the intensity value provided by LiDAR sensor, obtaining a total of 9,926 points belonging to road lines (Figure 18).

After the segmentation of the roadway and the extraction of road lines, Table 3 outlines the percentage of reduction of points and required computation time. We may observe that the roadway is defined using 3.5 million points, whereas the road lines are defined using 9,926 points.

The next step is the semantic classification of road lines, which allows us to cluster the different broken lines of the roadway along their principal direction (Figure 19a).

This step is really important, because the algorithm should discriminate between other types of road marks such as speed reduction marks or any mark painted on the road. In particular, the algorithm is robust rejecting other types of road marks, because it is based on the detection of longitudinal lines supported by the azimuthal direction along the road axis.

After the road lines were classified, a clustering of different broken lines of the roadway along their principal direction was performed (Figure 19b).

Supported by the road line classification, the geometric inventory of the road cross sections was obtained (Section 2.4). To successfully determine the cross sections (Figure 20b), the road axis must be defined, and the road lines must be fitted to the splines (Figure 20a).

Finally, with the obtained cross sections, we could provide its geometric inventory (see Table 4). This table shows the KP position, number of lanes, superelevation, width of the roadway, shoulders and lanes. Because of the huge volume of information, Table 4 only shows the results for the cross sections that were generated every 20 m.

From the results of Table 4 we can appreciate that three KP (KP 200, KP 320, and KP 380), present differences in the width of the roadway and in the left shoulder due to the presence of vehicles. In addition, it should be remarked that the library Georoad deals

Table 4
Results of the geometrical inventory of the road and comparison of its different geometric elements

KPs	*Number of lanes*	*Superelevation %*	*Width roadway (m)*	*Right shoulder (m)*	*Left shoulder (m)*	*Width Lane 1 (m)*	*Width Lane 2 (m)*
20	2	–1.89	8.43	0.51	0.49	3.73	3.71
40	2	–1.85	8.48	0.52	0.53	3.76	3.67
60	2	–1.92	8.42	0.54	0.48	3.75	3.65
80	2	–2.00	8.48	0.54	0.55	3.74	3.65
100	2	–1.90	8.25	0.53	0.34	3.73	3.64
120	2	–2.01	8.45	0.56	0.50	3.74	3.65
140	2	–1.87	8.31	0.56	0.38	3.74	3.63
160	2	–1.80	8.42	0.57	0.51	3.75	3.60
180	2	–1.89	8.46	0.54	0.54	3.80	3.57
200	2	–1.89	5.42	2.41	0.47	3.79	3.58
220	2	–1.85	8.36	0.55	0.43	3.77	3.61
240	2	–1.90	8.37	0.54	0.46	3.76	3.62
260	2	–1.86	8.47	0.53	0.54	3.78	3.62
280	2	–1.86	8.38	0.53	0.46	3.79	3.60
300	2	–1.88	8.44	0.54	0.53	3.71	3.67
320	2	–1.85	6.33	1.57	0.52	3.71	3.68
340	2	–1.91	8.36	0.54	0.44	3.66	3.72
360	2	–1.92	8.46	0.54	0.55	3.68	3.69
380	2	–1.85	5.89	2.01	0.54	3.70	3.66

successfully with the presence of multiple lanes, as well as with the presence of other types of road marks.

5 CONCLUSIONS

The methodology presented in this article contributes to the tasks of MLS processing because, based on road lines extraction, a geometric inventory of the road cross sections is provided. The novelty of the approach remains in the methodology developed which combining consolidated and well-known algorithms allows to provide automatically a geometric inventory of cross sections of roads.

As a result, a CAD model of road can be derived which can be used by the authorities in road maintenance- and management-related tasks.

The two study cases analyzed have tried to provide different significance and representative level of complexity, satisfying the authority expectations because successful results were obtained in the automatic extraction and inventory of road elements. In the first case, which was a 1-km-long motorway with varying number of lanes (e.g., additional lanes), the developed workflow again provided satisfactory results by correctly detecting and inventorying the road. In the second case, the presence of different types of road marks has been successfully solved both in the classification of road marks and the geometric inventory of the road.

Despite the great volume of data generated by these systems, a flexible, efficient and automatic methodology has been developed to extract semantic information. The idea is to extend these capabilities to the Open Source Point Cloud Library (PCL) to improve its computational and algorithmic capabilities in managing big point clouds. Finally, future research should focus on the detection and classification of different road markings using Machine Learning approaches, and integrate the results with the geometric inventory of roads presented in this investigation.

ACKNOWLEDGMENTS

The authors thank Ministerio Ciencia e Innovación (grant No. IPT-2012-1092-120000 and TIN2013-46801-C4-4-R) and Xunta de Galicia (Competitive Referenced Research Groups, Grant No. 2012/269) for the financial support.

REFERENCES

Catálogo de la RCE. (2010), Inventario de la Red de Carreteras del Estado. Dirección General de Carreteras, Ministerio de Fomento.

Belton, D. & Lichti, D. D. (2006), Classification and segmentation of terrestrial laser scanner point clouds using local

variance information. *International Archives of Photogrammetry, Remote Sensing and Spatial Information Sciences*, **36**(Part 5), 44–49.

Department for Transport. (2003), Traffic Signs Manual 2003, Road Markings. Published for the Department for Transport under Licence from the Controller of Her Majesty's Stationery Office (Chapter 5).

Departamento Nacional de Infraestrutura de Transportes – DNIT. (2010), Manual de Sinalização Rodoviária. Instituto de Pesquisas Rodoviárias – IPR. Publ. 743. Rio de Janeiro. 412 p.

Deshpande, S. S. (2013), Improved floodplain delineation method using high density LiDAR data, *Computer-Aided Civil and Infrastructure Engineering*, **28**(1), 68–79.

Ghosh-Dastidar, S., Adeli, H. & Dadmehr, N. (2008), Principal component analysis-enhanced cosine radial basis function neural network for robust epilepsy and seizure detection, *IEEE Transactions on Biomedical Engineering*, **55**(2), 512–18.

Gómez-García-Bermejo, J., Zalama, E. & Feliz, R. (2013), Automated registration of 3D scans using geometric features and normalized color data, *Computer-Aided Civil and Infrastructure Engineering*, **28**(2), 98–111.

Guan, H., Li, J., Yu, Y., Wang, C., Chapman, M. & Yang, B. (2014), Using mobile laser scanning data for automated extraction of road markings, *ISPRS Journal of Photogrammetry and Remote Sensing*, **87**(1), 93–107.

Guo, C., Meguro, J. I., Kojima, Y. & Naito, T. (2014, May). Automatic lane-level map generation for advanced driver assistance systems using low-cost sensors, in *Proceedings of the IEEE International Conference on Robotics and Automation (ICRA)*, 3975–82.

Highway Design Manual. California Department of Transportation, May 2012.

Hillel, A. B., Lerner, R., Levi, D. & Raz, G. (2014), Recent progress in road and lane detection: a survey. *Machine Vision and Applications*, **25**(3), 727–45.

Holgado-Barco, A., González-Aguilera, D., Arias-Sanchez, P. & Martinez-Sanchez, J. (2014), Semi-automatic extraction of road horizontal alignment from a mobile LiDAR system. *Computer-Aided Civil & Infrastructure Engineering*. http://dx.doi.org/10.1111/mice.12087.

Huang, A. S., Moore, D., Antone, M., Olson, E. & Teller, S. (2009), Finding multiple lanes in urban road networks with vision and lidar, *Autonomous Robots*, **26**(2-3), 103–22.

J.A.E.– Norma de Marcas Rodoviárias (1995), Junta Autónoma de Estradas, Almada.

Kumar, P. (2012), Road features extraction using terrestrial mobile laser scanning system. Doctoral dissertation, National University of Ireland Maynooth.

Kumar, P., McElhinney, C.P., Lewis, P. & McCarthy, T. (2013), "An automated algorithm for extracting road edges from terrestrial mobile LiDAR data", *ISPRS Journal of Photogrammetry and Remote Sensing*, **85**, 44–55.

Kumar, P., McElhinney, C. P., Lewis, P. & McCarthy, T. (2014), Automated road markings extraction from mobile laser scanning data, *International Journal of Applied Earth Observation and Geoinformation*, **32**, 125–37.

Lundgren, J., (2011), Splinefit. MATLAB Central File Exchange. Available at: www.mathworks.com/matlabcentral/fileexchange/13812-splinefit. Accessed: February 9, 2015.

Ministerio de Fomento (1987), Norma de carreteras. Norma 8.2 - I.C.: Marcas Viales. Boletín Oficial Del Estado, Número 185, De 4 De Agosto De 1987. Madrid,

Ministerio de Fomento (2000), Instrucción de carreteras. Norma 3.1 - I.C.: Trazado. Boletín Oficial Del Estado, Número 28, De 2 De Febrero De 2000. Madrid,

Pauly, M., Gross, M. & Kobbelt, L. P. (2002), Efficient simplification of point-sampled surfaces, in *Proceedings of the Conference on Visualization'02* 163–70.

Park, H. S. Lee, H. M., Adeli, H. & Lee, I. (2007), A new approach for health monitoring of structures: terrestrial laser scanning, *Computer-Aided Civil and Infrastructure Engineering*, **22**(1), 19–30.

Park, S. W., Park, H. S., Kim, J. H. & Adeli, H. (2015), 3D displacement measurement model for health monitoring of structures using a motion capture system, *Measurement*, **59**, 352–36.

Puente, I., González-Jorge, H., Riveiro, B. & Arias, P. (2013), Accuracy verification of the Lynx Mobile Mapper system, *Optics & Laser Technology*, **45**, 578–86.

Spear, B., Vandervalk, A. & Snyder, D. (2010), Roadway Geometry and Inventory Trade Study for IntelliDriveSM Applications (No. FHWA-HRT-10-073).

Takahashi, G., Takeda, H. & Shimano, Y. (2014), Automatic drawing for traffic marking with mms lidar intensity, in*ISPRS Annals of the Photogrammetry, Remote Sensing and Spatial Information Sciences*, **II-5**, 363–70.

Thuy, M. & León, F. (2010), Lane detection and tracking based on Lidar data, *Metrology and Measurement Systems*, **17**(3), 311–21.

Truong-Hong, L., Laefer, D. F., Hinks, T. & Carr, H. (2013), Combining an angle criterion with voxelization and the flying voxel method in reconstructing building models from LiDAR data, *Computer-Aided Civil and Infrastructure Engineering*, **28**(2), 112–29.

Tsai, M. J. & Han, J. Y. (2013) A preliminary study on the road surface feature extraction using MMS collected point clouds, in *Proceedings of the 34rd Asian Conference on Remote Sensing*, October 20–24, Bali, Indonesia.

Varela-González, M., González-Jorge, H., Riveiro, B. & Arias, P. (2014), Automatic filtering of vehicles from mobile LiDAR datasets, *Measurement*, **53**, 215–23.

Vosselman, G. & H.-G Maas, (2010), *Airborne and Terrestrial Laser Scanning*. Taylor and Francis Group, Boca Raton, FL, USA.

Yang, B., Fang, L., Li, Q. & Li, J. (2012), Automated extraction of road markings from mobile LiDAR point clouds, *Photogrammetric Engineering & Remote Sensing*, **78**(4), 331–38.

Yang, B, Fang, L. & Li, J. 2013. Semi-automated extraction and delineation of 3D roads of street scene from mobile laser scanning point clouds, *ISPRS Journal of Photogrammetry and Remote Sensing* **79**, 80–93.

Yu, Y., Li, J., Guan, H., Jia, F. & Wang, C. (2015), Learning hierarchical features for automated extraction of road markings from 3-D mobile lidar point clouds, *IEEE Journal of Selected Topics in Applied Earth Observations and Remote Sensing*, **8**(2), 709–26.

Zhou, H., Jalayer, M., Gong, J., Hu, S. & Grinter, M. (2013), Investigation of methods and approaches for collecting and recording highway inventory data, *FHWA-ICT*, 13-022.

CAPÍTULO 4

CONCLUSIONES Y PERSPECTIVAS FUTURAS

CONCLUSIONES Y PERSPECTIVAS FUTURAS

En esta Tesis Doctoral se ha demostrado que las herramientas desarrolladas contribuyen a la aplicación de sistemas de cartografiado móvil (MMS) y en concreto los sistemas LiDAR móvil (MLS), permitiendo automatizar tareas de inspección e inventario de carreteras y obteniendo unos resultados métricos precisos de los elementos geométricos que componen el trazado topográfico horizontal y vertical de la carretera, el inventario de elementos horizontales (nº carriles), así como la señalización horizontal (líneas de carretera). Las principales ventajas que nos ofrecen tanto los MLS como las herramientas desarrolladas son: documentar la totalidad de la carretera sin tener ningún impedimento a la circulación del resto de vehículos así como obtener la información geométrica de la carretera con las herramientas desarrolladas. La combinación de ambas hace que se pueda extraer la geometría de la carretera con mayor rapidez y eficacia, garantizando una gran reducción de los tiempos de procesado comparándolo con las técnicas tradicionales.

A continuación, tras la consecución de los objetivos propuestos en esta investigación, se desarrollarán en profundidad las conclusiones obtenidas correspondientes a cada uno de los artículos científicos, además de prever unas líneas de trabajo futuras basadas en la ampliación del estudio realizado que permiten seguir avanzando con esta geotecnología en constante evolución.

4.1. Conclusiones

En primer lugar en base al objetivo general se desarrolló un novedoso y eficiente método para la extracción semiautomática del eje de la carretera junto con la estimación de su trazado horizontal según las

especificaciones oficiales españolas (Norma 3.1- IC. Trazado). Dichas estimaciones son importantes para aplicaciones relacionadas con la inspección e inventariado de carreteras e incluso para proporcionar mapas de riesgos en accidentes de tráfico. En el método propuesto se desarrolló un protocolo para la detección de las calzadas, así como un sistema que nos permitiera detectar la marca vial que actuaría de eje de la carretera a partir de los datos LiDAR. Obtenido el eje se llevó a cabo una estrategia con la que obtener el trazado geométrico horizontal (rectas, curvas circulares y clotoides) a partir de dicho eje de la carretera. El proceso desarrollado es un método útil para automatizar de forma precisa las características geométricas asociadas al trazado horizontal de la carretera.

En segundo lugar se ha desarrollado una metodología con la que poder estimar las características geométricas del trazado vertical. En este proceso se aplicó el mismo protocolo desarrollado para la detección de las calzadas junto con una metodología en la que se aplican simples algoritmos con los que determinar los elementos geométricos que mejor definen su trazado vertical en la dirección longitudinal (rasantes y acuerdos verticales) y transversal (peraltes). El proceso desarrollado es un método útil para automatizar de forma precisa las características geométricas asociadas al trazado vertical de la carretera.

Sin embargo, la principal desventaja de estas metodologías radica en el establecimiento de umbrales por parte del usuario. El primero de ellos relacionado con el umbral angular fijado para segmentar tanto la calzada como la marca vial que actúa de eje de la carretera y el segundo basado en el umbral de intensidad necesario para la detección de las marcas viales. Dada la gran variedad de anchuras en marcas y carreteras, así como los diferentes estados de conservación de las propias marcas viales, esta umbralización no podrá ser universalizada. Con el objetivo de mejorar estas desventajas se ha desarrollado la tercera y última metodología con la que poder corregir este tipo de problemáticas.

Esta última metodología supone un avance en las tareas de procesamiento de datos MLS, ya que integra estrategias de segmentación de la plataforma, detección y clasificación de marcas viales, así como la

extracción de perfiles transversales a partir de los cuales obtener la información geométrica de la sección transversal de la carretera (nº carriles, ancho plataforma, ancho arcenes, ancho carriles).

La contribución más importante radica en la automatización completa de la carretera, la detección de las marcas viales, la clasificación semántica de las marcas viales longitudinales y la delineación CAD de las mismas, sin requerir la dependencia de umbrales angulares y de intensidad fijados por el usuario, así como ninguna limitación asociada al número de carriles de las carreteras, ni la dependencia de la trayectoria seguida por el vehículo MLS. Siendo un método robusto ante la presencia de múltiples carriles así como en la variación de los mismos (p. ej.: carriles de entrada o salida).

El poder generar el modelo CAD de la carretera de una forma automática y precisa es importante para poder realizar mapas de navegación que se podrían emplear para asistir de forma inteligente al conductor, así como para el inventario de carreteras que lo podrían utilizar las administraciones gestoras, para el mantenimiento de las mismas.

Como conclusión general de la Tesis Doctoral, se verifica que la aplicación de los sistemas de cartografiado móvil junto con las metodologías desarrolladas arrojan resultados satisfactorios a la hora de determinar el trazado tanto horizontal como vertical, así como el inventariado geométrico de los perfiles transversales, lo que implica la utilidad de estas metodologías hacia una alternativa a la hora de realizar los inventarios geométricos de carreteras, así como de la generación de modelos as-built de la carretera para verificar la construcción respecto al modelo diseñado.

4.2. Perspectivas Futuras

Debido a la ingente información capturada por los sistemas de cartografiado móvil, proponemos una serie de líneas futuras de investigación vinculadas al desarrollo de esta Tesis Doctoral. Algunas de

estas propuestas siguen en la línea de los inventarios geométricos como puede ser:

- El reconocimiento de la señalización vertical a partir de la integración de información LiDAR y RGB.
- La detección e inventario de la señalización horizontal.
- La extracción de los gálibos en los pasos superiores de las carreteras.
- El inventario del equipamiento de las carreteras (p. ej.: balizamiento, hitos, biondas, luminarias, etc.).
- Cartografía de detalle para vehículos autónomos.

También líneas relacionadas con los sistemas MMS pero en el ámbito urbano que permitirán ejecutar proyectos integrales de planeamiento urbanístico. A pesar de que se espera que el cartografiado urbano sea la aplicación que marque la senda futura de la tecnología MMS durante los años venideros, hasta el momento, únicamente un reducido número de compañías en todo el mundo están ofreciendo este tipo de solución enfocada específicamente a los ambientes urbanos. Es evidente que existe un número creciente de expertos en el mundo del MMS en ámbitos como la inspección de carreteras, la administración de infraestructuras o el cartografiado de minas o costas, pero, por el contrario, los MMS urbanos se encuentran todavía en su etapa inicial. Las soluciones MMS aplicadas a entornos urbanos proporcionan una mayor resolución espacial que otras técnicas tradicionales, como las que se basan en imágenes aéreas o de satélite, así como una toma de datos veloz en un periodo de tiempo corto.

CAPÍTULO 5

BIBLIOGRAFÍA

BIBLIOGRAFÍA

Alho, P., Kukko, A., Hyyppä, H., Kaartinen, H., Hyyppä, J., & Jaakkola, A. (2009). *Application of boat-based laser scanning for river survey*. Earth Surface Processes and Landforms, 34(13), 1831-1838.

Cheng, W., Hassan, T., El-Sheimy, N. & Lavigne, M. (2008), *Automatic road vector extraction for mobile mapping systems*, The International Archives of the Photogrammetry, Remote Sensing and Spatial Information Sciences, 37(Part B3b), 515–21.

Di Mascio, P., Di Vito, M., Loprencipe, G. & Ragnoli, A. (2012), *Procedure to determine the geometry of road alignment using GPS data*, Procedia-Social and Behavioral Sciences, 53, 1203–16.

Díaz-Vilariño, L., González-Jorge, H., Bueno, M., Arias, P., & Puente, I. (2016). *Automatic classification of urban pavements using mobile LiDAR data and roughness descriptors.* Construction and Building Materials, 102, 208-215.

El-Halawany, S. I., & Lichti, D. D. (2011, January). *Detection of road poles from mobile terrestrial laser scanner point cloud.* In Multi-Platform/Multi-Sensor Remote Sensing and Mapping (M2RSM), 2011 International Workshop on (pp. 1-6). IEEE.

El-Rabbany, A. (2002). *GPS Positioning Modes, Introduction to GPS: the Global Positioning System*, Artech House, Inc., Norwood, MA, pp.69-83.

El-Sheimy, N. (2005, April). *An overview of mobile mapping systems.* In FIG Working Week (pp. 16-21).

FARO, (2016).*Homepage of the company FARO Technologies*, Inc., URL: http://www.faro.com.

Goad, C. C. (1991). *The Ohio State University highway mapping project: the positioning component.* In Proceedings of the 47th Annual Meeting of The Institute of Navigation (pp. 117-120).

Gräfe, G. (2008). *Kinematic 3D laser scanning for road or railway construction surveys.* In Proceedings of the International Conference on Machine Control & Guidance (pp. 24-26).

Guan, H., Li, J., Yu, Y., Ji, Z., & Wang, C. (2015). *Using mobile LiDAR data for rapidly updating road markings.* Intelligent Transportation Systems, IEEE Transactions on, 16(5), 2457-2466.

Hervieu, A., & Soheilian, B. (2013). *Semi-Automatic Road/Pavement Modeling using Mobile Laser Scanning.* ISPRS Annals of Photogrammetry, Remote Sensing and Spatial Information Sciences, 1(3), 31-36.

Huerta, E., Mangiaterra, A., & Noguera, G. (2005). *GPS: posicionamiento satelital.* Rosario: UNR Editora, Universidad Nacional de Rosario, 148p.

Kaasalainen, S., Kaartinen, H., Kukko, A., Anttila, K., & Krooks, A. (2011). Brief communication, *Application of mobile laser scanning in snow cover profiling*. The Cryosphere, 5(1), 135-138.

Kavanagh, R. M. (2007). *Gyroscopes for orientation and inertial navigation systems.* Cartography and Geoinformation, 6, 255-271.

Lakakis, K., Savvaidis, P. & Wunderlich, T. (2013), *Evaluation of a low-cost mobile mapping and inspection system for road safety classification*, American Journal of Geographic Information System, 2(1), 6–14.

LEICA, (2016). *Homepage of the company Leica Geosystems*, URL: http://www.leica-geosystems.com.

Novak, K. (1991, June). *The Ohio State University highway mapping system: The stereo vision system component.* In Proceedings of the 47th Annual Meeting of The Institute of Navigation (pp. 121-124).

OPTECH, (2016). *Homepage of the company OPTECH*, URL: http://www. teledyneoptech.com.

Petrie, G. (2010). *Mobile mapping systems: An introduction to the technology*. GeoInformatics, 13(1), 32-43.

Pu, S., Rutzinger, M., Vosselman, G., & Oude Elberink, S. (2011). *Recognizing basic structures from mobile laser scanning data for road inventory studies.* ISPRS Journal of Photogrammetry and Remote Sensing, 66(6), S28-S39.

RIEGL, (2016). *Homepage of the company RIEGL Laser Measurement Systems GmbH*, URL: http://www.riegl.com.

SICK, (2016). *Homepage of the company SICK Group*, URL: http://www.sick.com.

Soheilian, B., Paparoditis, N., & Boldo, D. (2010). *3D road marking reconstruction from street-level calibrated stereo pairs.* ISPRS Journal of Photogrammetry and Remote Sensing, 65(4), 347-359.

Tin Leung, K., Whidborne, J. F., Purdy, D., & Dunoyer, A. (2011). *A review of ground vehicle dynamic state estimations utilising GPS/INS.* Vehicle System Dynamics, 49(1-2), 29-58.

Titterton, D., & Weston, J. L. (2004). *Strapdown inertial navigation technology* 2nd Edition, Institution of Engineering and Technology, Stevenage, UK.

TOPCON, (2016). *Homepage of TOPCON Global Gateway*, URL: http://www.topconpositioning.com.

TRIMBLE, (2016). *Homepage of the company TRIMBLE*, URL: http://www.trimble.com.

Tsai, Y. J., Ai, C., Wang, Z. & Pitts, E. (2013), *A mobile cross slope measurement method using LiDAR*, Technology, 2(3), 53–59.

Yang, B., Fang, L. & Li, J. (2013), *Semi-automated extraction and delineation of 3D roads of street scene from mobile laser scanning point clouds*, ISPRS Journal of Photogrammetry and Remote Sensing, 79, 80–93.

Yu, Y., Li, J., Guan, H., Jia, F., & Wang, C. (2015). *Learning hierarchical features for automated extraction of road markings from 3-D mobile LIDAR point clouds.* Selected Topics in Applied Earth Observations and Remote Sensing, IEEE Journal of, 8(2), 709-726.

Zarchan, P. and Musoff, H. (2009). *Fundamentals of Kalman Filtering: a practical Approach*, 3rd Edition, American Institute of Aeronautics & Astronautics (AIAA), Reston, VA, 854 p.

Zoller+Fröhlich, (2016). *Homepage of the company Zoller+Fröhlich GmbH*, URL: http://www.zf-laser.com.

APÉNDICE A

INDEXACIÓN Y FACTOR DE IMPACTO DE LAS PUBLICACIONES

Apéndice A. Indexación y factor de impacto de las publicaciones

Todos los artículos realizados en esta Tesis Doctoral se encuentran **publicados** en **revistas** del **primer decil**. En el caso del primer y tercer artículo se publicaron en la revista número 1 en el área de ingeniería civil (Computer-Aided Civil and Infrastructure Engineering). Respecto al segundo artículo se publicó en la revista número 6 en el área de sensor remoto (ISPRS Journal of Photogrammetry and Remote Sensing).

A.1. Semi-Automatic extraction of road horizontal alignment from a mobile LiDAR system

Descripción de factor de impacto y documentación de la revista

Nombre de la revista:	**Computer-Aided Civil and Infrastructure Engineering**
URL:	**http://onlinelibrary.wiley.com/journal/10.1111/%28ISSN%291467-8667**
Editorial:	**WILEY ONLINE LIBRARY**
ISSN:	**1467-8667**
Factor de impacto (2014):	**4.925**
Ranking de la revista:	**1/59 (Construction & Building Technology)** **1/125 (Engineering Civil)**
Cuartil:	**Q1**

ISI Web of Knowledge℠

Journal Citation Reports®

WELCOME | HELP | RETURN TO LIST

2014 JCR Science Edition

Journal: COMPUTER-AIDED CIVIL AND INFRASTRUCTURE ENGINEERING

Mark	Journal Title	ISSN	Total Cites	Impact Factor	5-Year Impact Factor	Immediacy Index	Citable Items	Cited Half-life	Citing Half-life
☐	COMPUT-AIDED CIV INF	1093-9687	1834	4.925	4.021	0.480	50	5.4	8.2

Cited Journal | Citing Journal | Source Data | Journal Self Cites

CITED JOURNAL DATA | CITING JOURNAL DATA | IMPACT FACTOR TREND | RELATED JOURNALS

Journal Information

Full Journal Title: COMPUTER-AIDED CIVIL AND INFRASTRUCTURE ENGINEERING
ISO Abbrev. Title: Comput.-Aided Civil Infrastruct. Eng.
JCR Abbrev. Title: COMPUT-AIDED CIV INF
ISSN: 1093-9687
Issues/Year: 10
Language: ENGLISH
Journal Country/Territory: UNITED STATES
Publisher: WILEY-BLACKWELL
Publisher Address: 111 RIVER ST, HOBOKEN 07030-5774, NJ,
Subject Categories: COMPUTER SCIENCE, INTERDISCIPLINARY APPLICATIONS
SCOPE NOTE | VIEW JOURNAL SUMMARY LIST | VIEW CATEGORY DATA
CONSTRUCTION & BUILDING TECHNOLOGY SCOPE NOTE
VIEW JOURNAL SUMMARY LIST | VIEW CATEGORY DATA
ENGINEERING, CIVIL SCOPE NOTE | VIEW JOURNAL SUMMARY LIST
VIEW CATEGORY DATA
TRANSPORTATION SCIENCE & TECHNOLOGY SCOPE NOTE
VIEW JOURNAL SUMMARY LIST | VIEW CATEGORY DATA

Journal Rank in Categories: JOURNAL RANKING

***Eigenfactor*® Metrics**
***Eigenfactor*® Score**
0.00394
***Article Influence*® Score**
1.037

Journal Impact Factor

Cites in 2014 to items published in: 2013 = 218, 2012 = 309, Sum: 527
Number of items published in: 2013 = 54, 2012 = 53, Sum: 107

Calculation: Cites to recent items 527 / Number of recent items 107 = **4.925**

5-Year Journal Impact Factor

Cites in {2014} to items published in: 2013 = 218, 2012 = 309, 2011 = 188, 2010 = 136, 2009 = 110, Sum: 961
Number of items published in: 2013 = 54, 2012 = 53, 2011 = 43, 2010 = 44, 2009 = 45, Sum: 239

Calculation: Cites to recent items 961 / Number of recent items 239 = **4.021**

Journal Self Cites

The tables show the contribution of the journal's self cites to its impact factor. This information is also represented in the cited journal graph.

Total Cites	1834	**Self Cites**	512 (27% of 1834)
Cites to Years Used in Impact Factor Calculation	527	**Self Cites to Years Used in Impact Factor Calculation**	207 (39% of 527)
Impact Factor	4.925	**Impact Factor without Self Cites**	2.991

Journal Immediacy Index

Cites in 2014 to items published in 2014 = 24
Number of items published in 2014 = 50
Calculation: Cites to current items 24 = **0.480**
Number of current items 50

Journal Cited Half-Life

The cited half-life for the journal is the median age of its items cited in the current JCR year. Half of the citations to the journal are to items published within the cited half-life.

Cited Half-Life: 5.4 years

Breakdown of the citations ***to the journal*** by the cumulative percent of 2014 cites to items published in the following years:

Cited Year	2014	2013	2012	2011	2010	2009	2008	2007	2006	2005	2004-all
# Cites from 2014	24	218	309	188	136	110	129	110	108	83	419
Cumulative %	1.31	13.20	30.04	40.29	47.71	53.71	60.74	66.74	72.63	77.15	100

Cited Half-Life Calculations:
The cited half-life calculation finds the number of publication years from the current JCR year that account for 50% of citations received by the journal. Read help for more information on the calculation.

Cited Journal Graph

Click here for Cited Journal data table

This graph shows the distribution by cited year of citations to items published in the journal COMPUT-AIDED CIV INF.

Citations to the journal (per cited year)

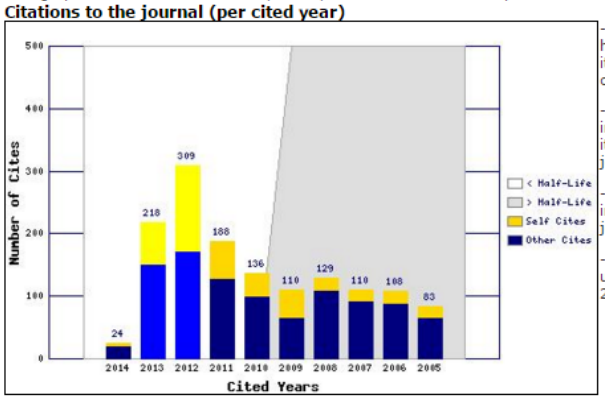

- The white/grey division indicates the cited half-life (if < 10.0). Half of the journal's cited items were published more recently than the cited half-life.

- The top (gold) portion of each column indicates Journal Self Citations: citations to items in the journal from items in the same journal.

- The bottom (blue) portion of each column indicates Non-Self Citations: citations to the journal from items in other journals.

- The two lighter columns indicate citations used to calculate the Impact Factor (always the 2nd and 3rd columns).

Journal Citing Half-Life

The citing half-life for the journal is the median age of the items the journal cited in the current JCR year. Half of the citations in the journal are to items published within the citing half-life.

Citing Half-Life: 8.2 years

Breakdown of the citations ***from the journal*** by the cumulative percent of 2014 cites to items published in the following years:

Cited Year	2014	2013	2012	2011	2010	2009	2008	2007	2006	2005	2004-all
# Cites from 2014	7	155	297	207	163	186	166	135	158	106	1115
Cumulative %	0.26	6.01	17.03	24.71	30.76	37.66	43.82	48.83	54.69	58.63	100

Citing Half-Life Calculations:
The citing half-life calculation finds the number of publication years from the current JCR year that account for 50% of citations in the journal. Read help for more information on the calculation.

Citing Journal Graph

Click here for Citing Journal data table

This graph shows the distribution by cited year of citations from current-year items in the journal COMPUT-AIDED CIV INF.

Citations from the journal (per cited year)

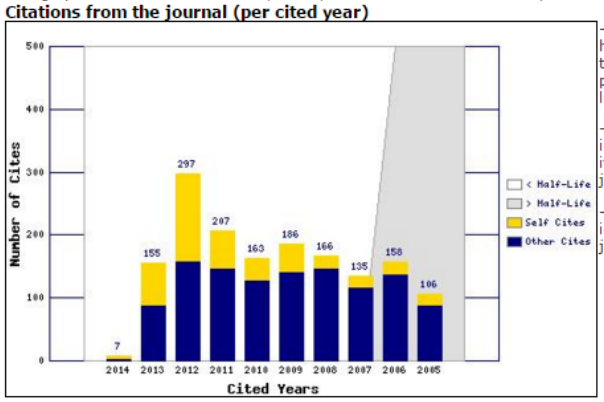

- The white/grey division indicates the citing half-life (if < 10.0). Half of the citations from the journal's current items are to items published more recently than the citing half-life.

- The top (gold) portion of each column indicates Journal Self-Citations: citations from items in the journal to items in the same journal.

- The bottom (blue) portion of each column indicates Non-Self Citations: citations from the journal to items in other journals.

Journal Source Data

	Citable items			
	Articles	**Reviews**	**Combined**	**Other items**
Number in JCR year 2014 (A)	50	0	50	5
Number of references (B)	2695	0	2695	0.00
Ratio (B/A)	53.9	0.0	53.9	0.0

Rank in Category: COMPUTER-AIDED CIVIL AND INFRASTRUCTURE ENGINEERIN...

Journal Ranking

For **2014**, the journal **COMPUTER-AIDED CIVIL AND INFRASTRUCTURE ENGINEERIN...** has an Impact Factor of **4.925**.

This table shows the ranking of this journal in its subject categories based on Impact Factor.

Category Name	Total Journals in Category	Journal Rank in Category	Quartile in Category
COMPUTER SCIENCE, INTERDISCIPLINARY APPLICATIONS	102	1	Q1
CONSTRUCTION & BUILDING TECHNOLOGY	59	1	Q1
ENGINEERING, CIVIL	125	1	Q1
TRANSPORTATION SCIENCE & TECHNOLOGY	33	1	Q1

Category Box Plot

For **2014**, the journal **COMPUTER-AIDED CIVIL AND INFRASTRUCTURE ENGINEERIN...** has an Impact Factor of **4.925**.

This is a box plot of the subject category or categories to which the journal has been assigned. It provides information about the distribution of journals based on Impact Factor values. It shows median, 25th and 75th percentiles, and the extreme values of the distribution.

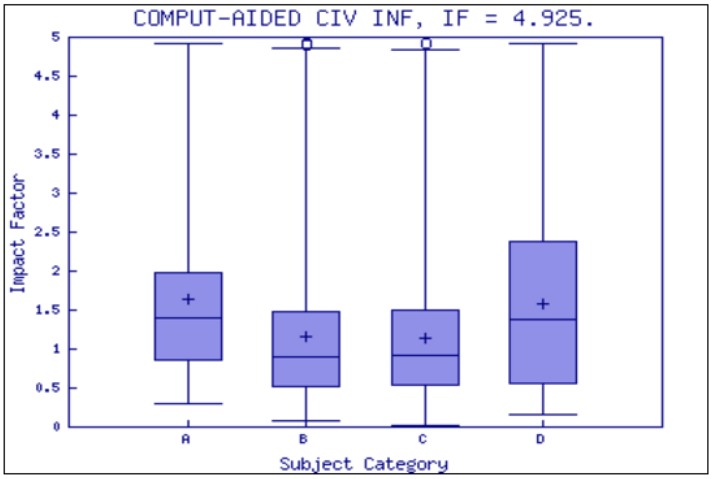

Key

A - COMPUTER SCIENCE, INTERDISCIPLINARY APPLICATIONS

B - CONSTRUCTION & BUILDING TECHNOLOGY

C - ENGINEERING, CIVIL

D - TRANSPORTATION SCIENCE & TECHNOLOGY

A.2. An automated approach to vertical road characterisation using mobile LiDAR systems: Longitudinal profiles and cross-sections

Descripción de factor de impacto y documentación de la revista

Nombre de la revista:	**ISPRS Journal of Photogrammetry and Remote Sensing**
URL:	**http://www.journals.elsevier.com/isprs-journal-of-photogrammetry-and-remote-sensing/**
Editorial:	**ELSEVIER**
ISSN:	**0924-2716**
Factor de impacto (2014):	**3.132**
Ranking de la revista:	**4/24 (Imaging Science & Photographic Technology)** **6/28 (Remote Sensing)**
Cuartil:	**Q1**

ISI Web of Knowledge℠

Journal Citation Reports®

WELCOME | HELP | RETURN TO LIST

2014 JCR Science Edition

Journal: ISPRS JOURNAL OF PHOTOGRAMMETRY AND REMOTE SENSING

Mark	Journal Title	ISSN	Total Cites	Impact Factor	5-Year Impact Factor	Immediacy Index	Citable Items	Cited Half-life	Citing Half-life
☐	ISPRS J PHOTOGRAMM	0924-2716	4120	3.132	4.652	0.890	172	5.5	7.4

Cited Journal | Citing Journal | Source Data | Journal Self Cites

CITED JOURNAL DATA | CITING JOURNAL DATA | IMPACT FACTOR TREND | RELATED JOURNALS

Journal Information

Full Journal Title: ISPRS JOURNAL OF PHOTOGRAMMETRY AND REMOTE SENSING
ISO Abbrev. Title: ISPRS-J. Photogramm. Remote Sens.
JCR Abbrev. Title: ISPRS J PHOTOGRAMM
ISSN: 0924-2716
Issues/Year: 4
Language: MULTI-LANGUAGE
Journal Country/Territory: NETHERLANDS
Publisher: ELSEVIER SCIENCE BV
Publisher Address: PO BOX 211, 1000 AE AMSTERDAM, NETHERLANDS
Subject Categories: GEOGRAPHY, PHYSICAL — SCOPE NOTE | VIEW JOURNAL SUMMARY LIST | VIEW CATEGORY DATA
GEOSCIENCES, MULTIDISCIPLINARY — SCOPE NOTE | VIEW JOURNAL SUMMARY LIST | VIEW CATEGORY DATA
REMOTE SENSING — SCOPE NOTE | VIEW JOURNAL SUMMARY LIST | VIEW CATEGORY DATA
IMAGING SCIENCE & PHOTOGRAPHIC TECHNOLOGY — SCOPE NOTE | VIEW JOURNAL SUMMARY LIST | VIEW CATEGORY DATA

***Eigenfactor*® Metrics**
***Eigenfactor*® Score** 0.00771
***Article Influence*® Score** 1.062

Journal Rank in Categories: JOURNAL RANKING

Journal Impact Factor

Cites in 2014 to items published in: 2013 = 343, 2012 = 415, Sum: 758
Number of items published in: 2013 = 142, 2012 = 100, Sum: 242

Calculation: Cites to recent items 758 / Number of recent items 242 = **3.132**

5-Year Journal Impact Factor

Cites in {2014} to items published in: 2013 = 343, 2012 = 415, 2011 = 519, 2010 = 439, 2009 = 410, Sum: 2126
Number of items published in: 2013 = 142, 2012 = 100, 2011 = 93, 2010 = 54, 2009 = 68, Sum: 457

Calculation: Cites to recent items 2126 / Number of recent items 457 = **4.652**

Journal Self Cites

The tables show the contribution of the journal's self cites to its impact factor. This information is also represented in the cited journal graph.

Total Cites	4120	**Self Cites**	461 (11% of 4120)
Cites to Years Used in Impact Factor Calculation	758	**Self Cites to Years Used in Impact Factor Calculation**	123 (16% of 758)
Impact Factor	3.132	**Impact Factor without Self Cites**	2.624

Journal Immediacy Index

Cites in 2014 to items published in 2014 = 153
Number of items published in 2014 = 172
Calculation: Cites to current items 153 = **0.890**
Number of current items 172

Journal Cited Half-Life

The cited half-life for the journal is the median age of its items cited in the current JCR year. Half of the citations to the journal are to items published within the cited half-life.

Cited Half-Life: 5.5 years

Breakdown of the citations ***to the journal*** by the cumulative percent of 2014 cites to items published in the following years:

Cited Year	2014	2013	2012	2011	2010	2009	2008	2007	2006	2005	2004-all
# Cites from 2014	153	343	415	519	439	410	240	270	181	99	1051
Cumulative %	3.71	12.04	22.11	34.71	45.36	55.32	61.14	67.69	72.09	74.49	100

Cited Half-Life Calculations:
The cited half-life calculation finds the number of publication years from the current JCR year that account for 50% of citations received by the journal. Read help for more information on the calculation.

Cited Journal Graph

Click here for Cited Journal data table

This graph shows the distribution by cited year of citations to items published in the journal ISPRS J PHOTOGRAMM.

Citations to the journal (per cited year)

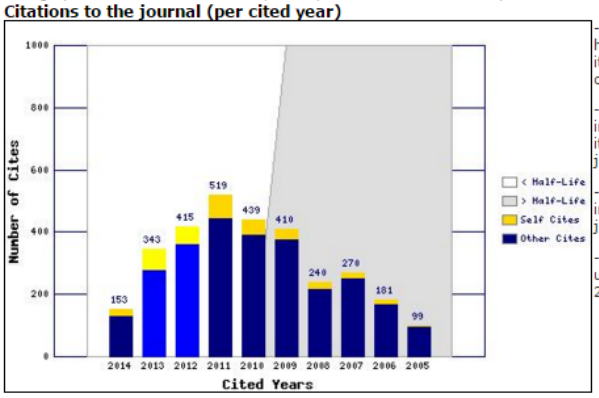

- The white/grey division indicates the cited half-life (if < 10.0). Half of the journal's cited items were published more recently than the cited half-life.

- The top (gold) portion of each column indicates Journal Self Citations: citations to items in the journal from items in the same journal.

- The bottom (blue) portion of each column indicates Non-Self Citations: citations to the journal from items in other journals.

- The two lighter columns indicate citations used to calculate the Impact Factor (always the 2nd and 3rd columns).

Journal Citing Half-Life

The citing half-life for the journal is the median age of the items the journal cited in the current JCR year. Half of the citations in the journal are to items published within the citing half-life.

Citing Half-Life: 7.4 years

Breakdown of the citations ***from the journal*** by the cumulative percent of 2014 cites to items published in the following years:

Cited Year	2014	2013	2012	2011	2010	2009	2008	2007	2006	2005	2004-all
# Cites from 2014	132	530	797	754	665	601	656	467	475	424	3136
Cumulative %	1.53	7.66	16.89	25.62	33.32	40.28	47.88	53.28	58.78	63.69	100

Citing Half-Life Calculations:
The citing half-life calculation finds the number of publication years from the current JCR year that account for 50% of citations in the journal. Read help for more information on the calculation.

Citing Journal Graph

Click here for Citing Journal data table

This graph shows the distribution by cited year of citations from current-year items in the journal ISPRS J PHOTOGRAMM.

Citations from the journal (per cited year)

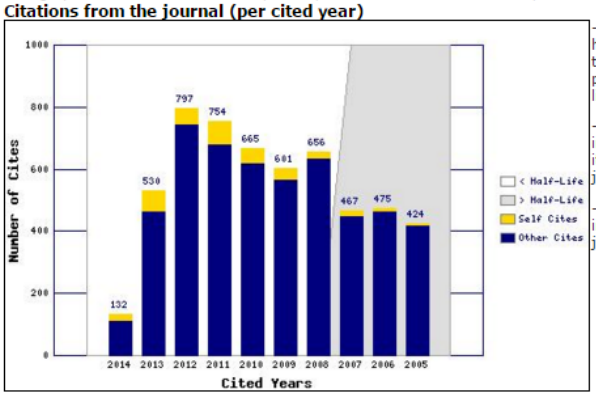

- The white/grey division indicates the citing half-life (if < 10.0). Half of the citations from the journal's current items are to items published more recently than the citing half-life.

- The top (gold) portion of each column indicates Journal Self-Citations: citations from items in the journal to items in the same journal.

- The bottom (blue) portion of each column indicates Non-Self Citations: citations from the journal to items in other journals.

Journal Source Data

	Citable items			
	Articles	**Reviews**	**Combined**	**Other items**
Number in JCR year 2014 (A)	166	6	172	1
Number of references (B)	8111	526	8637	0.00
Ratio (B/A)	48.9	87.7	50.2	0.0

Rank in Category: ISPRS JOURNAL OF PHOTOGRAMMETRY AND REMOTE SENSING

Journal Ranking

For **2014**, the journal **ISPRS JOURNAL OF PHOTOGRAMMETRY AND REMOTE SENSING** has an Impact Factor of **3.132**.

This table shows the ranking of this journal in its subject categories based on Impact Factor.

Category Name	Total Journals in Category	Journal Rank in Category	Quartile in Category
GEOGRAPHY, PHYSICAL	46	9	Q1
GEOSCIENCES, MULTIDISCIPLINARY	175	24	Q1
IMAGING SCIENCE & PHOTOGRAPHIC TECHNOLOGY	24	4	Q1
REMOTE SENSING	28	6	Q1

Category Box Plot

For **2014**, the journal **ISPRS JOURNAL OF PHOTOGRAMMETRY AND REMOTE SENSING** has an Impact Factor of **3.132**.

This is a box plot of the subject category or categories to which the journal has been assigned. It provides information about the distribution of journals based on Impact Factor values. It shows median, 25th and 75th percentiles, and the extreme values of the distribution.

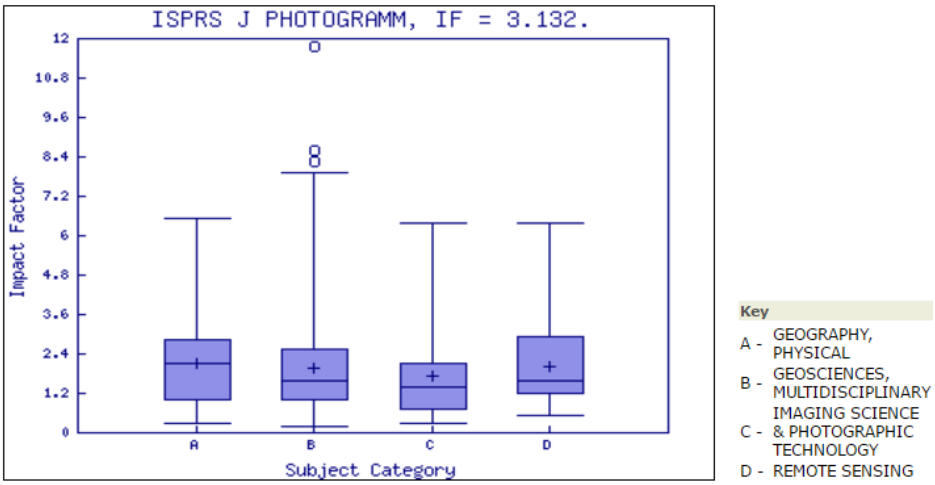
ISPRS J PHOTOGRAMM, IF = 3.132.
Impact Factor
12
10.8
9.6
8.4
7.2
6
4.8
3.6
2.4
1.2
0
A
B
C
D
Subject Category
Key
A - GEOGRAPHY, PHYSICAL
B - GEOSCIENCES, MULTIDISCIPLINARY
C - IMAGING SCIENCE & PHOTOGRAPHIC TECHNOLOGY
D - REMOTE SENSING

A.3. Automation in the geometric inventory of roads from a Mobile LiDAR System

Carta de aceptación

Re: Automatic inventory of road cross sections from Mobile Laser Scanning system

A. Holgado-Barco, **Belén Riveiro**, Diego González-Aguilera, and Pedro Arias (Spain)

Dear Dr. Riveiro:

I am pleased to inform you that your above-referenced-manuscript has been accepted for publication in **Computer-Aided Civil and Infrastructure Engineering**. You will receive the proofs of your article in due time. To expedite the publication process please return the proofs promptly by Email. Thank you.

Regards,

Hojjat Adeli, Distinguished Member ASCE, Fellow AAAS, Fellow IEEE, Fellow AIMBE, Fellow American Neurological Association
Professor
Editor-in-Chief, **Computer-Aided Civil and Infrastructure Engineering**
Mailing address:
College of Engineering
The Ohio State University
470 Hitchcock Hall, 2070 Neil Avenue
Columbus, Ohio 43210 U.S.A.

Descripción de factor de impacto y documentación de la revista

Nombre de la revista:	**Computer-Aided Civil and Infrastructure Engineering**
URL:	**http://onlinelibrary.wiley.com/journal/10.1111/%28ISSN%291467-8667**
Editorial:	**WILEY ONLINE LIBRARY**
ISSN:	**1467-8667**
Factor de impacto (2014):	**4.925**
Ranking de la revista:	**1/59 (Construction & Building Technology)** **1/125 (Engineering Civil)**
Cuartil:	**Q1**

ISI Web of Knowledge℠

Journal Citation Reports®

WELCOME | HELP | RETURN TO LIST

2014 JCR Science Edition

Journal: COMPUTER-AIDED CIVIL AND INFRASTRUCTURE ENGINEERING

Mark	Journal Title	ISSN	Total Cites	Impact Factor	5-Year Impact Factor	Immediacy Index	Citable Items	Cited Half-life	Citing Half-life
☐	COMPUT-AIDED CIV INF	1093-9687	1834	4.925	4.021	0.480	50	5.4	8.2

Cited Journal | Citing Journal | Source Data | Journal Self Cites

CITED JOURNAL DATA | CITING JOURNAL DATA | IMPACT FACTOR TREND | RELATED JOURNALS

Journal Information

Full Journal Title: COMPUTER-AIDED CIVIL AND INFRASTRUCTURE ENGINEERING
ISO Abbrev. Title: Comput.-Aided Civil Infrastruct. Eng.
JCR Abbrev. Title: COMPUT-AIDED CIV INF
ISSN: 1093-9687
Issues/Year: 10
Language: ENGLISH
Journal Country/Territory: UNITED STATES
Publisher: WILEY-BLACKWELL
Publisher Address: 111 RIVER ST, HOBOKEN 07030-5774, NJ,
Subject Categories: COMPUTER SCIENCE, INTERDISCIPLINARY APPLICATIONS
SCOPE NOTE | VIEW JOURNAL SUMMARY LIST | VIEW CATEGORY DATA
CONSTRUCTION & BUILDING TECHNOLOGY SCOPE NOTE
VIEW JOURNAL SUMMARY LIST | VIEW CATEGORY DATA
ENGINEERING, CIVIL SCOPE NOTE | VIEW JOURNAL SUMMARY LIST
VIEW CATEGORY DATA
TRANSPORTATION SCIENCE & TECHNOLOGY SCOPE NOTE
VIEW JOURNAL SUMMARY LIST | VIEW CATEGORY DATA

Journal Rank in Categories: JOURNAL RANKING

***Eigenfactor*® Metrics**
***Eigenfactor*® Score**
0.00394
***Article Influence*® Score**
1.037

Journal Impact Factor

Cites in 2014 to items published in: 2013 = 218, 2012 = 309, Sum: 527
Number of items published in: 2013 = 54, 2012 = 53, Sum: 107

Calculation: Cites to recent items 527 / Number of recent items 107 = **4.925**

5-Year Journal Impact Factor

Cites in {2014} to items published in: 2013 = 218, 2012 = 309, 2011 = 188, 2010 = 136, 2009 = 110, Sum: 961
Number of items published in: 2013 = 54, 2012 = 53, 2011 = 43, 2010 = 44, 2009 = 45, Sum: 239

Calculation: Cites to recent items 961 / Number of recent items 239 = **4.021**

Journal Self Cites

The tables show the contribution of the journal's self cites to its impact factor. This information is also represented in the cited journal graph.

Total Cites	1834	**Self Cites**	512 (27% of 1834)
Cites to Years Used in Impact Factor Calculation	527	**Self Cites to Years Used in Impact Factor Calculation**	207 (39% of 527)
Impact Factor	4.925	**Impact Factor without Self Cites**	2.991

Journal Immediacy Index

Cites in 2014 to items published in 2014 = 24
Number of items published in 2014 = 50
Calculation: Cites to current items 24 = **0.480**
Number of current items 50

Journal Cited Half-Life

The cited half-life for the journal is the median age of its items cited in the current JCR year. Half of the citations to the journal are to items published within the cited half-life.

Cited Half-Life: 5.4 years

Breakdown of the citations ***to the journal*** by the cumulative percent of 2014 cites to items published in the following years:

Cited Year	2014	2013	2012	2011	2010	2009	2008	2007	2006	2005	2004-all
# Cites from 2014	24	218	309	188	136	110	129	110	108	83	419
Cumulative %	1.31	13.20	30.04	40.29	47.71	53.71	60.74	66.74	72.63	77.15	100

Cited Half-Life Calculations:
The cited half-life calculation finds the number of publication years from the current JCR year that account for 50% of citations received by the journal. Read help for more information on the calculation.

Cited Journal Graph

Click here for Cited Journal data table

This graph shows the distribution by cited year of citations to items published in the journal COMPUT-AIDED CIV INF.

Citations to the journal (per cited year)

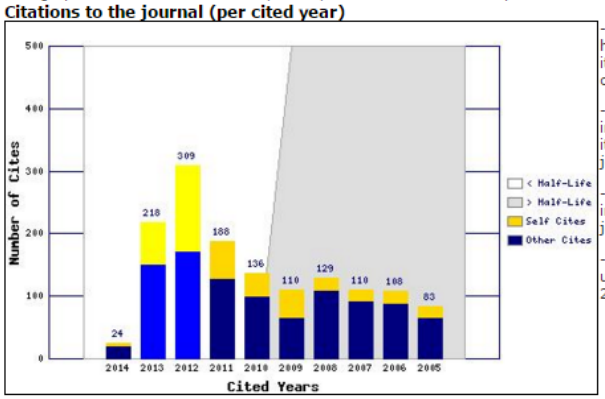

- The white/grey division indicates the cited half-life (if < 10.0). Half of the journal's cited items were published more recently than the cited half-life.

- The top (gold) portion of each column indicates Journal Self Citations: citations to items in the journal from items in the same journal.

- The bottom (blue) portion of each column indicates Non-Self Citations: citations to the journal from items in other journals.

- The two lighter columns indicate citations used to calculate the Impact Factor (always the 2nd and 3rd columns).

Journal Citing Half-Life

The citing half-life for the journal is the median age of the items the journal cited in the current JCR year. Half of the citations in the journal are to items published within the citing half-life.

Citing Half-Life: 8.2 years

Breakdown of the citations ***from the journal*** by the cumulative percent of 2014 cites to items published in the following years:

Cited Year	2014	2013	2012	2011	2010	2009	2008	2007	2006	2005	2004-all
# Cites from 2014	7	155	297	207	163	186	166	135	158	106	1115
Cumulative %	0.26	6.01	17.03	24.71	30.76	37.66	43.82	48.83	54.69	58.63	100

Citing Half-Life Calculations:
The citing half-life calculation finds the number of publication years from the current JCR year that account for 50% of citations in the journal. Read help for more information on the calculation.

Citing Journal Graph

Click here for Citing Journal data table

This graph shows the distribution by cited year of citations from current-year items in the journal COMPUT-AIDED CIV INF.

Citations from the journal (per cited year)

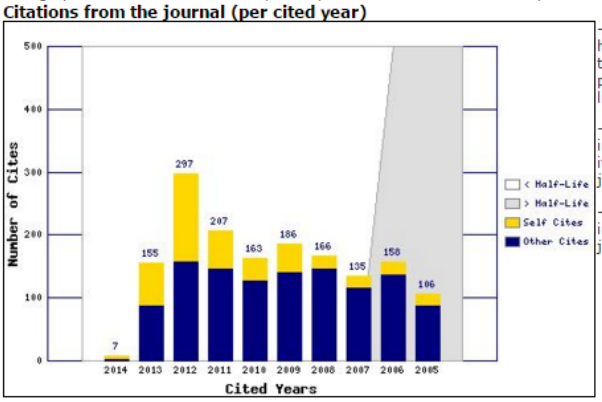

- The white/grey division indicates the citing half-life (if < 10.0). Half of the citations from the journal's current items are to items published more recently than the citing half-life.

- The top (gold) portion of each column indicates Journal Self-Citations: citations from items in the journal to items in the same journal.

- The bottom (blue) portion of each column indicates Non-Self Citations: citations from the journal to items in other journals.

Journal Source Data

	Citable items			
	Articles	**Reviews**	**Combined**	**Other items**
Number in JCR year 2014 (A)	50	0	50	5
Number of references (B)	2695	0	2695	0.00
Ratio (B/A)	53.9	0.0	53.9	0.0

Rank in Category: COMPUTER-AIDED CIVIL AND INFRASTRUCTURE ENGINEERIN...

Journal Ranking

For **2014**, the journal **COMPUTER-AIDED CIVIL AND INFRASTRUCTURE ENGINEERIN...** has an Impact Factor of **4.925**.

This table shows the ranking of this journal in its subject categories based on Impact Factor.

Category Name	Total Journals in Category	Journal Rank in Category	Quartile in Category
COMPUTER SCIENCE, INTERDISCIPLINARY APPLICATIONS	102	1	Q1
CONSTRUCTION & BUILDING TECHNOLOGY	59	1	Q1
ENGINEERING, CIVIL	125	1	Q1
TRANSPORTATION SCIENCE & TECHNOLOGY	33	1	Q1

Category Box Plot

For **2014**, the journal **COMPUTER-AIDED CIVIL AND INFRASTRUCTURE ENGINEERIN...** has an Impact Factor of **4.925**.

This is a box plot of the subject category or categories to which the journal has been assigned. It provides information about the distribution of journals based on Impact Factor values. It shows median, 25th and 75th percentiles, and the extreme values of the distribution.

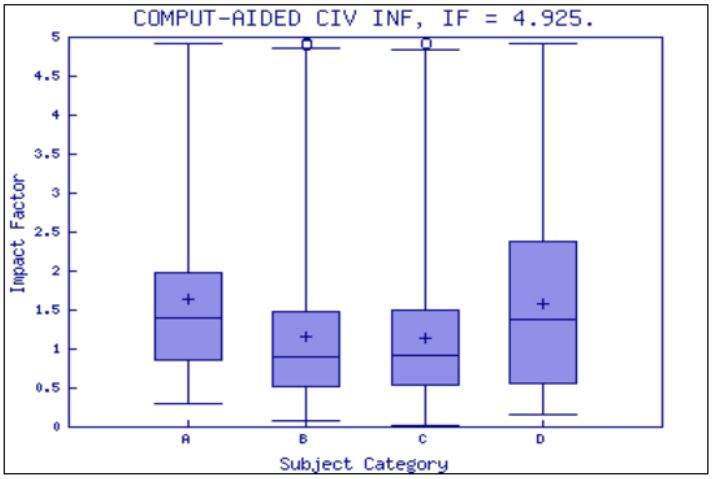

Key

A - COMPUTER SCIENCE, INTERDISCIPLINARY APPLICATIONS

B - CONSTRUCTION & BUILDING TECHNOLOGY

C - ENGINEERING, CIVIL

D - TRANSPORTATION SCIENCE & TECHNOLOGY

APÉNDICE B

SOFTWARE GEOROAD

Apéndice B. Software GEOROAD

Tipo: Registro de la propiedad intelectual

Referencia: SA-121-15

Universidad: Universidad de Salamanca

Códigos UNESCO:

- 3305.06 Ingeniería Civil
- 3305.29 Construcción de Carreteras
- 3317.10 Ingeniería del Trafico
- 3329.07 Transporte

Resumen:

GeoRoad (Road Geometry Extraction) es una herramienta para la extracción de características geométricas de la carretera a partir de modelos 3D obtenidos por un Sistema de Mapeado Móvil (MMS). El software se alimenta de las nubes de puntos 3D capturadas por un MMS, obteniendo como resultado los diagramas geométricos de la carretera tanto planimétricos como altimétricos (longitudinal y transversal), así como el resto de geometría contenida en los perfiles transversales de la carretera.

Su originalidad reside en el automatismo y facilidad de uso con la que obtener las características geométricas de la carretera.

Es de interés para empresas de ingeniería donde quieran obtener la geometría de la carretera tanto para el propio inventario geométrico, como para obras de ensanche y mejora de las carreteras.

Autores:

- Alberto Holgado Barco
- Diego González Aguilera
- Pedro Arias Sánchez
- Belén Riveiro Rodríguez
- Pablo Rodríguez Gonzálvez